

THESIS

INVESTIGATING CONTRIBUTIONS TO ELEVATED SURFACE OZONE IN THE
COLORADO FRONT RANGE DURING SUMMER 2015

Submitted by

Jakob Lindaas

Department of Atmospheric Science

In partial fulfillment of the requirements

For the Degree of Master of Science

Colorado State University

Fort Collins, Colorado

Spring 2018

Master's Committee:

Advisor: Emily V. Fischer

Delphine K. Farmer
A. R. Ravishankara

Copyright by Jakob Lindaas 2018

All Rights Reserved

ABSTRACT

INVESTIGATING CONTRIBUTIONS TO ELEVATED SURFACE OZONE IN THE COLORADO FRONT RANGE DURING SUMMER 2015

Tropospheric ozone (O_3) is a significant pollutant in the Colorado Front Range. The northern Front Range metropolitan area (NFRMA) has exceeded the U.S. EPA national ambient air quality standard for O_3 since 2008. While many regions in the country have experienced downward trends in ground-level O_3 , the NFRMA O_3 mixing ratios have remained stagnant despite efforts to reduce precursor emissions. Rapid population growth and a boom in oil and natural gas development over the past 15 years have changed the quantity and spatial distributions of many important O_3 precursors. O_3 precursors may also be transported into the NFRMA, such as during wildfire smoke events. Here I use *in situ* measurements of O_3 , a suite of volatile organic compounds (VOCs), and reactive oxidized nitrogen species collected during summer 2015 at the Boulder Atmospheric Observatory (BAO) in Erie, CO, to investigate the contribution of different VOC sources to elevated surface O_3 in the NFRMA.

The first analysis combines observations of acyl peroxy nitrates (APN) and a previously described positive matrix factorization of the VOCs to investigate the contribution of different VOC sources to high O_3 abundances at BAO. Based on the ratio of PPN to PAN, I find that anthropogenic VOC precursors dominate APN production when O_3 is most elevated. Propane and higher alkanes, primarily from oil and natural gas emissions in the Colorado Front Range, drive elevated PPN to PAN ratios during high O_3 events. The percentage of OH reactivity associated with oil and gas emissions is also positively correlated with O_3 and PPN/PAN. Lastly,

idealized box model simulations are used to probe the chemical mechanisms for these observations. I find that VOC precursor mixtures dominated by oil and gas emissions create abundant and more efficient peroxy radical intermediates compared to mixtures dominated by traffic or biogenic emissions. This work may help guide efforts to control O₃ precursors in the NFRMA.

The second analysis examines the impact of wildfire smoke on O₃ abundances via a case study. Aged wildfire smoke impacted BAO during two distinct time periods during summer 2015: 6 – 10 July and 16 – 30 August. The smoke was transported from the Pacific Northwest and Canada across much of the continental U.S. Carbon monoxide and particulate matter increased during the smoke-impacted periods, along with acyl peroxy nitrates and several VOCs that have atmospheric lifetimes longer than the transport timescale of the smoke. During the August smoke-impacted period, nitrogen dioxide was also elevated during the morning and evening compared to the smoke-free periods. There were nine empirically defined high O₃ days during our study period at BAO, and two of these days were smoke-impacted. I examined the relationship between O₃ and temperature at BAO and found that for a given temperature, O₃ mixing ratios were greater (~10 ppbv) during the smoke-impacted periods. Enhancements in O₃ during the August smoke-impacted period were also observed at two long-term monitoring sites in Colorado: Rocky Mountain National Park and the Arapahoe National Wildlife Refuge near Walden, CO. Given that the relative importance of wildfire smoke for air quality over the western U.S. is expected to increase as the climate warms and anthropogenic emissions decline, this case study offers important insights into how aged wildfire smoke can influence atmospheric composition at an urban site.

ACKNOWLEDGMENTS

I would like to thank my advisor, Dr. Emily Fischer, for her mentorship, support, and never-ending enthusiasm for all things atmospheric chemistry. The environment she creates for her students to learn and grow can only be described in superlative terms.

Thank you also to my committee members, Dr. Delphine Farmer and Dr. A. R. Ravishankara, for advice along the course of these two research projects and for always asking tough and insightful questions.

It takes many people to make the measurements that form the basis for this thesis, and to complete the analyses on whose shoulders this thesis stands upon. To Ilana Pollack, Andrew Abeleira, Frank Flocke, Rob Roscioli, Scott Herndon, Jake Zaragoza, and Steven Brey, thank you for your hard work during and after the summer 2015 field campaign.

I'd like to acknowledge partial funding support from the American Meteorological Society Graduate Fellowship, and thank the AMS for the variety of other opportunities it has provided me to learn and grow.

Thank you also to all the current and former members of the Fischer Group for being wonderful office and floor mates. That extends to you too, members of the Pierce Group and fellow travelers of the second floor.

I would be remiss if I didn't thank the spectacularly helpful front office staff in the Atmos Department. They truly make the wheels of science turn more smoothly here.

Lastly, thank you to all the family and friends who accompany me on adventures, big and small, every day.

TABLE OF CONTENTS

ABSTRACT.....	ii
ACKNOWLEDGMENTS	iv
CHAPTER 1: INTRODUCTION.....	1
CHAPTER 2: METHODS AND DATA	8
2.1 Research Location	8
2.2 Measurements.....	8
2.3 Smoke-free period	11
2.3.1 PMF factors.....	12
2.3.2 Box model setup.....	12
2.4 Smoke-impacted periods	16
CHAPTER 3: THE CONTRIBUTION OF DIFFERENT VOC PRECURSORS TO HIGH OZONE ABUNDANCES IN THE COLORADO FRONT RANGE DURING SUMMER 2015	20
3.1 Empirical Results.....	20
3.1.1 Spatial Variability in NRFMA O ₃ and its precursors.....	20
3.1.2 Ozone and PANs	21
3.1.3 Ozone, PPN/PAN and VOCs	24
3.2 Insights from idealized modeling	27
CHAPTER 4: CHANGES IN OZONE AND PRECURSORS DURING TWO AGED WILDFIRE SMOKE EVENTS IN THE COLORADO FRONT RANGE IN SUMMER 2015	37
4.1 CO, CH ₄ , and VOC Abundances.....	37
4.2 Reactive Oxidized Nitrogen (NO _y) Species	45
4.3 Ozone.....	48
CHAPTER 5: CONCLUSIONS AND FUTURE WORK.....	58
REFERENCES	63
APPENDIX A: SUPPLEMENTARY INFORMATION TO CHAPTER 3	76
APPENDIX B: SUPPLEMENTARY INFORMATION TO CHAPTER 4	78

CHAPTER 1: INTRODUCTION¹

Formed by the oxidation of volatile organic compounds (VOCs) in the presence of nitrogen oxides (NO_x) and sunlight (Sillman, 1999), tropospheric ozone (O_3) negatively affects human health (*e.g.*, Bates, 2005; Ito et al., 2005), especially in sensitive populations such as children and the elderly, and has adverse effects on vegetation (Fowler, 1992). As such, ground-level O_3 is regulated by the U.S. Environmental Protection Agency (EPA) as one of six key criteria pollutants, with the National Ambient Air Quality Standard (NAAQS) recently revised to a 70 ppbv maximum 8 hour average (EPA, 2015).

The northern Colorado Front Range metropolitan area (NFRMA) has been in violation of the EPA NAAQS for O_3 since 2008 (CDPHE, 2009). Rapid population growth and increasing oil and natural gas development since the early 2000s have changed the quantity and distribution of emissions of many important O_3 precursors (*e.g.*, Evans and Helmig, 2017; McDuffie et al, 2016). However, these emission sources are heterogeneously distributed across the NFRMA (Pfister et al., 2017b). NO_x ($= \text{NO} + \text{NO}_2$) is emitted predominately from traffic and power generation, and in the NFRMA NO_x is most abundant near major roadways and population centers (Wild et al., 2017) (yellow lines and grey areas in Figure 1). These urban areas are also sources of aromatic hydrocarbons, hydrocarbons associated with traffic (*e.g.*, ethyne), and industrial solvents, among other compounds (Swarthout et al., 2013). Oil and natural gas extraction operations in the Denver-Julesberg Basin are clustered in Weld County around Greeley, and extend into areas south and west, abutting the northern Denver metropolitan area (blue dots in Figure 1). Oil and

¹ Portions of this chapter contain published work. Citation: Lindaas, J., Farmer, D. K., Pollack, I. B., Abeleira, A., Flocke, F., Roscioli, R., Herndon, S., and Fischer, E. V.: Changes in ozone and precursors during two aged wildfire smoke events in the Colorado Front Range in summer 2015, *Atmos. Chem. Phys.*, 17, 10691-10707, 10.5194/acp-17-10691-2017, 2017.

natural gas activities emit a range of alkanes and aromatic hydrocarbons (Pétron et al., 2012; Gilman et al., 2013; Pétron et al., 2014; Thompson et al., 2014; Halliday et al., 2016). Biogenic emissions from dispersed broadleaf trees throughout urban neighborhoods in the NFRMA contribute small amounts of isoprene, and needle-leaf forests in the Rocky Mountain foothills along the western edge of the NFRMA have been shown to emit small amounts of several alkene species (Rhew et al., 2017a).

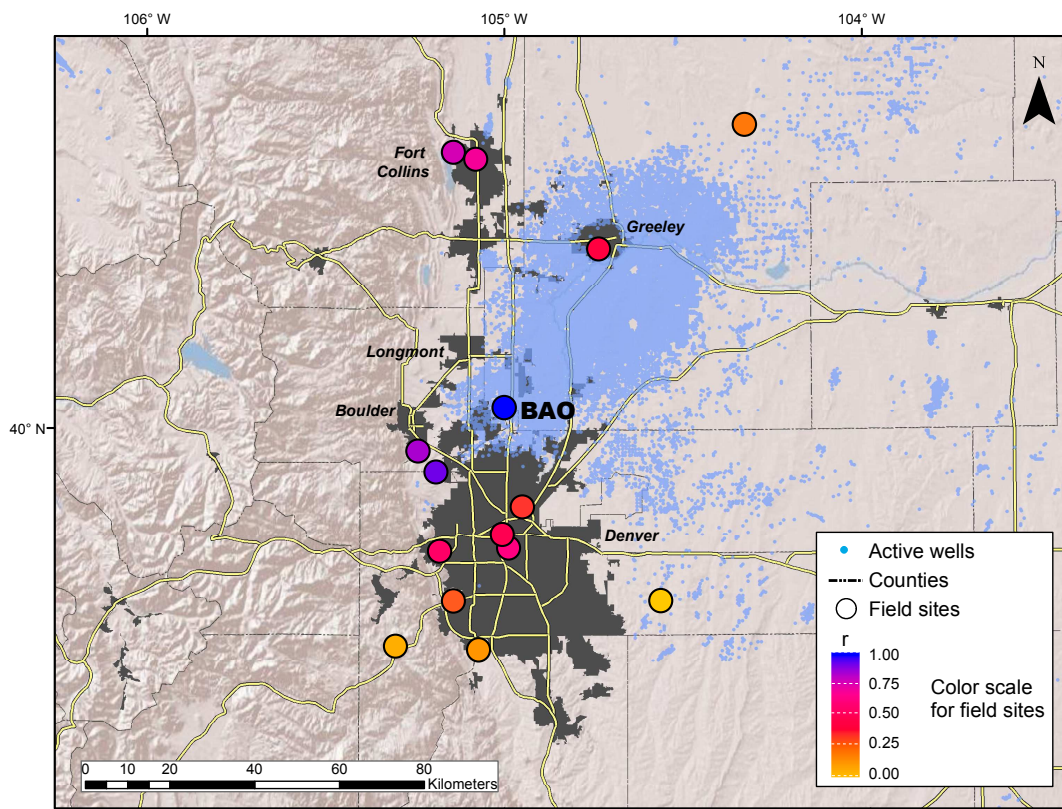


Figure 1. Positive correlations of maximum daily O₃ at BAO with air quality monitoring sites in the Northern Colorado Front Range. Dark grey regions are urban areas, with yellow lines representing major roads and dotted lines delineating county boundaries. Small blue dots are the locations of active oil and natural gas wells. Large points are CDPHE air quality monitoring locations that measure O₃. For sites that routinely exceed the NAAQS standard (https://www.colorado.gov/airquality/html_resources/ozone_summary_table.pdf; Rocky Flats N, NREL, Fort Collins West, Welch, Chatfield State Park, and Greeley Weld Tower), correlation coefficients with BAO are $r = 0.77, 0.67, 0.76, 0.54, 0.47,$ and 0.57 respectively.

The photolysis of NO_2 is the only known mechanism for chemically producing O_3 in the troposphere (Monks et al., 2015). Net O_3 production occurs when NO , is recycled back to NO_2 without the subsequent destruction of O_3 . Oxidation of VOCs offers a way to convert NO to NO_2 while cycling HO_x , thereby propagating or catalyzing the formation of O_3 . This formation of O_3 is initiated by the reaction of OH with a VOC, which begins a process whereby NO_x is interconverted as the VOC oxidation products are further oxidized.

The hydroxyl radical (OH) is the primary daytime oxidant for most VOC species. The VOC OH reactivity (OHR) is then defined as the product of the rate constant associated with the reaction of a species with OH ($k_{\text{OH,VOC}}$) with the concentration of that species. OHR provides information on which species are likely to initiate the catalytic O_3 production cycle. OHR does not, however, give insight into how oxidation products of that VOC may propagate or terminate the NO_x and HO_x catalytic cycles. For instance, alkanes tend to have lower $k_{\text{OH,VOC}}$ values than alkenes or aromatic hydrocarbons, but the degradation products of alkane oxidation (namely aldehydes) are relatively more efficient at producing O_3 than their parents, whereas the degradation products (namely ketones) of alkenes tend to be less efficient at O_3 production than their parents (Calvert, 2008).

The oxidation pathways of most VOCs are complex, and the fate of oxidation products (such as RO and RO_2 radicals) plays a large role in the extent to which the reactions supporting catalytic O_3 production continue or whether these cycles terminate. This leads to complex and non-linear chemistry that is impacted by the relative abundances of NO_x and VOCs. Reactions that terminate the cycling of NO_x and HO_x can be temporary or permanent sinks for these radical families, and include the production of nitric acid, hydrogen peroxide, organic nitrates and acyl peroxy nitrates (*e.g.*, Sillman et al., 1995; Farmer et al., 2011; Thornton et al., 2002).

Acyl peroxy nitrates are secondary species that are formed concurrently with O_3 from specific VOC precursors. Therefore, the relative abundances of different APN species offers important evidence for the extent to which their respective parent VOCs impacted the photochemistry of a given air mass. The most common APN, peroxyacetyl nitrate (PAN), also has the widest variety of VOC precursors (Fischer et al., 2014). Comparatively, two other commonly measured APNs, peroxypropionyl nitrate (PPN) and peroxyacryloyl nitrate (MPAN), have more limited VOC precursors. PPN is formed from oxidation products of primarily anthropogenic VOCs (Roberts et al., 2001), and the main precursor of MPAN is isoprene, a primarily biogenic species (Williams et al., 1997). APNs are a temporary sink for NO_x , due to thermal dissociation. Under warm temperatures, such as those during summer in the Colorado Front Range, this thermal dissociation considerably shortens the lifetime of APNs to less than one day. Because background APN abundances are very low and transport of APNs into the Front Range is negligible (Zaragoza et al., 2017), this means that most of the variability in measured APN mixing ratios in the Front Range is due to local photochemical production.

In addition to local production of O_3 , the Colorado Front Range experiences exacerbated O_3 pollution due to wildfire smoke. Wildfires emit many trace gas species that contribute to tropospheric O_3 production. Along with carbon monoxide (CO), methane (CH_4), and carbon dioxide (CO_2), hundreds of different non-methane volatile organic compounds (NMVOCs) with lifetimes ranging from minutes to months (Atkinson and Arey, 2003) are emitted during biomass burning (Akagi et al., 2011; Gilman et al., 2015). Due to relatively large emissions of CO_2 , CO, and CH_4 , the contribution of VOCs to the total emission of carbon from fires on a molar basis is small (<1%). However, VOCs dominate the OH reactivity in smoke plumes (Gilman et al., 2015). Recent observations of the evolution of VOCs within aging smoke plumes indicate that OH can

be elevated in young biomass burning plumes (Hobbs et al., 2003; Yokelson et al., 2009; Akagi et al., 2012; Liu et al., 2016) in part due to the photolysis of oxygenated VOCs (Mason et al., 2001), which make a large contribution to the total emitted VOC mass (Stockwell et al., 2015). Elevated OH may reduce the lifetime of emitted VOCs and increase oxidation rates and potential O₃ production.

Fires are also a major source of oxidized nitrogen; emissions from biomass and biofuel burning represent approximately 15% of total global NO_x emissions (Jaegle et al., 2005). However, there are major uncertainties in NO_x emission estimates from biomass burning, particularly at a regional scale (Schreier et al., 2015). NO_x emissions depend on the nitrogen content of the fuel (Lacaux et al., 1996; Giordano et al., 2016) as well as the combustion efficiency (Goode et al., 2000; McMeeking et al., 2009; Yokelson et al., 2009). Emitted NO_x is quickly lost in the plume, either by conversion to HNO₃ (Mason et al., 2001) or via PAN formation (Alvarado et al., 2010; Yates et al., 2016). HNO₃ is not often observed in plumes because it either rapidly forms ammonium nitrate or is efficiently scavenged by other aerosols (Tabazadeh et al., 1998; Trentmann et al., 2005).

There are multiple lines of observational evidence indicating that wildfires in the western U.S. increase the abundance of ground level O₃. Background O₃ mixing ratios across the western U.S. are positively correlated with wildfire burned area (Jaffe et al., 2008), and daily episodic enhancements in O₃ at ground sites can be > 10 ppbv (Lu et al., 2016). There are well-documented case studies of within plume O₃ production (see Jaffe and Wigder (2012), Heilman et al. (2014), and references within) and time periods where smoke contributed to exceedances of the U.S. EPA National Ambient Air Quality Standard (NAAQS) for O₃ (Morris et al., 2006; Pfister et al., 2008), currently a maximum daily 8 hour average of 70 ppbv. Brey and Fischer

(2016) investigated the impacts of smoke on O₃ abundances across the U.S. via an analysis of routine *in situ* measurements and NOAA satellite products. Their analysis demonstrated that higher expected O₃ mixing ratios are higher when smoke is present in many areas of the U.S., and that this relationship is not driven by temperature. Regions with the largest smoke-induced O₃ enhancements (*e.g.* the southeast and Gulf coast) can be located substantially downwind of the wildfires producing the most smoke.

Over the past 30 years, the number of large wildfires that occur each year in the western U.S. has increased, and this trend will likely continue under future climate change (Westerling, 2016). Wildfire smoke can be transported over thousands of kilometers, and exposure to wildfire smoke has significant impacts on human health (Künzli et al., 2006; Rappold et al., 2011; Elliott et al., 2013). While U.S. emissions of most major air pollutants are declining (Pinder et al., 2008), increasing fire activity suggests that wildfires may have a greater relative impact on U.S. air quality in the future (Val Martin et al., 2015).

Despite several recent studies showing that smoke contributes to elevated O₃, there have been relatively few detailed studies of wildfire smoke mixing with anthropogenic air masses near the surface. Morris et al. (2006) demonstrated that smoke from wildfires in Alaska and Canada exacerbated O₃ pollution in Houston during two days in July 2004, but did not have *in situ* measurements of other chemical species apart from O₃. Singh et al. (2012) used aircraft measurements from summer 2008 over California to document significant O₃ enhancements in nitrogen-rich urban air masses mixed with smoke plumes. Accompanying air quality simulations were not successful in capturing the mechanisms responsible for these enhancements. In general, measurements of O₃ precursors are hard to make routinely. Instrumentation and calibration

methods tend to be time and labor intensive, and thus unpredictable wildfire smoke plumes and their effects on surface O_3 are sparsely sampled.

This thesis presents two analyses that investigate the contribution of different O_3 precursors to elevated surface O_3 in the Colorado Front Range during summer 2015. In Chapter 3 we explore the contribution of different VOC precursors to high O_3 events at the Boulder Atmospheric Observatory during smoke-free time periods in summer 2015. We build on previous measurements made at BAO during summer 2014 and report similar patterns in the relationships between measured APN species and O_3 . We pair this analysis with a concurrently measured dataset of 40+ VOCs (Abeleira et al., 2017), and examine the empirical relationships between different VOC sources O_3 and APNs. Next we present a series of idealized box model simulations to probe the underlying causes for the empirical relationships we observe. Lastly, we use the box model to investigate the primary precursors of PPN and provide support for the hypothesis presented in Zaragoza et al. (2017) that alkane precursors dominate the production of APNs in the NFRMA. In Chapter 4 we present a case study of aged wildfire smoke mixed with anthropogenic pollution in the Colorado Front Range and show its impact on atmospheric composition and O_3 . First we describe the research location and measurements. Next, we identify the smoke-impacted time periods and show the origin, approximate age, and wide horizontal extent of the smoke plumes. We characterize significant changes in atmospheric composition with respect to the two major classes of O_3 precursors, VOCs and oxidized reactive nitrogen (NO_y). Finally, we present the impact of smoke on O_3 abundances during this period and discuss the underlying causes of this impact. Conclusions from both analyses are presented in Chapter 5, and suggestions for future work are discussed.

CHAPTER 2: METHODS AND DATA²

2.1 RESEARCH LOCATION

During summer 2015, we made measurements of a suite of trace gases at the Boulder Atmospheric Observatory (BAO), located north of Denver, CO, in the middle of the rapidly developing northern Colorado Front Range [40.05°N, 105.01°W, 1584m ASL]. BAO has a history of atmospheric trace gas and meteorological measurements stretching back nearly four decades (Kelly et al., 1979; Gilman et al., 2013). Our research campaign from 1 July – 7 September 2015 measured a suite of O₃ precursor species as well as several NO_x oxidation products and greenhouse gases. The intended goal of the field campaign was to improve our understanding of the complex O₃ photochemistry in the Colorado Front Range and the contributions of oil and natural gas activities as well as other anthropogenic emissions to O₃ production. All measurements were made by instruments housed in two trailers located at the base of the BAO tower. Here we briefly describe the measurements used in this thesis. Data are available at <https://esrl.noaa.gov/csd/groups/csd7/measurements/2015songnex/>.

2.2 MEASUREMENTS

We measured CO and CH₄ at ~3 second time resolution with a commercial cavity ring-down spectrometer (Picarro, model G2401) (Crosson, 2008). The inlet was located 6 m above ground level (a.g.l.), and a PTFE filter membrane with 1 μm pore size (Savillex) at the inlet was changed weekly. Laboratory instrument calibrations were performed pre- and post-campaign using three NOAA standard reference gases (<http://www.esrl.noaa.gov/gmd/ccl/refgas.htmls>;

² Portions of this chapter contain published work. Citation: Lindaas, J., Farmer, D. K., Pollack, I. B., Abeleira, A., Flocke, F., Roscioli, R., Herndon, S., and Fischer, E. V.: Changes in ozone and precursors during two aged wildfire smoke events in the Colorado Front Range in summer 2015, *Atmos. Chem. Phys.*, 17, 10691-10707, 10.5194/acp-17-10691-2017, 2017.

CA06969, CB10166, and CA08244). Field calibration was performed every 3 hours using high, low and middle reference gas mixtures (Scott Marin Cylinder IDs CB10808, CB10897, CB10881). Mixing ratios were calculated using the WMO-CH₄-X2004 and WMO-CO-X2014 scales. The uncertainty associated with the CH₄ and CO data is estimated to be 6% and 12% respectively, and it was estimated as the quadrature sum of measurement precision, calibration uncertainty and uncertainty in the water vapor correction.

A custom 4-channel cryogen-free gas chromatography (GC) system (Sive et al., 2005) was used to measure selected non-methane hydrocarbons (NMHCs), C₁ – C₂ halocarbons, alkyl nitrates (ANs), and oxygenated volatile organic compounds (OVOCs) at sub-hourly time resolution; approximately one sample every 45 minutes. The inlet was located at 6 m a.g.l. with a 1 μm pore size teflon filter. Ambient air for each sample was collected and pre-concentrated over 5 minutes, with a one litre total sample volume. A calibrated whole air mixture was sampled in the field after every ten ambient samples to monitor sensitivity changes and measurement precision. A full description of this instrument and the associated uncertainties for each detected species is provided in (Abeleira et al., 2017).

Ozone data at BAO for this time period were provided by the NOAA Global Monitoring Division surface ozone network (McClure-Begley et al., 2014; data available at aftp.cmdl.noaa.gov/data/ozwv/SurfaceOzone/BAO/). Ozone was measured via UV-absorption using a commercial analyzer (Thermo-Scientific Inc., model 49), which is calibrated to the NIST standard over the range 0 – 200 ppbv and routinely challenged at the site. The inlet height was 6m a.g.l. on the BAO tower, located about 50 feet from the two trailers, and measurements were reported at a 1 minute averaging interval with an estimated error of 1%.

Nitrogen oxides ($\text{NO}_x \equiv \text{NO} + \text{NO}_2$) and total reactive nitrogen (NO_y) were measured via $\text{NO}-\text{O}_3$ chemiluminescence detection (Kley and McFarland, 1980) using a commercial analyzer (Teledyne, model 200EU). Two commercial converters, a 395 nm -LED converter (Air Quality Designs, Inc., model BLC) for chemically-selective photolysis of NO_2 to NO and a molybdenum in stainless steel converter (Thermo Scientific Inc.) heated to 320 °C for reduction of NO_y to NO , were positioned as close to the inlet tip as possible (<10 cm). A 7 mm stainless steel particulate filter was affixed to the upstream end of the molybdenum converter; otherwise no other filters were used. The analyzer switched between sampling from the LED (NO_x) converter and the molybdenum (NO_y) converter every 10 seconds, and the LEDs were turned on (to measure $\text{NO} + \text{NO}_2$) and off (to measure NO only) every minute. NO_2 was determined by subtraction of measured NO from measured $\text{NO} + \text{NO}_2$ divided by the efficiency of the LED converter. All three species are reported on a consistent two-minute average timescale. The detector was calibrated daily by standard addition of a known concentration of NO , NIST-traceable (Scott-Marrin Cylinder ID CB098J6), to synthetic ultrapure air. Both converters were calibrated with a known concentration of NO_2 generated via gas phase titration of the NO standard. The NO_y channel was further challenged with a known mixing ratio of nitric acid (HNO_3) generated using a permeation tube (Kintech, 30.5 ± 0.8 ng/min at 40 °C), which was used to confirm >90% conversion efficiency of HNO_3 by the molybdenum converter. Uncertainties of $\pm 5\%$ for NO , $\pm 7\%$ for NO_2 , and $\pm 20\%$ for NO_y are determined from a quadrature sum of the individual uncertainties associated with the detector, converters, and calibration mixtures; an LOD of 0.4 ppbv for all species is dictated by the specifications of the commercial detector.

Acyl peroxy nitrates (APNs) were measured using the National Center for Atmospheric Research gas chromatograph with an electron capture detector (NCAR GC-ECD) (Flocke et al.,

2005). The instrument configuration was the same as was used during the summer 2014 FRAPPE field campaign (Zaragoza, 2016). The NCAR GC-ECD analyzed a sample every five minutes from a 6 m a.g.l. inlet with 1 μ m pore size teflon filter. A continuous-flow acetone photolysis cell generated a known quantity of PAN used to calibrate the system at 4-hour intervals. Three APN species were quantified: peroxyacetyl nitrate (PAN), peroxypropionyl nitrate (PPN) and peroxyethacryloyl nitrate (MPAN).

An Aerodyne dual quantum cascade laser spectrometer was used to measure HNO₃ (McManus et al., 2011). The instrument employed a prototype 400 m absorption cell for increased sensitivity during the first month of the campaign, after which it was replaced by a 157 m absorption cell. An active passivation inlet (Roscioli et al., 2016) was used to improve the time response of the measurement to ~0.75 s. This technique utilized a continuous injection of 10-100 ppb of a passivating agent vapor, nonafluorobutane sulfonic acid, into the inlet tip. The inlet tip was made of extruded perfluoroalkoxy Teflon (PFA), followed by a heated, fused silica inertial separator to remove particles larger than 300 nm from the sample stream. The inlet was located 8 m a.g.l. with a 18 m heated sampling line (PFA, 1/2" diameter OD) to the instrument. The system was calibrated every hour by using a permeation tube that was quantified immediately prior to the measurement period.

2.3 SMOKE-FREE PERIOD

The first analysis, presented in Chapter 3, uses valid measurements from the period July 11 – August 15. The days within the campaign study period but before and after July 11 – August 15 have been determined to be impacted by aged wildfire smoke, and measurements from these periods will be described in Section 2.4 and Chapter 4. Measurements used in the first analysis are further restricted in two ways. Chromatograms from the PAN instrument were

not adjusted to clearly display the MPAN peak until July 18. Thus, analysis using the APN measurements is restricted to July 18 – August 15. Valid VOC measurements for this analysis were likewise restricted to July 24 – August 14 due to water issues in the GC system (Abeleira et al., 2017).

2.3.1 PMF FACTORS

Abeleira et al. (2017) characterized the VOC measurements made at BAO during summer 2015. They used Positive Matrix Factorization (PMF) to differentiate multiple source classifications and to partition the species measured among these factors. For summer 2015 they identified 6 source factors: short-lived oil and gas, long-lived oil and gas, traffic, secondary, biogenic, and background.

In Chapter 3 we use the reconstructed time series of the summed OH reactivity (OHR) for these factors to investigate the empirical connections between these source classifications and our secondary species of interest, O_3 and the APNs. The reconstructed OHR time series was created by calculating the OHR of each species, using the time series of the reconstructed mixing ratios for that species, the temperature-dependent $k_{OH,VOC}$, and the ambient 10m air temperature time series, and then aggregating the reconstructed OHR time series across all species in a given factor. For simplicity, we group the short and long-lived oil and gas factors into one oil and gas factor, and note that the biogenic factor solely consists of isoprene.

2.3.2 BOX MODEL SETUP

In Chapter 3 we use BOXMOX (Knote et al., 2015; https://boxmodeling.meteo.physik.uni-muenchen.de/online_tools/boxmox.html), an online extension to the Kinetic PreProcessor (Sandu et al., 2003), to simulate idealized photochemistry

in the Front Range. We use the full set of equations from the Master Chemical Mechanism version 3.3 (MCMv3.3; Emmerson and Evans, 2009; Jenkin et al., 2015) with fixed environmental parameters, summarized in Appendix A in Table 3. The MCM explicitly simulates thousands of reactions and has been extensively used in past studies of urban photochemistry (*e.g.*, Sommariva et al., 2011).

For all simulations the mixing height is set to 1km and the ambient temperature is set to 300K. No deposition, turbulent mixing, or entrainment/dilution parameters are included. The simulations are run for eight hours at a ten-minute time step. Photolysis rates were calculated from the NCAR Tropospheric Ultraviolet and Visible (TUV; Madronich, 1992) radiation model for 40°N and 105°W, 1700 magl (Rebecca Hornbrook, personal communication). The full set of TUV parameters are listed in Appendix A in Table 3. The photolysis rates were held constant for the duration of each simulation.

Additionally, NO and NO₂ emissions are added at each time step such that NO_x mixing ratios stay approximately constant throughout each simulation. The goal of this setting is to allow VOC oxidation to proceed under a consistent VOC/NO_x regime in each simulation. For the first group of simulations, each VOC mixture is run with a series of five NO_x scaling factors: 0.25, 0.5, 1, 2, and 3. With all other initial conditions held constant, both the NO and NO₂ initial conditions and NO and NO₂ emissions at each time step are multiplied by the given NO_x scaling factor. This treatment resulted in reasonably stable NO_x mixing ratios for all simulations with the exception of those run under the largest NO_x scaling factor. In these simulations NO_x mixing ratios slowly increased to around 180% of the initial values.

We present two groups of BOXMOX simulations. The first group of simulations is initialized with five different VOC mixtures for the set of five NO_x scaling factors. The five

different mixtures include a baseline mixture (“baseline”), high oil and natural gas influenced mixture (“high ong”), high biogenic influenced mixture (“high bio”), high traffic influenced mixture (“high traffic”), and a perturbation on the high bio mixture wherein a small quantity of isoprene ($3 \times 10^{11} \text{ molec cm}^{-2} \text{ s}^{-1}$) was emitted into the box at every timestep to keep isoprene approximately constant in the simulation. Initial mixing ratios in the “baseline” are initialized with the median value of every measured VOC for the smoke free period between daytime hours of 10AM - 6PM MDT, while the three other mixtures are created by adding the mixing ratio equivalent of 0.5 s^{-1} of OH reactivity, distributed among respective sets of species, to the baseline initial conditions. Thus, the “high ong” mixture has an additional 0.5 s^{-1} of OHR, achieved by proportionately increasing the initial mixing ratios of species that were unambiguously factored into the combined oil and gas PMF factor in Abeleira et al. (2017). Accordingly, isoprene increased by the mixing ratio equivalent of 0.5 s^{-1} OHR in the “high bio” mixture. And species that are predominately associated with the traffic PMF factor are proportionately increased by 0.5 s^{-1} OHR mixing ratio equivalent to create the “high traffic” mixture. While the initial mixing ratios for the oil and gas species and isoprene in the high ong and high bio mixtures remained within the range of measured values during our field campaign, traffic species’ abundances in the high traffic mixture were well above even the maximum measured mixing ratios. Thus, the high traffic mixture is not included in the visualization of the simulations as it is not consistent with the measurements. Values for all initial mixing ratios in each mixture are summarized in Table 1.

The second group of three BOXMOX simulations is initialized with same OHR (2 s^{-1}) and NO_x scaling factor of 1. In this group, the first simulation (“100% isoprene”) is initialized with the mixing ratio of isoprene needed for the total OHR to be completely comprised of isoprene. The second simulation (“100% propane”) is initialized such that the OHR is completely

comprised of propane. The third BOXMOX simulation in this group is initialized with a 50% mixture of each isoprene and propane (“even mix”); the initial mixing ratios of both isoprene and propane are set to be 1 s^{-1} OHR. The initial mixing ratios for these three simulations are summarized in Table 1.

We compared the NO_2/NO ratio in our simulations to that observed at BAO. For all of our simulations, the initial NO_2/NO ratio was ~ 2 , which is slightly lower than average daytime from field data (~ 5), but the NO_2/NO ratio adjusts within 2-3 time steps to a level consistent with the average ratio of the BAO field measurements. OH concentrations were also similar to those measured in the NFRMA during the FRAPPE aircraft campaign in summer 2014 (Ebben et al., 2017).

Table 1. Initial conditions for all BOXMOX simulations. All environmental parameters and NO_x emissions were held constant throughout the simulations, which were run for 8 hours at a 10 minute time step. Initial conditions for the first group of simulations are given for a NO_x scaling factor of 1.

^a Multiply by the NO_x scaling factor if needed.

^b TUV input parameters given in Table 3 in Appendix A.

	First group				Second group		
	baseline	high_ong	high_bio	high_traf	100% isoprene	even mix	100% propane
Temperature	300 K						
Mixing Height	1000 m						
Deposition	NA						
Turbulent Mixing	NA						
Entrainment	NA						
Photolysis Rates	constant, from TUV ^b						
NO emissions ^a	$3 \times 10^{11} \text{ molec cm}^{-2} \text{ s}^{-1}$						
NO_2 emissions ^a	$3 \times 10^{10} \text{ molec cm}^{-2} \text{ s}^{-1}$						
NO^a	0.5 ppbv						
NO_2^a	1 ppbv						
O_3	50 ppbv						
H_2O	1%						
CH_4	1900 ppbv						
CO	110.9 ppbv						
M	1e9 ppbv						
N_2	78.084%						
O_2	20.946%						
OH	0 ppbv						
Initial $\Sigma \text{OHR}_{\text{voc}} [\text{s}^{-1}]$	1.58	2.08	2.08	2.08	2	2	2
Oil and gas species [ppbv]							
	baseline	high_ong	high_bio	high_traf	100% isoprene	Even mix	100% propane
Ethane	5.4	12.3	5.4	5.4	0	0	0

Propane	2.39	5.4	2.39	2.39	0	38	76
i-butane	0.41	0.95	0.41	0.41	0	0	0
n-butane	1.0	2.28	1.0	1.0	0	0	0
i-pentane	0.9	2.05	0.9	0.9	0	0	0
n-pentane	0.71	1.62	0.71	0.71	0	0	0
n-hexane	0.1	0.23	0.1	0.1	0	0	0
Cyclohexane	0.053	0.12	0.053	0.053	0	0	0
2-methylhexane	0.024	0.055	0.024	0.024	0	0	0
n-heptane	0.042	0.096	0.042	0.042	0	0	0
n-octane	0.021	0.047	0.021	0.021	0	0	0
Cis-2-butene	0.016	0.036	0.016	0.016	0	0	0
Traffic species [ppbv]							
	baseline	high_ong	high_bio	high_traf	100% isoprene	Even mix	100% propane
Toluene	0.111	0.111	0.111	2.07	0	0	0
Ethylbenzene	0.012	0.012	0.012	0.22	0	0	0
Ortho-xylene	0.015	0.015	0.015	0.28	0	0	0
Ethyne	0.14	0.14	0.14	2.61	0	0	0
3-methylhexane	0.02	0.02	0.02	0.372	0	0	0
Biogenic species [ppbv]							
	baseline	high_ong	high_bio	high_traf	100% isoprene	Even mix	100% propane
Isoprene	0.167	0.167	0.37	0.167	0.83	0.415	0
Other species [ppbv]							
	baseline	high_ong	high_bio	high_traf	100% isoprene	Even mix	100% propane
Ethene	0.123	0.123	0.123	0.123	0	0	0
Propene	0.035	0.035	0.035	0.035	0	0	0
Benzene	0.091	0.091	0.091	0.091	0	0	0
Acetaldehyde	1.915	1.915	1.915	1.915	0	0	0
Acetone	3.16	3.16	3.16	3.16	0	0	0
MEK	0.344	0.344	0.344	0.344	0	0	0
CH ₂ Cl ₂	0.021	0.021	0.021	0.021	0	0	0
CHCl ₃	0.007	0.007	0.007	0.007	0	0	0

2.4 SMOKE-IMPACTED PERIODS

Chapter 4 concerns the time periods impacted by aged wildfire smoke during the campaign. Two distinct smoke-impacted periods were observed at BAO, identified by large enhancements in CO and fine aerosol (PM_{2.5}). Figure 2 presents CO observations from BAO and fine particulate matter (PM_{2.5}) observations from the Colorado Department of Public Health and Environment (CDPHE) CAMP air quality monitoring site (www.epa.gov/airdata), located in downtown Denver, approximately 35km south of BAO. PM_{2.5} was similarly elevated during the smoke-impacted periods at nine other CDPHE monitoring sites across the Colorado Front Range: BOU, CASA, CHAT, COMM, FTCF, GREH, I25, LNGM, NJH (Figure 19 in Appendix B). For

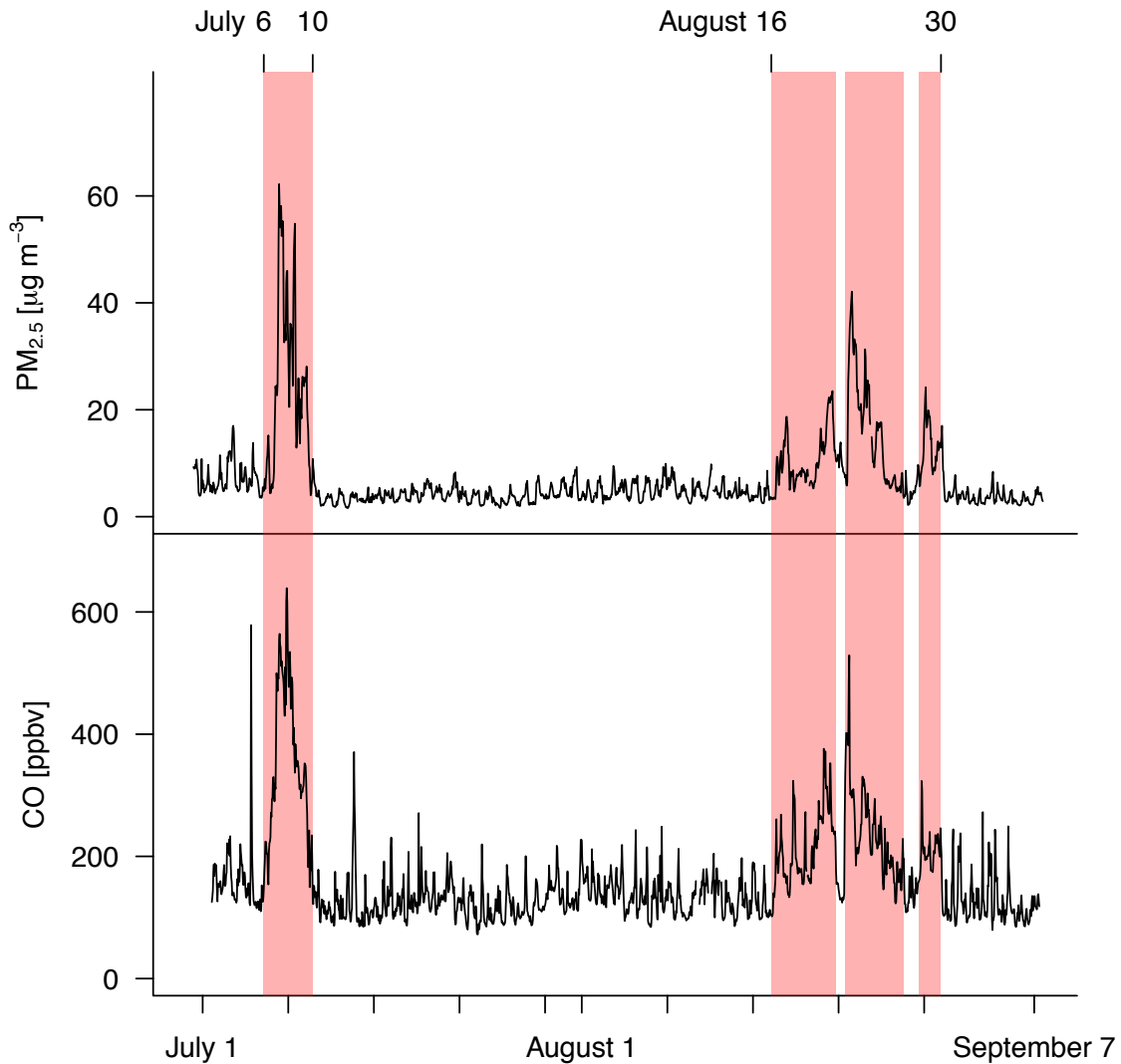


Figure 2. Top panel: Time series of hourly PM_{2.5} concentrations for the CDPHE CAMP air quality monitoring site (www.epa.gov/airdata) located in downtown Denver (39.75', -104.98'). Bottom panel: Time series of hourly CO mixing ratios at the Boulder Atmospheric Observatory (BAO: 40.05', -105.01'). Red shading denotes periods during which smoke is present at BAO.

our analysis, we defined a July smoke-impacted period and an August smoke-impacted period. The July smoke-impacted period lasted for 4 days from 00 MDT 6 July 2015 to 00 MDT 10 July 2015. The August smoke-impacted period was significantly longer (~14 days). For the subsequent analysis, we combined three distinct waves of smoke-impact in this 14 day period into one August smoke-impacted period: 00 MDT 16 August 2015 – 18 MDT 21 August 2015,

12 MDT 22 August 2015 – 18 MDT 27 August 2015, and 14 MDT 28 August 2015 – 09 MDT 30 August 2015. We omitted the brief periods between these times from the analysis due to uncertainty on the influence of smoke during them. All other valid measurements were considered part of the smoke-free data.

Figure 3 presents the extent of the presence of smoke in the atmospheric column during representative smoke-impacted days, 7 July and 21 August 2015. The NOAA Hazard Mapping System smoke polygons show that the smoke events observed at BAO were large regional events. The HMS smoke product is produced using multiple NASA and NOAA satellite products (Rolph et al., 2009). Smoke in the atmospheric column is detected using both visible and infrared imagery and is fully described in Brey et al. (2017). The extent of smoke plumes within the HMS dataset represents a conservative estimate, and no information is provided on the vertical extent or vertical placement of the plumes. Figure 3 also shows active MODIS fire locations for the previous day (Giglio et al., 2003; Giglio et al., 2006) and 5 day NOAA Air Resources Laboratory Hybrid Single Particle Lagrangian Integrated Trajectory (HYSPLIT) back trajectories initialized each hour of the day from BAO at 1000m above ground level (Stein et al., 2015). Trajectories were run using the EDAS (Eta Data Assimilation System) 40 km x 40 km horizontal resolution reanalysis product (Kalnay et al., 1996). In total, Figure 3 demonstrates that the smoke that impacted BAO during both periods was transported from large extreme fire complexes in the Pacific Northwest and Canada, with approximate transport timescales on the order of two to three days. Front Range surface temperatures were not anomalously high in July and August 2015 based on a comparison of reanalysis data for this period to the 1981 – 2010 climatology. Surface precipitation, surface relative humidity, and soil moisture in the Front Range were all lower than this referent period. The extreme fires in Washington and Idaho were associated with

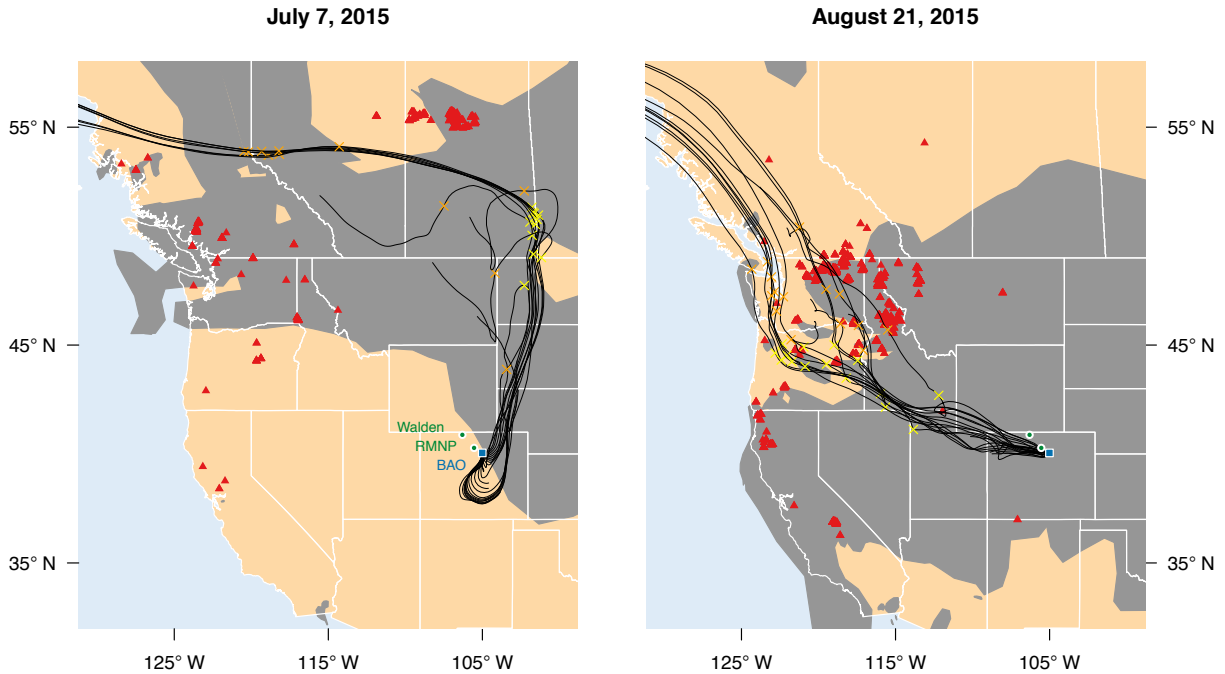


Figure 3. Representative days during each smoke period observed at the Boulder Atmospheric Observatory (BAO: blue square). NOAA Hazard Mapping System (<http://www.ssd.noaa.gov/PS/FIRE/>) smoke polygons are plotted in dark grey shading with MODIS fire locations (<http://modis-fire.umd.edu/index.php>) from the previous day plotted as red triangles. The thin black lines show HYSPLIT 120 hour back trajectories from the BAO site initiated at 1000 m a.g.l. for each hour of the day plotted. Yellow cross hatches display the location of each trajectory 48 hours back and orange cross hatches indicate the 72 hour location. The green points show the location of the Rocky Mountain National Park and Walden measurement locations.

warmer and dryer than average summer temperatures in the Pacific Northwest (Kalnay et al., 1996). Creamean et al. (2016) provide a more detailed description of smoke transport and the sources of the aerosols associated with the August smoke-impacted period. Summer 2015 was the largest wildfire season in Washington, and the Okanogan Complex fire, which likely contributed to the smoke observed at BAO, was the largest fire complex in state history. Summer 2015 was also one of the largest fire seasons for northern Idaho, with approximately 740,000 acres burned.

CHAPTER 3: THE CONTRIBUTION OF DIFFERENT VOC PRECURSORS TO HIGH OZONE ABUNDANCES IN THE COLORADO FRONT RANGE DURING SUMMER 2015

3.1 EMPIRICAL RESULTS

The results and discussion section is divided into two subsections. First, we present the results of our empirical analysis using *in situ* measurements at BAO. Second, we investigate the potential mechanisms behind our empirical results using the set of idealized box modeling simulations described in Section 3.2.

3.1.1 SPATIAL VARIABILITY IN NRFMA O₃ AND ITS PRECURSORS

Strong spatial gradients in emissions and meteorology in the NRFMA make this region particularly heterogeneous (Pfister et al., 2017b). The sources of O₃ precursors differentially impact ground-level O₃ across the Front Range. Denver and surrounding suburban and industrial areas (large grey area in Figure 1) are characterized by large NO_x emissions and certain VOC emissions. Outside of Denver and its suburbs there are also several more disperse population centers (*e.g.*, the cities of Boulder, Longmont, Fort Collins, Greeley), and oil and natural gas production closely border, if not overlap with these regions (small blue dots in Figure 1). Though likely less relevant for O₃ production, agricultural activities are also a major source of air pollutants in the Front Range (Eilerman et al., 2016; Townsend-Small et al., 2016; Tevlin et al., 2017). Recirculation and upslope-downslope regimes mix these sources of emissions throughout the NRFMA (Sullivan et al., 2016; Vu et al., 2016; Pfister et al., 2017b).

The BAO is located north of the Denver urban area and at the southeast corner of the region with the most dense oil and gas development. This site has hosted a variety of recent field experiments. For example, *in situ* observations from this location have been used to investigate specific aspects of nighttime chemistry (Brown et al., 2013), the relative importance of different

sources on VOC abundances in the Colorado Front Range (*e.g.*, Gilman et al., 2013; Swarthout et al., 2013; Pétron et al., 2014; Abeleira et al., 2017), and the impact of oil and gas emissions on summertime O₃ chemistry in this region (McDuffie et al., 2016). Recent measurements near BAO in Erie, CO, indicate that atmospheric composition near BAO is similar to other sites throughout the northern Colorado Front Range in the types of species present and their relative abundances (Thompson et al., 2014). Analogously, we find that O₃ measurements at BAO are positively correlated with O₃ measurements across the Front Range. Figure 1 shows the correlation coefficient (*r*) of the relationship between daily maximum hour-averaged O₃ mixing ratios at BAO and daily maximum hour-averaged O₃ mixing ratios at CDPHE air quality monitoring sites. Correlation coefficients > 0.6 exist for most sites along the Denver to Fort Collins corridor, with lower correlations between BAO and further afield sites such as rural Weld County and east Aurora. Variability of O₃ abundances is also similar at BAO as compared to other sites. The standard deviation in maximum hourly O₃ mixing ratios at BAO (10.5 ppbv) also falls very close to the median standard deviation (9.9 ppbv) of all locations and it is within the range of standard deviations (5.5 – 12.2 ppbv) at other Front Range locations.

3.1.2 OZONE AND PANS

APNs are secondary species produced by the reaction of VOC oxidation products and NO₂. APNs are lost via thermal decomposition, reaction with OH, and dry deposition; the total lifetime can be less than a day in the summer mid-latitude boundary layer. The strong relationship between APN lifetime and temperature is partially responsible for the positive relationship between O₃ and temperature (Sillman and Samson, 1995). PAN is considered to be an excellent tracer of photochemical activity because it is not emitted and it has a low background (Fischer et al., 2014). APN species at BAO have already been shown to be a good

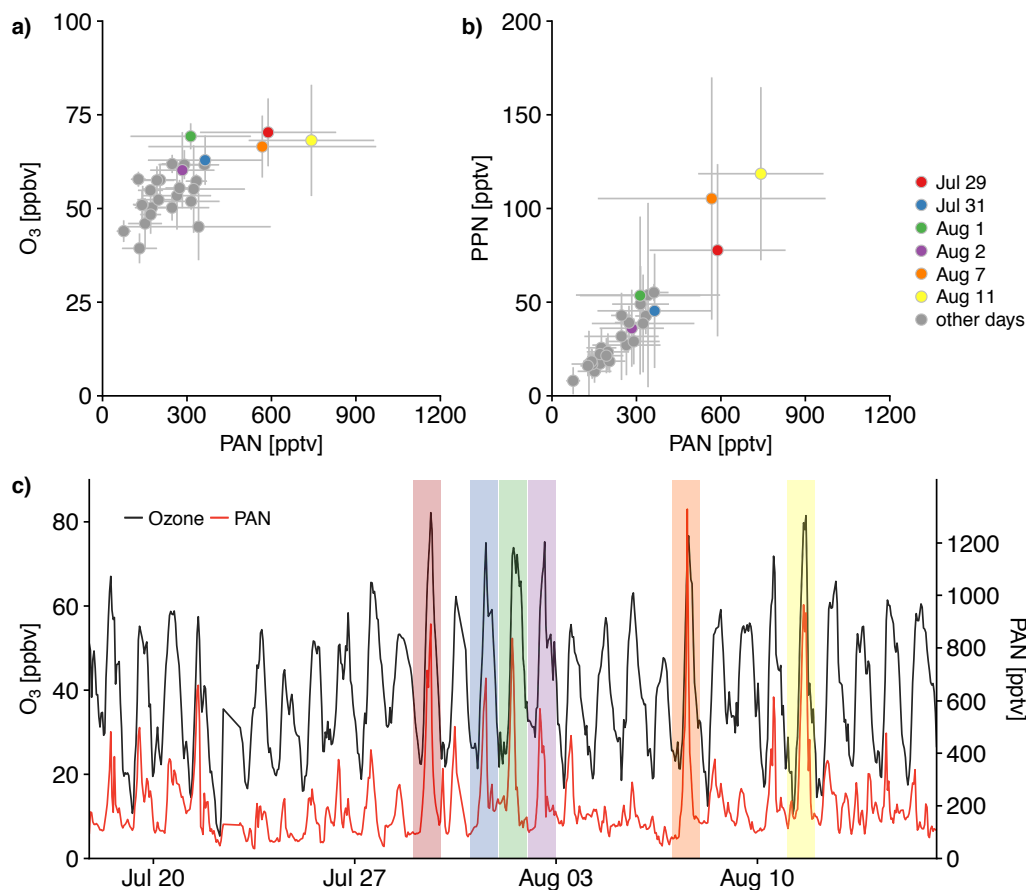


Figure 4. Relationship between O₃ and PAN (a), and PPN and PAN (b). Points represent afternoon (12pm – 6pm MDT) average mixing ratios for each day during the study period. Error bars indicate +/- 1 standard deviation. c) Time series of O₃ in black and PAN in red. The colors of the rectangular shading denote the corresponding days in panels a) and b).

tracer of local photochemistry (Zaragoza et al., 2017). Conversely, periods of elevated O₃ driven by long-range transport or a large contribution of O₃ from the upper troposphere in 2014 were not found to be associated with elevated APNs (Zaragoza et al., 2017). We do not find any days in our study period that display evidence of long-range transport or stratospheric intrusion. Significant periods during our measurement campaign were influenced by wildfire smoke (Lindaas et al., 2017), including several days with high O₃, but these periods are not included this analysis.

Similar to prior measurements at BAO and other locations, Figure 4a shows a positive relationship ($R^2 = 0.51$) between daily average (12PM – 6PM MDT) O_3 and PAN mixing ratios over the study period. Zaragoza et al. (2017) also found a strong relationship between PPN and PAN, and Figure 4b indicates a similar strong relationship during summer 2015 ($R^2 = 0.93$). The ratio of PPN to PAN can tell us about the precursors that dominated the secondary production preceding a given measurement (Roberts et al., 1998). Zaragoza et al. (2017) hypothesized that PPN/PAN ratios > 0.15 were indicative of alkane dominated photochemistry in the Front Range, and we discuss this further in later sections. Figure 4c presents the time series of hourly average

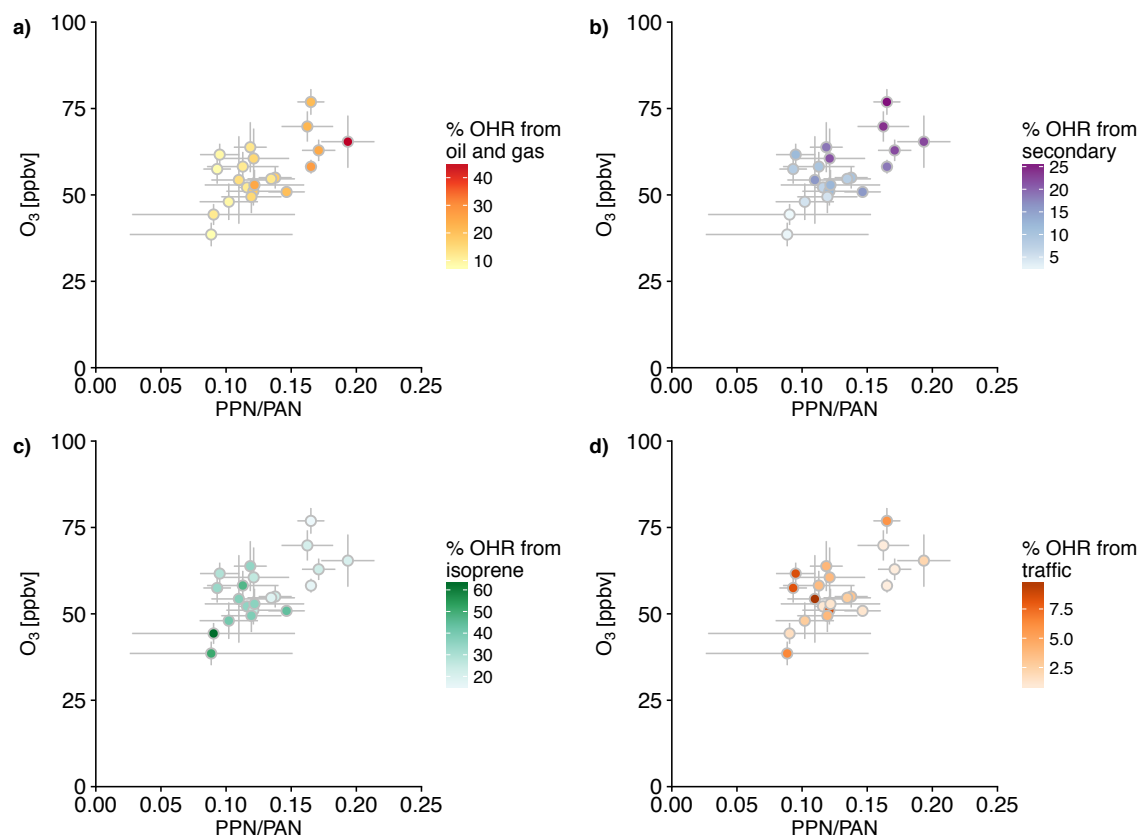


Figure 5. Afternoon (12PM – 6PM MDT) average O_3 mixing ratios versus the ratio of PPN to PAN at BAO for each day during the study period. Error bars indicate ± 1 standard deviation. Points are colored by a) the percentage of total calculated OH reactivity (OHR) from the oil and natural gas PMF factor, b) the percentage of total calculated OH reactivity from the secondary PMF factor, c) the percentage of total calculated OH reactivity from the biogenic PMF factor, which consists exclusively of isoprene, and d) the percentage of total calculated OH reactivity from the traffic PMF factor.

O₃ and PAN mixing ratios for summer 2015. The shaded colors designate six days with the highest maximum hourly average O₃ abundances. These same colors are used to denote the corresponding points in panels 4a and 4b. These six days are not only among the days with the highest daily average O₃, they also are associated with hourly PAN mixing ratios > 500 pptv. Similar to the observations from summer 2014 (Zaragoza et al., 2017), we again find that MPAN is closely correlated with PAN ($R^2 = 0.69$) and PPN ($R^2 = 0.72$) as well, but the absolute mixing ratios we observe (afternoon mean = 8.3 pptv) are very low compared to other regions such as the southeastern or northeastern U.S. with larger isoprene emissions (*e.g.*, Roberts et al., 1998; Roberts et al., 2003; Roberts et al., 2007).

3.1.3 OZONE, PPN/PAN AND VOC

We observe a positive relationship between daily average (12PM – 6PM MDT) O₃ mixing ratios and the ratio of PPN/PAN ($R^2 = 0.41$; Figure 5), suggesting that there is increasing influence from PPN precursors when O₃ abundances are higher in the Front Range. The colors in Figure 5 designate the percentage of total calculated VOC OH reactivity (OHR) from various PMF VOC factors identified by Abeleira et al. (2017) (see section 2.3). This percentage is calculated as the sum of OHR for individual species in the factor divided by the summed OHR across all species in all factors. Figure 5a shows that when the PPN/PAN ratio is high, the percentage contribution of oil and gas OHR to total OHR is also high. Conversely, Figure 5c shows that when PPN/PAN is low, the percentage contribution of biogenic species (largely isoprene) to OHR is high. The ratio of MPAN/PAN is also anti-correlated with O₃, following the same pattern as the percentage of biogenic OHR. As expected, other secondary species such as alkyl nitrates that are included in the secondary factor are positively correlated with PPN/PAN

(Figure 5b). Lastly, the percentage of OHR attributed to traffic shows no relationship with PPN/PAN, and is consistently below 10% of the total estimated OHR (Figure 5d).

While these observations support the conclusion that oil and gas emissions make an important contribution to high O₃ abundances at BAO, it is clear that the variability in PPN/PAN and OHR from the oil and gas factor do not explain all of the variability in O₃ mixing ratios. Meteorological factors such as temperature, relative humidity, and stagnation events have been shown to drive variability on multiple time scales in the NFRMA (Reddy and Pfister, 2016) and other regions (*e.g.*, Jacob et al., 1993; Sillman and Samson, 1995; Camalier et al., 2007). We do not find a relationship between mean afternoon air temperatures or mean afternoon relative humidity measured at BAO and mean afternoon O₃ abundances during our time period. We do, however, find a negative relationship between mean afternoon wind speed and mean afternoon O₃ ($R^2 = 0.52$), such that lower wind speeds are linked to high O₃ and vice versa. These low wind speed days likely exhibit lower ventilation or stagnation. This relationship is strong enough to explain some of the variability unexplained by PPN/PAN. This is not necessarily inconsistent with our inferences based on atmospheric composition made above; under more calm conditions emissions would have time to build up and react, increasing the potential for oil and gas emissions to contribute to O₃ production.

Another variable that may contribute to variability in measured surface mean afternoon O₃ is the residual O₃ from the previous day. O₃ produced during the previous day persists in the residual layer and can be entrained into the planetary boundary layer the next day as it develops. This residual O₃ will then influence the “starting” mixing ratio as O₃ production begins. There can be considerable variability in this residual O₃ (McDuffie et al., 2016), but without coincident O₃ LIDAR measurements at BAO such as those during summer 2014 (Wang et al., 2017) it is

difficult to estimate. Thus, we acknowledge this as a source of variability, but we lack the tools to effectively separate out the O₃ production from the current day from the residual O₃ component.

There are several possible complications to using the mean afternoon estimated PMF factor percentage contributions to total OHR (i.e. VOC measurements made at the same time as O₃ and APNs) as the basis for supporting the conclusions reached by the APN and O₃ relationship analysis. First, APN species and O₃ are produced concurrently in the air mass as it is transported to BAO and reflect the chemistry influenced by the same mixtures, while the VOCs measured in the afternoon may represent different mixtures from those that influenced earlier photochemistry. A possible method for addressing this potential issue could be to use VOC measurements from earlier in the day. However, in that case one must assume that the earlier measurements represent the same air mass and the same emission sources as the air mass measured in the afternoon. We know that there is considerable recirculation in the NFRMA, and that complex circulation patterns are common (Sullivan et al., 2016; Vu et al., 2016). Thus, this assumption may not be valid. A more conservative assumption is that the coincident afternoon VOC mixture reflects the same mixture that produced O₃ and APNs, though short-lived species may no longer be present.

Very short-lived VOCs may contribute to the photochemistry of the air masses en route to BAO, but these VOCs may not have been quantified at BAO because they were also consumed en route. For example, isoprene has a lifetime on the order of an hour (for [OH] = 10⁶ molec. cm⁻³) and a light and temperature dependent emission rate (Guenther et al., 2006). Isoprene could have been emitted into an air mass en route to BAO, but may have been oxidized before the air mass reaches BAO. However, the very low MPAN abundances observed at BAO

do not support the hypothesis that isoprene abundances are large in the region on our days of interest.

Our inference that oil and gas emissions significantly influence high O₃ mixing ratios at BAO is consistent with other recent research. McDuffie et al. (2016) combined observations from two summers (2012 and 2014) at BAO and employed the MCM box model to estimate the average contribution of oil and gas emissions to O₃ production in summer 2014. They found that oil and gas emissions are responsible for about 17% of average local O₃ production at BAO. Evans and Helmig (2017) partitioned O₃ measurements made over four years (2009 - 2012) at two Front Range locations by wind direction and observed that a majority of elevated O₃ measurements were characterized by transport from areas with large oil and gas emissions. Cheadle et al. (2017) used measurements from three individual days in Greeley as case studies to show that a larger abundance of oil and gas related species is correlated with higher O₃ mixing ratios. And lastly, regional chemical transport modeling conducted by NCAR as a follow up to the Front Range Air Pollution and Photochemistry Experiment (FRAPPÉ) indicate that oil and gas and traffic emissions generally make the largest contributions to local O₃ production during summer 2014 in the NFRMA (Pfister et al., 2017a).

3.2 INSIGHTS FROM IDEALIZED MODELING

Section 3.1 shows empirically that O₃ mixing ratios at BAO are positively correlated with coincident measurements of PAN mixing ratios and PPN/PAN ratios. These results suggest that anthropogenic precursors, specifically those from oil and gas development, play an important role in O₃ production in the NFRMA during periods with the most elevated O₃. Though Abeleira et al. (2017) show that biogenic isoprene was a large temperature-dependent component of VOC reactivity in summer 2015 at BAO, Figure 5 indicates that the proportion of OHR attributed to

isoprene is negatively correlated with O_3 . In this section, we turn to two groups of idealized box model experiments to gain insight into the mechanisms behind these empirical observations.

Compared to the baseline simulation initialized with the median value of every measured VOC, the high oil and gas simulations as well as the high initial biogenic simulations produce more O_3 at every NO_x scaling factor (panel a) in Figure 6, with the high oil and gas set of simulations producing the most O_3 . Full details of these simulations are described in Section 2.4 and all input parameters are provided in Table 1. In the empirical analysis outlined in Section 3.1.2 and 3.2.3, O_3 and the PPN/PAN ratio are positively related (Figure 5). The simulation that includes isoprene emissions produces more O_3 , but shifts the PPN/PAN ratio down, toward more PAN production. This pattern is inconsistent with the observations, which consistently shows that the MPAN/PAN ratio and the amount of isoprene are lower during high O_3 events at BAO in summer 2015 compared to low O_3 periods. Conversely, the simulation that has greater initial influence from oil and gas VOCs both produces more O_3 and maintains a higher PPN/PAN ratio compared to the baseline. The percentage of OHR attributed to oil and gas VOCs in this

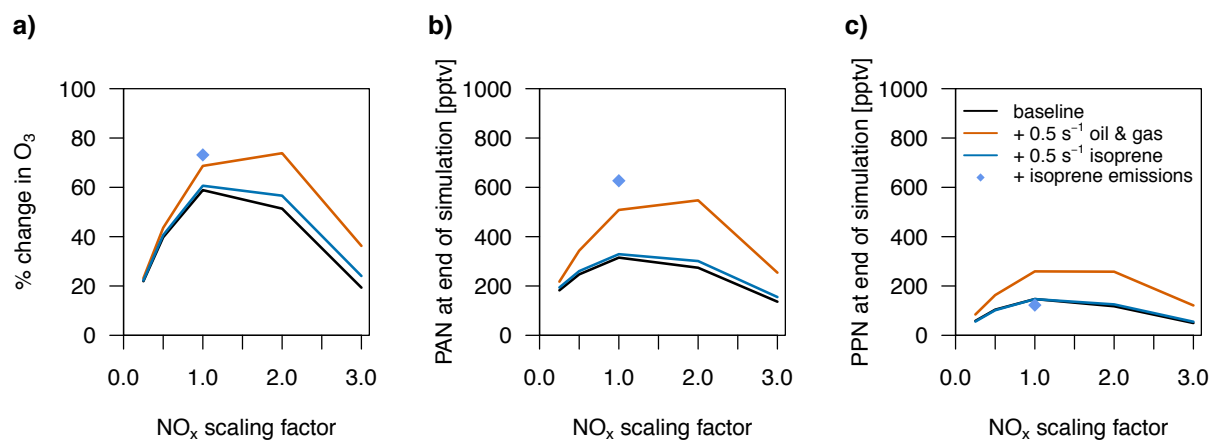


Figure 6. Results from the first set of BOXMOX simulations. The x-axis in each plot is the scaling factor by which the initial conditions and emissions of NO and NO_2 were multiplied for each simulation and each mixture. a) The percent change in the mixing ratio of O_3 between the end of the simulation and the initial value. b) The mixing ratio of PAN at the end of the simulation. c) The mixing ratio of PPN at the end of the simulation.

simulation is also more similar to the observed percentage of oil and gas VOC OHR during observed high O₃ mixing ratios at BAO in summer 2015 than the baseline mixture. Of the mixtures we tested with BOXMOX, the high oil and gas influenced mixture appears to be the closest analog to the observations during high O₃ events at BAO in summer 2015.

To assess the percentage contribution of each VOC factor to O₃ production in each simulation we employ a local first-order sensitivity analysis, similar to that performed by Jin et al. (2008) in their investigation of a local high O₃ episode in the central valley of California. In this sensitivity analysis the initial mixing ratios of each group of VOCs as well as CO and CH₄ are

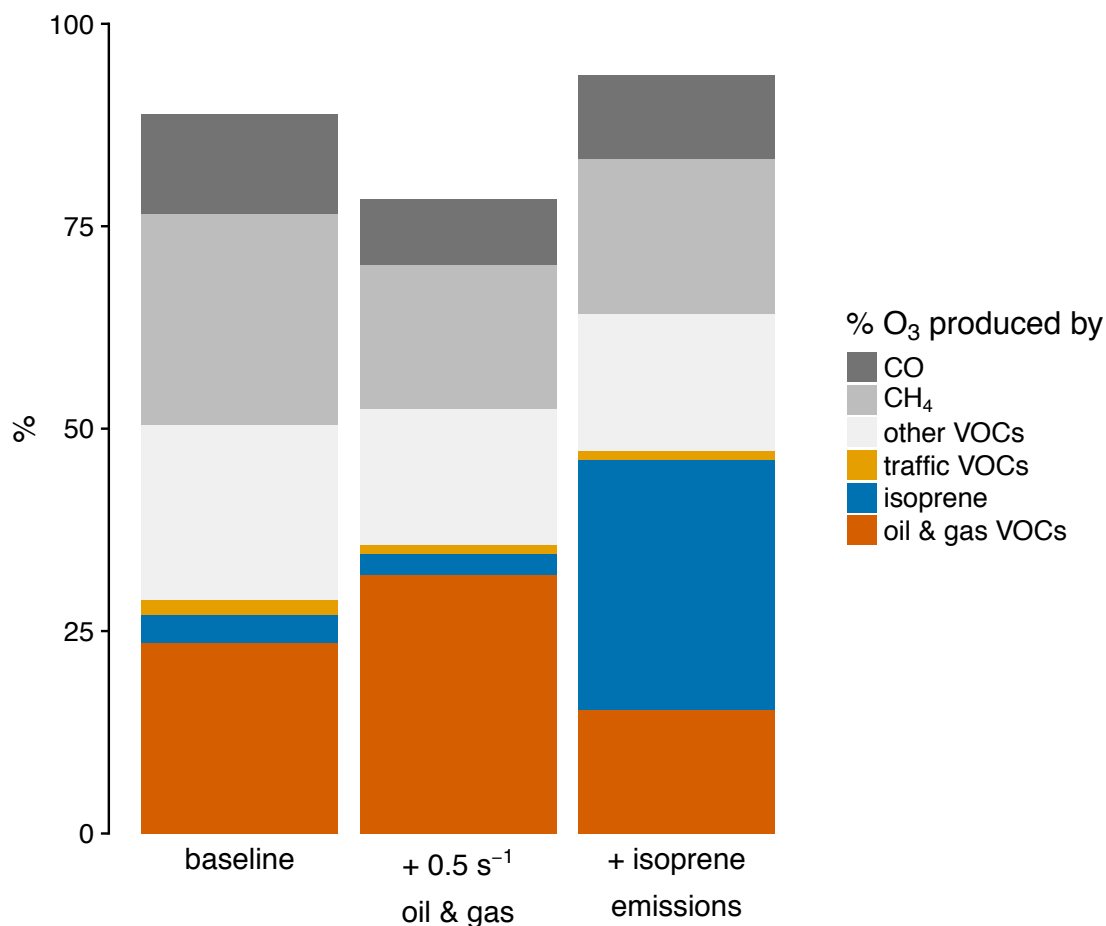


Figure 7. Percentage contribution to O₃ production by group of hydrocarbon for three mixtures simulated at a NO_x scaling factor of 1.

perturbed by -10% in separate additional simulations. The difference in O₃ abundances between each sensitivity simulation and the original simulation is calculated and multiplied by 10 to approximate the total contribution of that group of VOCs (or CO or CH₄) to the overall O₃ production in the original simulation. This linearization of the effect is subject to small errors given the nonlinearity of O₃ chemistry and the potential for interactions between species, but we achieve greater than 85% closure of the total O₃ production for every simulation. Thus, this local first-order sensitivity analysis is a reasonable approximation of the contribution of each VOC factor to O₃ production in each simulation.

Figure 7 presents the results of this sensitivity analysis for 3 mixtures at a NO_x scaling factor of 1: the baseline, the high oil and gas influenced mixture, and the mixture with isoprene emissions. These mixtures are displayed to highlight the range of percentage contributions attributable to oil and gas sources and to isoprene. As expected, the two mixtures with larger abundances of oil and gas VOCs or isoprene display larger percentage contributions to O₃ production for those respective groups of species. However, Traffic VOCs make only a small contribution to O₃ production (< 2%) in all simulations (excepting the unrealistic high traffic mixture), which is consistent with the empirical observation of low overall percentage contributions of traffic VOCs to measured VOC OHR. CO and CH₄ make significant contributions to O₃ production (8-12% and 17-26% respectively) in all simulations, which reflects the combination of contributions from background abundances and their relatively high local enhancements in the NFRMA. The mixture dominated by isoprene emissions shows a large contribution from isoprene to O₃ production (~30%), although for the reasons discussed earlier in this section this mixture is not representative of the observed mixtures during high O₃ events at BAO in summer 2015. We consider this mixture to represent a lower bound (15%) for the

contribution of oil and gas VOCs to O₃ production. More reasonable estimates from the baseline and high oil and gas mixtures are 23% and 31%. Given that the high oil and gas mixture most closely represents the observed mixture of VOCs associated with high O₃ mixing ratios (> 70 ppbv), we suggest that ONG VOCs contribute at least 30% of the O₃ production during high O₃ events at BAO in summer 2015. We expect these estimates could actually be a lower bound given that full closure of O₃ production was not fully achieved by this sensitivity analysis and that the “other VOCs” category includes species such as benzene and MEK, which have oil and gas sources or precursors. For instance the largest precursor of MEK in the Front Range is likely n-butane, which is largely emitted from the oil and gas sector. Additionally, some fraction of the locally emitted CH₄ is from oil and gas sources. Given that these species have other sources as well, they were not lumped with the group of VOCs we used to represent VOCs largely from oil and gas operations in the region.

O₃ is only formed in the troposphere from the photolysis of NO₂ (Monks et al., 2015). The rate of formation of NO₂, largely from the reaction of NO with HO₂ or peroxy radicals (RO₂), is considered to be the rate-limiting step in the production of tropospheric O₃. RO₂ species have different parent VOCs, meaning that the relative abundance of certain RO₂ species can offer insight into which parent VOCs are contributing the most to the rate-limiting step in O₃ production. To investigate this, we calculate the relative contribution of different reaction pathways to the formation of NO₂ (and thereby O₃) by tagging RO₂ species according to their precursors and then aggregating the rate at which they produce NO₂ by PMF factor. In this way, we can use RO₂ radicals as a lens into the contribution of different VOCs to O₃ production in our simulations in addition to the first-order sensitivity analysis.

For each VOC associated with a given factor (oil and gas, traffic, or biogenic) we identify every RO₂ produced during the oxidation of that group of VOCs. RO₂ radicals that react with NO to produce NO₂ were then combined into one of 5 categories: 1) RO₂ radicals that are formed solely from the precursors largely associated with oil and gas activities, 2) RO₂ radicals that are only produced from isoprene oxidation, 3) RO₂ radicals that are only produced from the oxidation of traffic-related precursors, 4) RO₂ radicals that are formed in the oxidation of VOCs

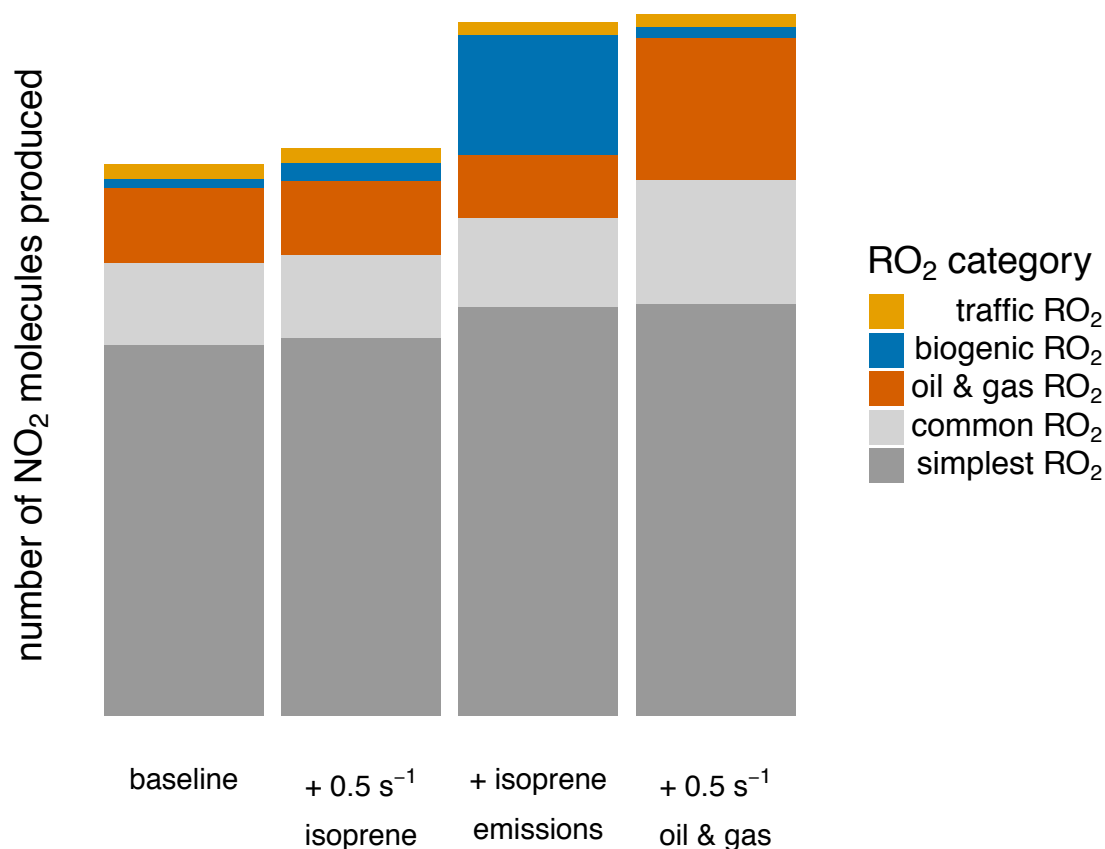


Figure 8. For four mixtures in the first group of BOXMOX simulations, this figure shows the sum of the RO₂ reactions that generate NO₂, broken down by the precursor category of the RO₂ radical. Traffic, biogenic, and oil and gas RO₂ categories include RO₂ radicals that are solely products of parent species within each representative group of VOCs. Common RO₂ radicals include those with precursors from multiple categories, and the simplest RO₂ radicals include the methyl-, ethyl-, and acetyl- peroxy radicals, which are the most abundant common products of all the factors.

not exclusive to one of the factors (i.e. they are commonly produced), and 5) the three simplest RO₂ radicals (methyl peroxy, acetyl peroxy, and ethyl peroxy radicals), which are often the most abundant RO₂ radicals and are produced by all of our three target precursor classes. Thus, we have classified all the RO₂ in the simulations into five groups named: oil and gas RO₂, biogenic RO₂, traffic RO₂, common RO₂, and the simplest RO₂. To calculate the rate of production of NO₂, and therefore gross O₃ production, we multiply the individual concentration of each RO₂ species in a given group by the concentration of NO and the rate constant for each time step. Lastly, we aggregate the results across all RO₂ species in the group and across all time steps in the simulation. The final product is the aggregated contribution of a given set of representative VOCs to the total gross production of NO₂, and by extension O₃, for a given simulation.

Figure 8 displays the results of this RO₂ categorization and calculation of total NO₂ production for the set of simulations with a NO_x scaling factor of 1. The high oil and gas mixture produces more RO₂ radicals specific to oil and gas as compared to the baseline simulation, and the same pattern holds true for the mixtures with greater influence from isoprene. The high oil and gas mixture also produces more NO₂ in general than the other mixtures, and proportionately more simple and common RO₂ as well. Thus simulations based on the suite of VOCs quantified at BAO in 2015 show that for a given starting initial OHR, VOCs from oil and gas sources lead to greater RO₂ radical production. Even though most of the individual trace gases associated with the oil and gas activities (i.e. alkanes) have relatively low initial OHR, the abundance of RO₂ radicals from the oil and gas activities is likely large. VOCs associated with the oil and gas activities provide abundant opportunities to recycle NO_x through RO₂ production at multiple stages of oxidation.

We present a second group of simple single-precursor simulations to again compare with the empirical conclusions. This set of three simple simulations controls for the initial OH reactivity, set at 2 s^{-1} , and is initialized with either 100% of the OH reactivity apportioned as isoprene (i.e. solely biogenic; “100% isoprene”), 100% of the OH reactivity apportioned as propane (i.e. solely oil and gas; “100% propane”), or an even mix of the two species with respect to the OH reactivity apportioned to each (“even_mix”). We again use a NO_x scaling factor of 1 for these simulations. Full simulation specifications are described in Chapter 2 and in Table 1.

Figure 9 shows the results from these simulations, and these figures show the change in O_3 and the ratio of PPN to PAN as a function of the percentage of initial OH reactivity associated with propane. Propane in the NFRMA is primarily associated with emissions from oil and natural gas operations (Gilman et al., 2013; Abeleira et al., 2017), and most of the VOC species in the oil and gas PMF factor from Abeleira et al. (2017) are alkanes. As the propane (i.e. alkane) contribution to initial OHR increases, O_3 and PPN/PAN ratio increase. These results are

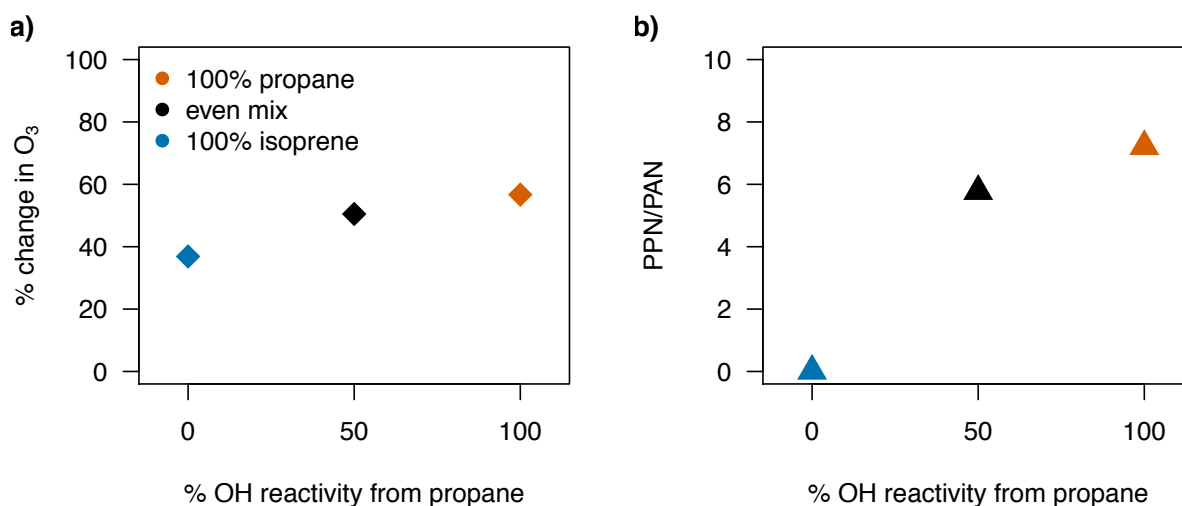


Figure 9. Results from the second set of BOXMOX simulations. Each mixture has an initial OH reactivity of 2 s^{-1} , and is initialized with either 100% of this initial reactivity in the form of isoprene or propane, or with the OH reactivity being divided evenly between each species. The x-axis in both plots is the percentage of OH reactivity from propane. Panel a) displays the percent change in the mixing ratio of O_3 between the beginning and the end of the simulation, and b) shows the final ratio of PPN to PAN at the end of the simulation.

consistent with the results of the first group of more complex simulations as well as the empirical results in Section 3.1.

Figure 10 displays the results of the calculation of gross NO_2 production for the second group of simulations via the same RO_2 categorization method used for the first group. As the contribution from propane to the mixture increases from left to right, the number of oil and gas RO_2 reactions rises along with the number of more complex common RO_2 radicals, while the total number of the simplest RO_2 steadily decreases. These results are in line with the hypothesis put forward stating that oil and gas species recycle more NO to NO_2 , and therefore produce more

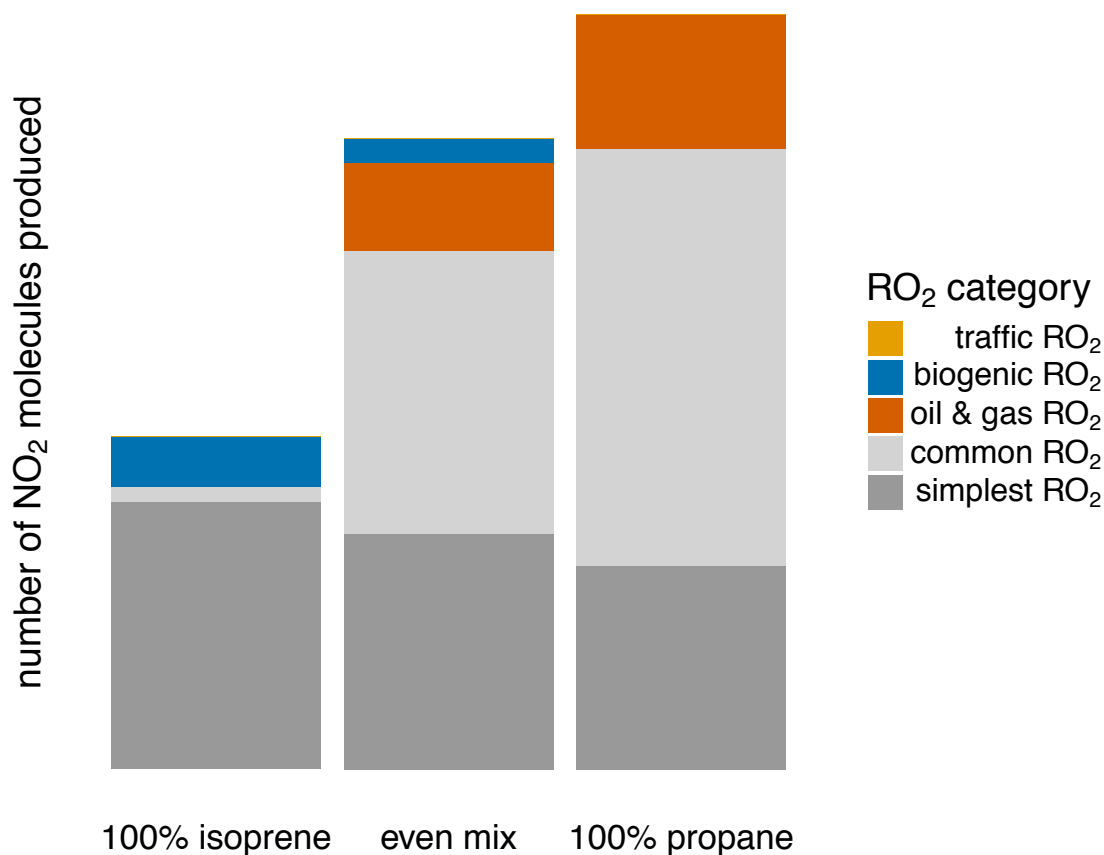


Figure 10. For each mixture in the second group of BOXMOX simulations, this figure shows the sum of the RO_2 reactions that generate NO_2 , broken down by the precursor category of the RO_2 radical. Traffic, biogenic, and oil and gas RO_2 categories include RO_2 radicals that are solely products of parent species within each respective PMF factor. Common RO_2 radicals include those with precursors from multiple categories, and the simplest RO_2 radicals include the methyl-, ethyl-, and acetyl- peroxy radicals, which are the most abundant common products of all the factors.

O₃. This occurs despite their lower initial rates of reaction with OH. Our results reaffirm the idea that OHR alone cannot be used to understand the contribution of different VOCs to gross O₃ production because this metric only provides insight into the initial step of oxidation, and does not reflect either the catalytic nature of O₃ production or the radical termination steps.

The observations from BAO show that the highest O₃ mixing ratios are also associated with the largest PPN/PAN ratios. Surface and aircraft observations during the summer 2014 FRAPPÉ field campaign produced similar relationships (Zaragoza et al., 2017). We can use the BOXMOX simulations to investigate which species are the most dominant PPN precursors. As discussed above, nearly any VOC can serve as a precursor to PAN, though the yields vary widely (Roberts, 2008; Fischer et al., 2014). In contrast, propanal is the main oxidation intermediate for PPN (Roberts et al., 2001; Roberts et al., 2007). We test the sensitivity of PPN and PAN formation to a series of perturbations to individual precursors using the baseline simulation with a NO_x scaling factor of 1. We tested the sensitivity of PPN and PAN production to the full set of possible PPN precursors that were measured during the summer 2015 field campaign at BAO using a final set of simulations where the initial mixing ratio for each species was individually increased by 10%. All other precursors were set to the median mixing ratio observed during the campaign (the same as the baseline simulation). We find that propane and n-pentane are the dominant precursors for PPN in our simulations. Given that alkanes are attributed primarily to oil and gas activities in the NFRMA, these sensitivity results support the hypothesis that alkane emissions from oil and gas activities dominate the production of PPN and PAN in the NFRMA and are responsible for periods with high (> 0.15) PPN/PAN ratios reported here and in Zaragoza et al. (2017). Results from these sensitivity tests are presented in Appendix A (Figures A1 and A2).

CHAPTER 4: CHANGES IN OZONE AND PRECURSORS DURING TWO AGED WILDFIRE SMOKE EVENTS IN THE COLORADO FRONT RANGE IN SUMMER 2015³

4.1 CO, CH₄, AND VOC ABUNDANCES

We quantified CO, CH₄, and 40+ VOC species including C₂-C₁₀ non-methane hydrocarbons (NMHCs), C₁-C₂ halocarbons, and several oxygenated species (methyl ethyl ketone, acetone, and acetaldehyde) at BAO. The focus of the BAO field intensive was to study the photochemistry of local emissions from oil and gas development (*e.g.* Gilman et al., 2013; Swarthout et al., 2013; Thompson et al., 2014; Abeleira et al., 2017), and the GC system was not set up to quantify species with known large biomass burning emission ratios (*e.g.* hydrogen cyanide, acetonitrile, most oxygenated organic species) (Akagi et al., 2011). The system did not have a mass spectrometer on-line, and the calibration standards did not contain HCN and acetonitrile, thus the detection of these species was not possible. In addition, early campaign issues with the on-line multichannel gas chromatography system compromised the data for the July smoke period and thus we restrict our comparison of VOCs in smoke-free versus smoke-impacted periods to a comparison between 16 – 30 August, the *August smoke-impacted period*, and 24 July – 16 August, the *smoke-free period*. The brief smoke-free times during 16 – 30 August (denoted by white between the red shading in Figure 2) were not included in either period since it is difficult to determine whether they were smoke-impacted. GC measurements were made approximately every 45 minutes and we compared 251 measurements of VOCs during the August smoke-period to 583 measurements during the smoke-free period. A statistical summary of all VOC measurements for each period is available in Table 4 in Appendix B.

³ This chapter contains published work. Citation: Lindaas, J., Farmer, D. K., Pollack, I. B., Abeleira, A., Flocke, F., Roscioli, R., Herndon, S., and Fischer, E. V.: Changes in ozone and precursors during two aged wildfire smoke events in the Colorado Front Range in summer 2015, *Atmos. Chem. Phys.*, 17, 10691-10707, 10.5194/acp-17-10691-2017, 2017.

In this section, we describe significant changes in VOC abundances and notable exceptions. The HYSPLIT trajectories (Figure 3) suggest that the age of the smoke impacting the Front Range during the August smoke-period was 2-3 days. We observed enhancements in the abundances of CO, CH₄, and VOCs with lifetimes longer than the transport time of the smoke, with the exception of some alkanes that have a large background concentration in the Front Range due to emissions from oil and gas production. Three of the alkenes we quantified (isoprene, ethene, and propene) were generally near the limit of detection during the August smoke-impacted period, although notably cis-2-butene abundances were not changed. Significant differences were not observed in the four oxygenated VOCs quantified between smoke-impacted and smoke-free periods.

Mean hourly CO mixing ratios were significantly enhanced by 223 ppbv, or 170% during the July smoke-impacted period and by 92 ppbv, or 70%, during the August smoke-impacted period (Figure 2). This enhancement was present across the diurnal cycle (Figure 11) and both smoke periods displayed a higher range of CO mixing ratios (July: 127 – 639 ppbv, August: 101 – 529 ppbv, smoke-free: 72 – 578 ppbv). The two smoke periods differed in their sources fires, length, and meteorology, with higher average CO and PM_{2.5} measurements in the July smoke period (Figure 2). Average enhancements of CH₄ were similar for both periods (July: 52 ppbv, August: 50 ppbv, or ~ 2.5% increase). Methane has a relatively high background at BAO due to large emissions of CH₄ in nearby Weld County from livestock production and oil and gas development (Pétron et al., 2014; Townsend-Small et al., 2016). Taken together, the larger background of CH₄ and the large local sources of CH₄ in the Front Range served to mute the impact of the August smoke on overall CH₄ abundances. The diurnal cycle of CH₄ did not change during the smoke-impacted period as compared to the smoke-free period and we

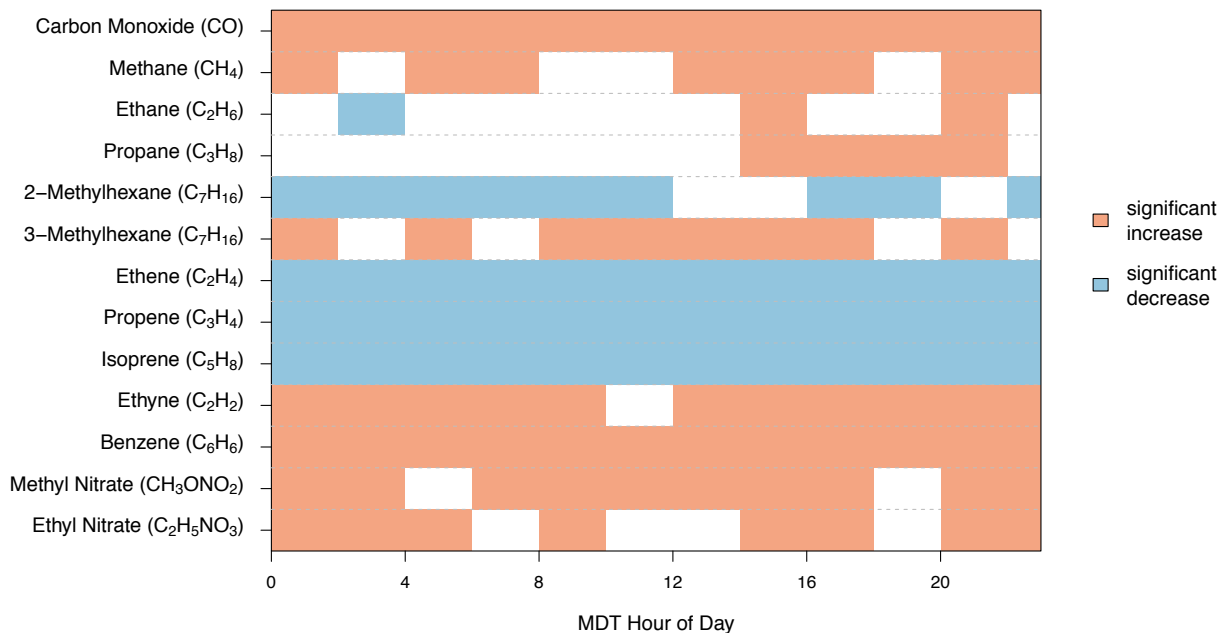


Figure 11. Significant changes (two sided Student’s t-test, 90% confidence interval) in hourly averaged mixing ratios of a subset of species measured at BAO between smoke-free periods and the 16 - 30 August smoke period. Significant increases during smoke-impacted periods compared to smoke-free periods are shown in red, significant decreases are in blue.

observed a similar range of mixing ratios (~1,840 – 3,360 ppbv) in the both smoke-free and smoke-impacted periods. We note several large spikes in CH_4 on the order of minutes during the August smoke-impacted period, but we do not believe that these are related to the presence of smoke because they were not correlated with similar excursions in CO and PANs, and exhibited strong correlations with propane and other tracers of oil and gas and other anthropogenic activity. Due to the availability of valid data, the rest of the discussion on VOC composition will focus on changes during the August smoke-impacted period.

Similar to CO, ethane has an atmospheric lifetime on the order of a month during summertime at mid-latitudes (Rudolph and Ehhalt, 1981) and is emitted by wildfires (Akagi et al., 2011). However, average ethane mixing ratios were not higher during the August smoke-impacted period compared to the smoke-free period. One potential reason for this may be the

large local sources of alkanes from oil and natural gas activities within the Denver-Julesberg Basin which contribute to relatively high local mixing ratios of these species (Gilman et al., 2013; Swarthout et al., 2013; Thompson et al., 2014; Abeleira et al., 2017). The range of ethane mixing ratios observed at BAO was also not different between smoke-free (0.3 - 337 ppbv) and smoke-impacted periods (1 - 362 ppbv). Similarly, we did not observe significant changes in most of the C₃-C₉ alkanes we measured. Figure 11 shows there were two exceptions to the general alkane observations: 2-methylhexane showed a significant decrease in average abundances (-39 pptv or -45%) and 3-methylhexane showed a significant increase (63 pptv or 75%) during the smoke-impacted period, despite both having similar smoke-free abundances and similar rate constants for reaction with the hydroxyl radical (OH; $k_{\text{OH}} \sim 7 \times 10^{12} \text{ cm}^3 \text{ molec}^{-1} \text{ s}^{-1}$).

Table 2. Summary of alkene statistics at the Boulder Atmospheric Observatory during the smoke-free period and the August smoke-impacted period in summer 2015.

^a Standard deviation in parentheses

* Indicates statistically significant change in mean during August smoke-impacted period as compared to the smoke-free period

Compound	Smoke-free period (ppbv)				August smoke-impacted period (ppbv)			
	min	median	mean ^a	max	min	median	mean ^a	max
ethene*	0.001	0.2	0.253 (0.212)	1.94	0.001	0.001	0.0464 (0.128)	0.918
propene*	0.002	0.041	0.051 (0.04)	0.41	0.002	0.008	0.011 (0.012)	0.086
cis-2-butene	0.001	0.018	0.0236 (0.0292)	0.345	0.001	0.014	0.023 (0.07)	1.08
isoprene*	0.003	0.141	0.223 (0.268)	2.02	0.001	0.048	0.0804 (0.114)	1.16

The atmospheric lifetimes of the four alkenes we quantified (isoprene, propene, ethene, and cis-2-butene) range from tens of minutes to hours. Surprisingly, we observed significant decreases in the abundance of isoprene, propene, and ethene during the August smoke-impacted period compared to the smoke-free period: -64% (-143 pptv), -77% (-39 pptv), and -81% (-206 pptv) respectively (for summary statistics see Table 2). The shape of the diurnal cycles did not change (Figure 20 in Appendix B), though propene and ethene were near their respective limits of detection for the majority of each day during the smoke-impacted period. Given the short

lifetimes of these species, this indicates that the presence of the smoke changed either local anthropogenic or biogenic emissions of these species, or their respective rates of oxidation by OH or O₃. We present several potential mechanisms here, but we do not have sufficient information to determine if one of these is solely responsible for the pattern we observed.

Our first hypothesis is that fewer anthropogenic emissions of these alkenes drove the observed decreases in alkene abundances. However, there is no evidence that anthropogenic emissions were different during the August smoke-impacted period. Specifically, the August smoke-impacted period encompassed both weekdays and weekends and did not contain any state or federal holidays. Therefore we move to our second hypothesis, that changes in the biogenic emissions of alkenes accounted for the decreased alkene mixing ratios. Isoprene is widely known to be emitted by broad leaf vegetation, and emission rates are positively correlated with light and temperature (Guenther et al., 2006). Recent measurements quantified ethene and propene emissions from a ponderosa pine forest near Colorado Springs, CO, with an inter-daily light and temperature dependence similar to isoprene (Rhew et al., 2017b). Interestingly, emissions and mixing ratios of ethene and propene were not closely correlated with isoprene within the diurnal cycle, indicating they have different vegetative/soil sources than isoprene at that site. Ponderosa pine stands are present in the foothills on the western edge of the plains in the Front Range, and several species of broad leaf trees are present along waterways, in urban areas, and in the foothills of this region. Thus, biogenic sources of ethene, propene, and isoprene in the region around BAO are reasonable. Given the August smoke-impacted period was on average colder than the smoke-free period, and potentially saw a reduction in photosynthetic active radiation (PAR) at the surface due to the increased number of aerosols, it is possible that biogenic emissions of isoprene, ethene, and propene were suppressed. However, biogenic fluxes of these

compounds are unavailable for the region around BAO during summer 2015, and extrapolating emissions from one ponderosa pine stand to the rest of the Front Range may be overly ambitious. Further, we note that a positive matrix factorization analysis of the VOC data from this site did produce a ‘biogenic factor’ dominated by isoprene, but with negligible contribution of any other hydrocarbon, suggesting that the biogenic component of these C₂-C₃ alkenes was small (Abeleira et al., 2017). Thus, while the hypothesis that smoke suppressed biogenic emissions remains feasible, we consider other potential causes for the observed decrease in alkene abundances below.

The alkenes we measured all have high reactivities with respect to OH ($> 8 \times 10^{12} \text{ molec}^{-1} \text{ cm}^3 \text{ s}$) and O₃ ($> 0.1 \times 10^{17} \text{ molec}^{-1} \text{ cm}^3 \text{ s}$) (Atkinson and Arey, 2003). Enhancements in OH abundances have been inferred in wildfire smoke plumes by several studies (*e.g.* Akagi et al. (2012); Hobbs et al. (2003); Liu et al. (2016); Yokelson et al. (2009)). If the August smoke-impacted period was characterized by higher than normal OH mixing ratios, then a third hypothesis is that the observed decreases in alkene abundances could be due to a higher oxidation rate by OH due to higher OH concentrations. However, other measured VOCs such as o-xylene or methylcyclohexane have similar OH reactivities to ethene (Atkinson and Arey, 2003), and we do not see associated decreases in abundances of these other VOCs. Thus, the hypothesis of increased oxidation by OH causing decreased alkene abundances in the August smoke period is not supported by the full suite of measurements at BAO.

Lastly, we move on to our final hypothesis. Alkenes have much higher rates of reaction with O₃ than the other VOCs we quantified. As we will demonstrate in Section 4.3, the August smoke-impacted period was characterized by higher O₃ abundances than would otherwise be expected. Therefore, the fourth hypothesis regarding decreased alkene abundances is that

enhanced alkene oxidation by O₃ decreased the observed mixing ratios. Two factors complicate this hypothesis though. First, we do not observe a negative relationship between O₃ and alkene abundance during the smoke-free time periods (i.e. increased O₃ is not correlated with decreased alkenes when no smoke is present). Second, despite having a higher reaction rate with O₃ compared to propene and ethene, *cis*-2-butene does not decrease during the August smoke-impacted period.

After careful consideration, there is no strong evidence supporting any of these four hypotheses over the others (suppressed anthropogenic emissions, suppressed biogenic emissions, increased OH, increased O₃). It is possible that more than one of these processes could have contributed to the observation of decreased alkene abundances during the 2 week-long August smoke-influenced period. Future field campaigns and modeling work are necessary to understand how common suppressed alkene abundances may be in smoke-impacted air masses, and what processes might control this phenomenon.

The only alkyne measured was ethyne. Ethyne is emitted by wildfires (Akagi et al., 2011) and has a lifetime of ~1 month during summer. We observed a significant increase in the abundance of ethyne during the August smoke-impacted period. These enhancements were small in absolute mixing ratio (0.163 ppbv), but represented a large percentage increase (67%) and were consistently present throughout the day.

It is well known that wildfires produce carcinogenic aromatic hydrocarbons including benzene (Fent et al., 2014). During the smoke-impacted periods, we observed significantly enhanced benzene throughout the day with an average increase of 0.117 ppbv and a percentage increase of 67%. These enhancements followed the pattern of CO and ethyne; there were consistent increases throughout the day and the diurnal cycle retained its shape. Wildfires also

produce toluene (Fent et al., 2014); however, it has a substantially shorter lifetime (< 2 days) than benzene (~12 days). Toluene showed no significant changes in its mean mixing ratio, diurnal cycle, or range of values measured at BAO during the smoke-impacted periods. The other aromatic hydrocarbons we quantified (o-xylene and ethyl-benzene) also did not change significantly.

As mentioned in Chapter 1, oxygenated VOCs are emitted by wildfires and make a large contribution to the total emitted VOC mass in wildfire smoke (Stockwell et al., 2015). Additionally they are produced as oxidation intermediates (Atkinson and Arey, 2003). Acetaldehyde, acetone, and methyl ethyl ketone (MEK) showed no consistent changes in their abundances, diurnal cycles, or range during the smoke-impacted period compared to the smoke-free period. Small increases in average acetone (~350 pptv) and MEK (~150 pptv) mixing ratios during late afternoon and evening hours were not statistically significant.

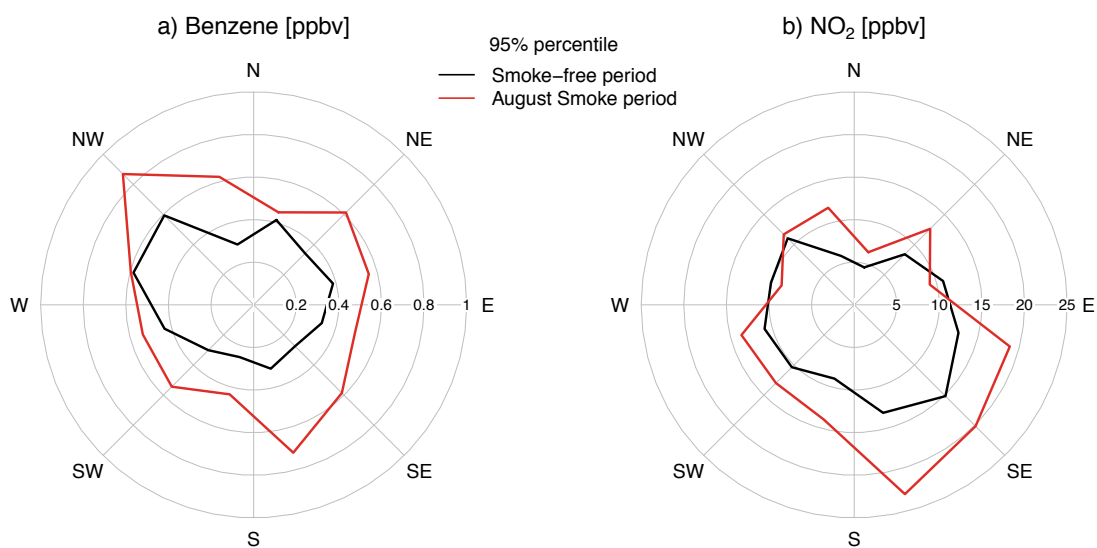


Figure 12. 95th percentiles of all hourly average measurements of a) benzene and b) NO₂ during the smoke-free period (in black) and the August smoke-impacted period (in red), as a function of wind direction.

Given the diversity of emission sources across the northern Colorado Front Range, previous studies of atmospheric composition at BAO have noted a strong dependence of VOC composition on wind direction (Pétron et al., 2012; Gilman et al., 2013). Recent housing development and oil and gas production surrounding the BAO site have made analyses based on wind direction more challenging in recent years (McDuffie et al., 2016). Importantly for our analysis, we found that the statistically significant changes in all species during the smoke-impacted periods occurred across all wind directions. Figure 12 shows this for two representative species: benzene and NO₂. We also did not find statistically significant changes in wind direction or wind speed patterns between smoke-free and smoke-impacted periods. Thus, we attribute the changes in atmospheric composition during the August smoke-impacted period to the presence of smoke.

4.2 REACTIVE OXIDIZED NITROGEN (NO_y) SPECIES

Acyl peroxy nitrates and HNO₃ were successfully measured from 10 July – 7 September and alkyl nitrates were measured from 24 July – 30 August. Thus we report significant changes in these species for the August smoke-impacted period only. We observed significant enhancements in both peroxyacetyl nitrate (PAN) and peroxypropionyl nitrate (PPN) during the August smoke-impacted period. PAN and PPN abundances were consistently elevated across the day by an average of 183 and 22 pptv respectively, corresponding to a ~100% change for both species. The peak of each diurnal cycle was shifted later in the day by about 3-4 hours for the smoke-impacted period. This cannot be accounted for merely by the shift in the timing of solar noon given that the total decrease in daylight between 10 July and 30 August is ~2 hours. The C₁ – C₂ alkyl nitrates measured at BAO exhibited similar behaviors; methyl nitrate and ethyl nitrate saw average enhancements during the August smoke period of 1.2 and 0.77 pptv, 41% and 31%

respectively, though the average mixing ratios of these species are smaller by an order of magnitude compared to other alkyl nitrates quantified. Propyl-, pentyl-, and butyl-nitrate did not display significant changes in their average mixing ratio, though we observed a similar shift in the peak of their diurnal cycles of 2-4 hours. We did not observe significant changes in the abundances of HNO_3 . There were no changes to the diurnal cycle of HNO_3 or the range of mixing ratios observed.

NO and NO_2 measurements were made during the entire campaign, 1 July – 7 September 2015, so both the July and August smoke-impacted periods were analyzed with respect to potential changes in NO_x . NO was present in the same abundances between the two periods and showed the same diurnal cycle during the August smoke-impacted period as compared to the smoke-free period (Figure 13). During the July smoke-impacted period the morning build-up of NO was slower than the smoke-free period, though the mixing ratios were within the range of smoke-free values and the duration of the July smoke-impacted period was much shorter than the August smoke-impacted period.

Figure 13 shows that NO_2 abundances exhibited more significant changes than NO . During the July smoke-impacted period, NO_2 was within the range of smoke-free measurements. In contrast NO_2 during the August smoke-impacted period followed the same diurnal cycle but had pronounced significant increases in average mixing ratios during the morning and evening hours of ~ 8 ppbv (17%) following sunrise and 3 ppbv (60%) following sunset. These enhanced peak abundances appeared during multiple days during the August smoke-impacted period. Out of 7 morning peaks in NO_2 during the August smoke-impacted period, 3 had concurrent toluene and ethyne peaks. One of these days occurred on a weekend, and the others occurred on weekdays. Toluene and ethyne are common tracers of traffic/industrial emissions. However, 4 of

the days did not have corresponding ethyne and toluene peaks. Thus, we can't rule out that traffic did not impact some of the NO_2 enhancements we observed, however there is also likely another contributing mechanism. There are a few potential hypotheses for a non-traffic related NO_2 enhancement during the August smoke period. One hypothesis is that the photolysis frequency

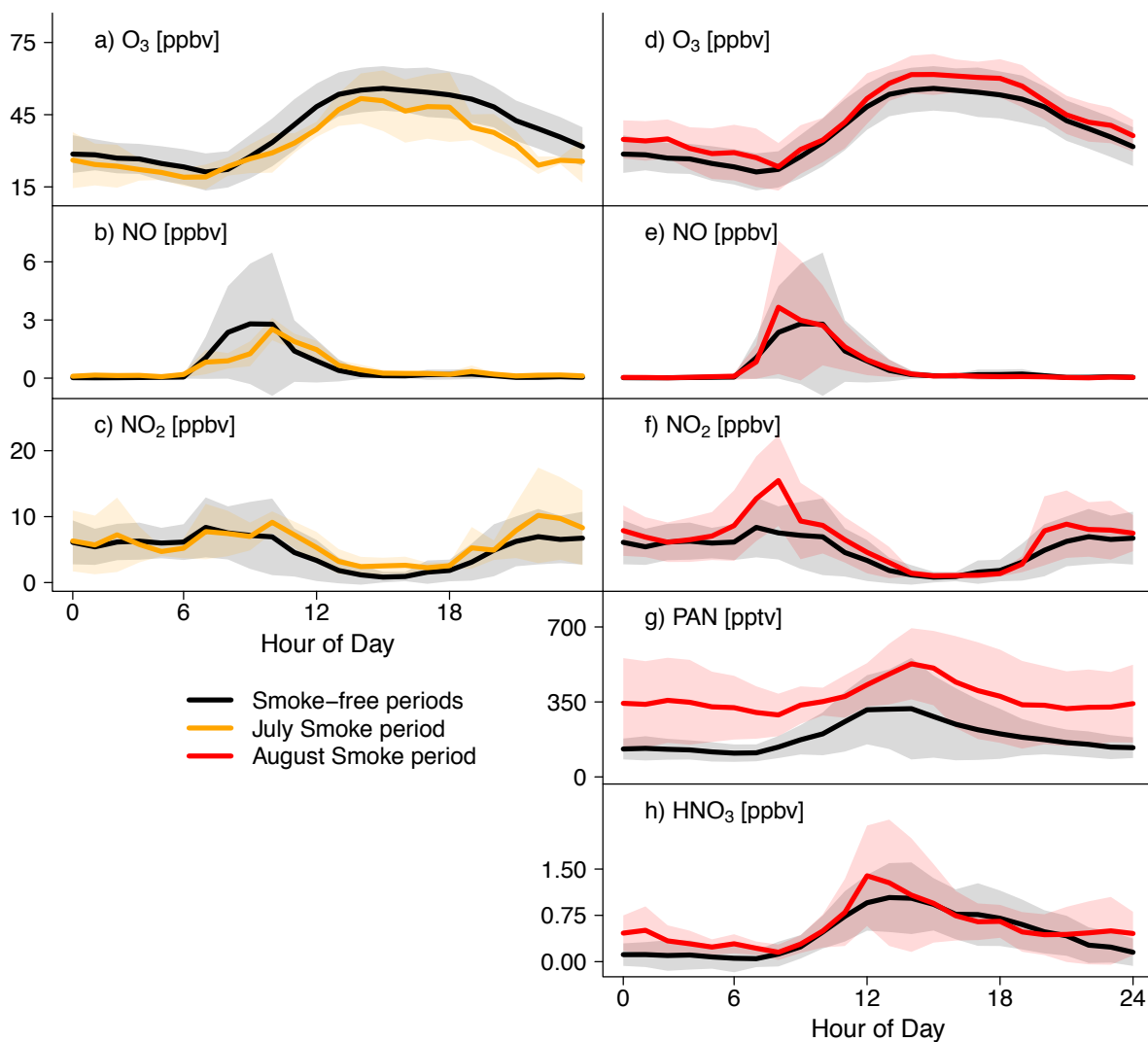


Figure 13. Average diurnal cycles in MDT of O_3 and oxidized reactive nitrogen species at BAO. Panels a), b), and c) compare average diurnal cycles from smoke-free time periods (black) to average diurnal cycles from the July smoke-impacted period (orange). Panels d) – h) show average diurnal cycles during the August smoke-impacted period (red) to the same average diurnal cycles from smoke-free periods (black). Grey, orange, and red shading indicates plus and minus one standard deviation. PAN and HNO_3 measurements were not available during the July smoke-impacted period. Solar noon on 1 July 2015 was at 1:03 PM, solar noon on 7 September 2015 was at 12:57 PM.

(J_{NO_2}) was most impacted (i.e. reduced) by the smoke near sunrise and sunset. Another hypothesis concerns the equilibrium between PAN and NO_2 . The thermal decomposition of PAN can be a source of NO_2 (Singh and Hanst, 1981), but the concurrently observed PAN abundances during the August smoke-impacted period can only account for at most 1 ppbv of additional NO_2 . However, there could have been significantly higher PAN abundances in the smoke plume prior to reaching BAO so this hypothesis for the NO_2 enhancements cannot be fully ruled out. We do not have measurements of other reactive nitrogen species (e.g. HONO, ClNO_2 , NO_3 , and N_2O_5) to test other potential hypotheses for a different chemical mechanism to explain the observed NO_2 enhancements.

4.3 OZONE

As discussed in the introduction, wildfire smoke has been found to produce O_3 within plumes and to be correlated with enhanced surface O_3 in areas to which it is advected. The total amount of O_3 at a location is a complex combination of the relative abundances of VOCs and NO_x , meteorological conditions supporting local O_3 production, and the amount of O_3 present in the air mass before local production. In this section, we describe the significant increases in O_3 during both smoke-impacted periods, show that these enhancements were most likely not due to changes in meteorological conditions, and discuss evidence pointing to whether these changes may be due to enhanced local production or transport of O_3 produced within the smoke plume.

Figure 13d shows that there were significant increases in O_3 mixing ratios during nighttime and midday during the August smoke-impacted period compared to the average smoke-free diurnal cycle. The mean O_3 mixing ratio across all hours of the day was 6 ppbv (14%) larger during the August smoke-impacted period than the smoke-free period (Figure 14), significant at the 99% confidence level based on a two-sample difference of means t-test. There

were no significant changes in the average O_3 mixing ratios during the July smoke-impacted period (Figure 13a). The average mixing ratio of O_3 during the July smoke-impacted period was not greater than absolute average during the smoke-free period. However, as discussed in Section 2, this period in particular was much colder on average than the smoke-free period.

O_3 mixing ratios generally increase with temperature, and this relationship has been attributed to several specific processes including 1) warm and often stagnant anti-cyclonic atmospheric conditions that are conducive to O_3 formation, 2) warmer air temperatures that

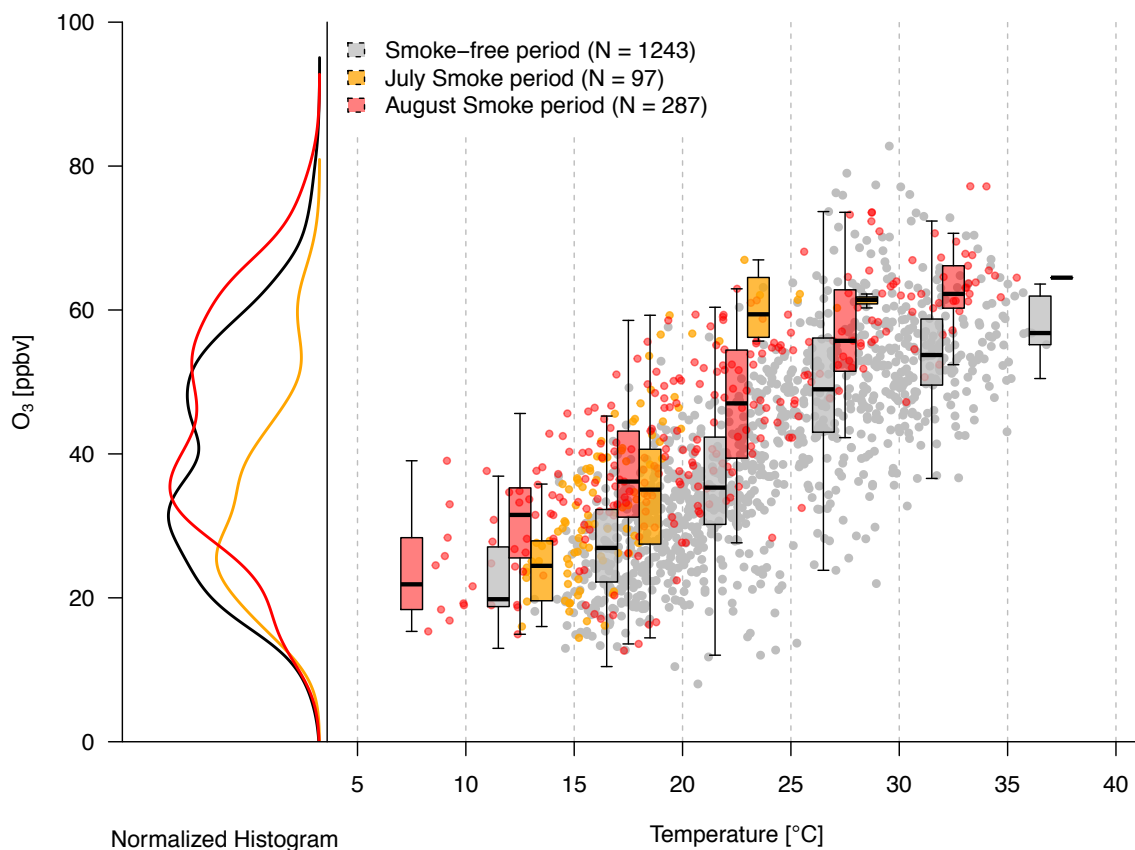


Figure 14. Hourly O_3 data from BAO plotted against hourly temperature data show a positive correlation between temperature and O_3 abundances for the smoke-free time periods in grey and both smoke-impacted periods (July in orange and August in red). Overlaid are boxplots (5th, 25th, 50th, 75th, and 95th percentiles) for each 5 °C bin. On the left normalized histograms of the hourly O_3 data are plotted, with all smoke-free measurements in black, and all hourly measurements made during the July smoke-impacted period in orange and August smoke-impacted period in red.

reduce the lifetime of PAN, releasing NO₂, and 3) lower relative humidity that reduces the speed of termination reactions to the O₃ production cycle (Jacob et al., 1993; Camalier et al., 2007). Specific to the Front Range, Abeleira and Farmer (2017) show that ozone in this region has a temperature dependence, but it is smaller than other U.S. regions, consistent with the smaller local biogenic VOC emissions compared to many other locations in the eastern U.S. Finally, there is an additional meteorological factor in the Front Range that can impact the temperature dependence of ozone. Gusty westerly winds are often associated with high temperatures, and these winds serve to weaken or eliminate cyclical terrain-driven circulations that normally enhance O₃ mixing ratios across the Front Range. Figure 14 presents hourly average O₃ and temperature at BAO and shows a positive relationship between O₃ and temperature for both the smoke-free period and August smoke-impacted period. The increase in O₃ mixing ratios during the August smoke-impacted period compared to the smoke-free period is present across the entire range of comparable temperatures. The same result is apparent during the July smoke-period, where, for comparable temperatures, the July smoke-period has higher O₃ than would be expected from the O₃-temperature relationship during the smoke-free period. Across both smoke-impacted periods and for a given temperature, the magnitude of the increase in average O₃ was 10 ± 2 ppbv. This was calculated as the mean difference between medians within each temperature bin weighted by the total number of hourly measurements within each bin. The weighted standard deviation was calculated in the same way. The magnitude of this difference is greater than the average difference in means between the smoke-free O₃ mixing ratios and the August smoke-impacted period because there were several periods during the July and August smoke-impacted period where air temperatures were colder ($\sim 5^\circ\text{C}$) than most observations during the smoke-free period. Thus the lower O₃ mixing ratios associated with these smoke-

impacted periods (*e.g.* $\sim 20 - 40$ ppbv) were not included in the weighted difference in medians since there were not commensurate smoke-free O₃ measurements at those same temperatures.

In addition to a positive relationship with surface temperature, elevated O₃ in the western U.S. has also been found to be correlated with monthly average 500 hPa geopotential heights, 700 hPa temperatures, and surface wind speeds on an interannual basis (Reddy and Pfister, 2016). We tested the day-to-day variability in the relationship between O₃ and these meteorological variables during our study period using observations from the 0Z and 12Z atmospheric soundings conducted in Denver (<http://mesonet.agron.iastate.edu/archive/raob/>). The positive relationships between MDA8 O₃ and 700 mb temperature, 500 mb geopotential height, and surface winds are very weak, $R^2 = 0.04$, and $R^2 = 0.08$, and $R^2 = 0.0009$ respectively. Thus, we did not find any evidence to support the hypothesis that differences in meteorological conditions were solely responsible for the significant differences in composition or O₃ that we observed during the smoke-impacted period.

To determine if a change in synoptic scale transport in smoke-impacted versus smoke-free periods could have contributed to different abundances, we performed a k-means cluster analysis on 72-hour HYSPLIT back trajectories. The trajectories were calculated using the methods described above, and initiated each hour at 2000 m a.g.l. from BAO. We chose to initialize the trajectories at 2000 m a.g.l. so that fewer trajectories intersect the ground in the Rocky Mountains. Trajectories are unlikely to capture the complex circulations (*e.g.* potential Denver Cyclones or up/down slope winds) characteristic of summertime in the Front Range, but they should capture synoptic scale air mass motions. The k-means analysis clustered each trajectory into a predetermined number of clusters by minimizing the distance between each trajectory and its nearest neighbor; this technique has been used to classify air mass history in air

quality studies (Moody et al., 1998). We found 4 predominate trajectory clusters during our study period: northwesterly flow, westerly flow, southwesterly flow, and local/indeterminate flow (Figure 21 in Appendix B). We then compared afternoon (12PM – 5PM MDT) hourly O₃ measurements separated by trajectory cluster and binned by temperature between the smoke-free period and the August smoke-impacted period. Most hours during the August smoke-impacted period were associated with northwesterly flow and we found a similar enhancement in O₃ for a given temperature when comparing smoke-impacted observations to smoke-free observations assigned to this cluster as we found for the complete dataset (Figures 22 and 23 in Appendix B). Thus we conclude that potential changes in O₃ driven by synoptic scale transport conditions cannot account for the observed O₃ enhancements during the August smoke-impacted period at BAO.

Following the definition in (Cooper et al., 2012), we define a “high O₃ day” as any day in our study period with at least one hour above the 95th percentile (71.75 ppbv) of all 11am – 4pm MDT hourly average O₃ measurements during the campaign. We found 9 individual high O₃ days during our study period, of which 2 occurred during the August smoke-impacted period (Figure 15). The total number of high O₃ days is lower than normal for the same time period in previous years. As we stated above, high O₃ during the August smoke period was not a result of abnormal meteorological variables, such as higher than normal temperatures. The lower portion of Figure 15 again shows that maximum daily temperatures during the smoke-impacted periods were the same as or lower than maximum daily temperatures during the smoke-free period. Denver cyclones and in-basin wind patterns can also contribute to O₃ production and re-circulation in the Front Range (see Sullivan et al. (2016), Vu et al. (2016) and references within). We examined surface wind observations (<http://mesowest.utah.edu>) on the 2 high O₃ days during

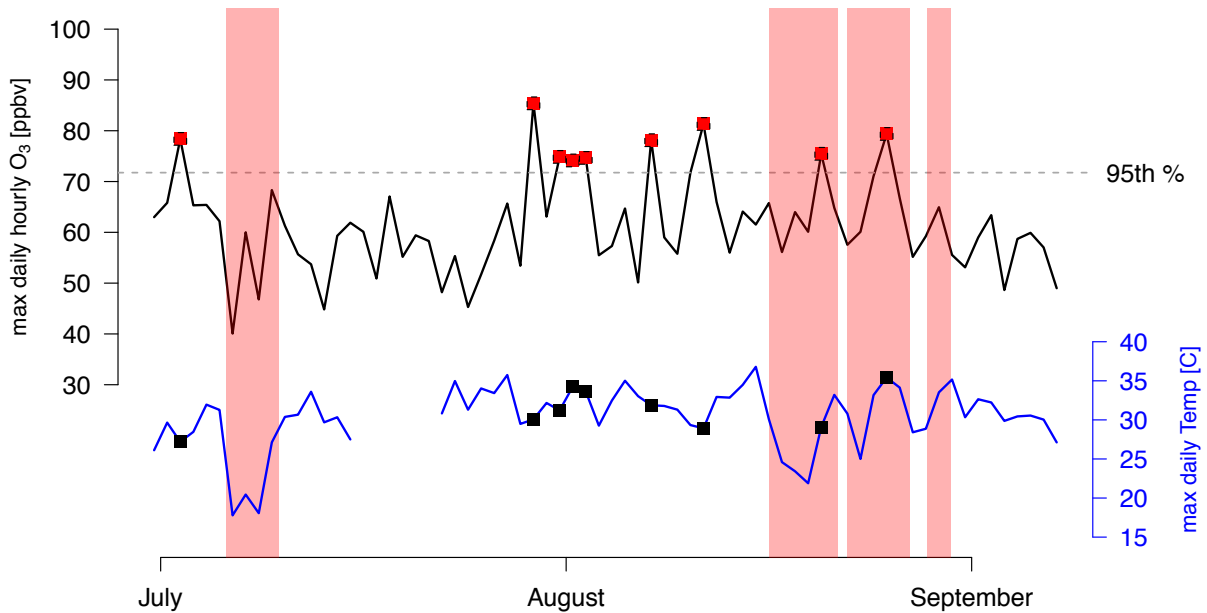


Figure 15. Maximum hourly average O₃ mixing ratios for each day at BAO plotted in black with maximum daily temperature at BAO in blue. Red boxes denote days that exceed the 95th percentile of all hourly average O₃ mixing ratios between 11am – 4pm MDT. Black boxes pinpoint these same days in the temperature timeseries.

the smoke impacted period: 20 August and 25 August. There is no evidence of the establishment of Denver Cyclones on either of these days. Sullivan et al. (2016) point out that thermally driven recirculation can manifest as a secondary increase in O₃ at surface sites. We did observe a secondary maximum at 17:00 MT on 25 August, but this feature was not present on 20 August.

Several Front Range O₃ monitors recorded elevated ozone during the August smoke-impacted period. Specifically, the maximum daily 8-hour average O₃ mixing ratio at Aurora East exceeded 75 ppbv on 21 August. This was the first highest maximum for this station for summer 2015. The second highest maximum for summer 2015 coincided with the August smoke-impacted period at Fort Collins West, Greeley, La Casa, Welby and Aurora East. The third highest maximum for summer 2015 coincided with the August smoke-impacted period at Aurora East, South Boulder Creek, Rocky Mountain National Park, and Fort Collins – CSU.

The presence of smoke was not always associated with high absolute abundances of O₃ at BAO. The July smoke-impacted period and most of the days in the August smoke period did not have maximum hourly mixing ratios greater than the 95th percentile. However, it is important to note that many of these days did have higher O₃ abundances than would otherwise be expected given their temperatures (see Figure 14). Therefore we conclude that the presence of wildfire smoke contributed to higher O₃ mixing ratios than would otherwise be expected during the two smoke events we sampled, and that during 2 of these days the smoke contributed to an empirically defined “high O₃ day”.

As mentioned in the Introduction, wildfire smoke can produce O₃ within the plume as it is transported, as well as contribute to O₃ photochemistry by mixing additional precursors into surface air masses. To assess the possibility of O₃ production with the plume, we analyzed hourly O₃ measurements from two National Park Service (NPS) Air Resources Division (<http://ard-request.air-resource.com/data.aspx>) measurement locations that are located outside the polluted Front Range urban corridor. The Rocky Mountain National Park long-term monitoring site (ROMO; 40.2778°N, 105.5453°W, 2743 meters A.S.L.) is located on the east side of the Continental Divide and co-located with the Interagency Monitoring of Protected Visual Environments (IMPROVE) and EPA Clean Air Status and Trends Network (CASTNet) monitoring sites. Front Range air masses frequently reach this site during summer afternoons (Benedict et al., 2013). The Arapahoe National Wildlife Refuge long-term monitoring site (WALD; 40.8822°N, 106.3061°W, 2417 meters A.S.L.) near Walden, Colorado, is a rural mountain valley site with very little influence from anthropogenic emissions. These two sites follow a rough urban to rural gradient; from primarily influenced by anthropogenic emissions (BAO), to sometimes influenced by anthropogenic emissions (ROMO), to very little influence

from anthropogenic emissions (WALD). Figure 16 shows that the August smoke-impacted period produced increases in O₃ mixing ratios across all three sites. When comparing all data for a given temperature, there are average weighted enhancements of 10 ± 2 ppbv, 10 ± 2 ppbv, and 6 ± 2 ppbv O₃ at BAO, ROMO and WALD respectively. O₃ enhancements across all three sites, across an approximate urban to rural gradient, suggest that some amount of the O₃ enhancement observed at BAO during the August smoke-impacted period is the result of O₃ production within the plume during transit. O₃ during the July smoke-impacted period in Figure 16 shows a different pattern. As we saw in Figure 14, O₃ is enhanced above the level predicted by the ambient temperature at BAO. But no statistically significant enhancements are observed at ROMO and WALD for the July smoke-impacted period. One possible reason for this nuance is that, based on the HMS smoke product shown in Figure 3, it is less obvious that smoke was present at ROMO and WALD during the July smoke-impacted period.

One measure of local production of O₃ is the ozone production efficiency (OPE). OPE is calculated as the slope of the relationship between O₃ and NO_z ($= \text{NO}_y - \text{NO}_x$) (Trainer et al., 1993). OPE is a measure of the number of molecules of O₃ that are produced before a given NO_x molecule is oxidized. To calculate OPE we used one minute O₃ and NO_z data in 30 minute chunks from 12PM - 5PM MDT. The slopes were calculated using a reduced major axis regression (package lmodel2 for R software) and only OPE values corresponding to an $R^2 > 0.3$ were retained. We do not find any significant differences in average calculated OPE between the smoke-impacted (8 ± 3 ppbv/ppbv) and smoke-free periods (7 ± 3 ppbv/ppbv). Thus from the OPE perspective it does not appear there were any changes in the local production efficiency of O₃ due to the presence of smoke. On the other hand, we documented many changes to the atmospheric composition of O₃ precursors, particularly with respect to CO, benzene, ethyne, the

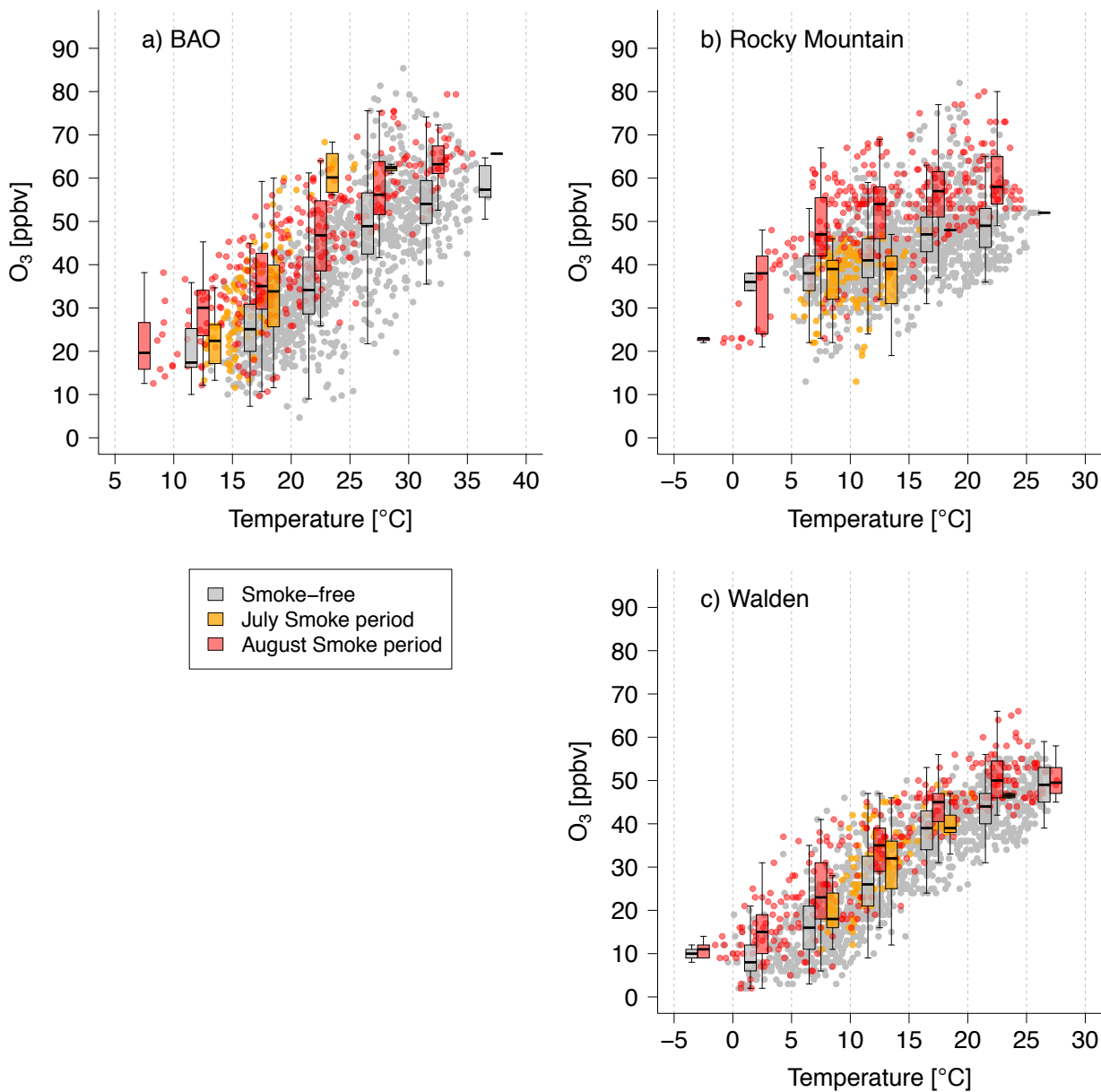


Figure 16. Hourly O_3 versus temperature for a) BAO, b) the Rocky Mountain National Park long-term monitoring site (ROMO), and c) the Arapahoe National Wildlife Refuge long-term monitoring site near Walden, CO (WALD). Plotted here are all hourly data, with boxplots showing standard percentiles of 5 °C binned O_3 data the same as was shown in Figure 14.

alkenes, and PANs. Additionally the smoke may have added many O_3 precursors that we were not set up to measure (*e.g.* many OVOCs). Due to the nonlinear nature of O_3 chemistry, the different mix of precursors could have caused enhanced local O_3 production, depressed local O_3 production, or had no effect on local O_3 production. Taken together, the observations do not

suggest a single mechanism that describes smoke influence on O₃ in Front Range air masses during these case studies. Instead, the observations point to the presence of smoke resulting in a complex array of processes that will require more detailed observations and chemical transport modeling to clearly identify and quantify.

CHAPTER 5: CONCLUSIONS AND FUTURE WORK⁴

In this thesis we report on a time series of detailed gas-phase ground measurements in the northern Colorado Front Range during summer 2015. We divide the measurement period into multiple time periods, characterized by the presence or absence of aged wildfire smoke, and completed separate analyses of these different periods. Chapter 3 presented the first analysis, an assessment of the contribution of different local VOC sources to elevated surface O₃ at BAO during the smoke-free time period. Empirical observations and idealized box model simulations support the hypothesis that emissions from oil and gas extraction activities in the northern Colorado Front Range contribute to O₃ photochemical production in the region. We have four main conclusions. First, the highest mixing ratios of PAN occur on the same days with the highest abundance of O₃, and these periods of elevated secondary species are consistently associated with ratios of PPN/PAN > 0.15. Additionally, when O₃ and the PPN/PAN ratio are most elevated, a large (25 – 45 %) percent of the concurrently estimated VOC OHR is attributed to VOCs from oil and gas development. These observations suggest that emissions of VOCs from oil and natural gas production play an important role in contributing to high O₃ days at BAO in summer 2015. Second, a larger percentage (30 – 60 %) of the measured VOC OHR is attributed to isoprene when O₃ and PPN/PAN ratios are lower (< 0.13). MPAN mixing ratios are also low and MPAN/PAN ratios are anti-correlated with O₃ abundance. This suggests that biogenic VOCs do not play the dominant role in driving high O₃ events at BAO in summer 2015. Third, given the current relative abundances of measured VOC species, our model simulations

⁴ Portions of this chapter contain published work. Citation: Lindaas, J., Farmer, D. K., Pollack, I. B., Abeleira, A., Flocke, F., Roscioli, R., Herndon, S., and Fischer, E. V.: Changes in ozone and precursors during two aged wildfire smoke events in the Colorado Front Range in summer 2015, *Atmos. Chem. Phys.*, 17, 10691-10707, 10.5194/acp-17-10691-2017, 2017.

suggest that O_3 mixing ratios are more sensitive to a given percentage increase in oil and gas VOCs than a percentage increase in traffic VOCs. The high oil and gas mixtures appear to produce more abundant, and more efficient RO_2 radical intermediates, as compared to mixtures dominated by other VOC sources. Following a local first-order sensitivity analysis, we conservatively estimate that the percentage contribution to O_3 production from oil and gas VOCs is at least 15%-31%. And fourth, out of the VOC species we measured, propane and several larger alkanes such as n-pentane are the dominant contributors to PPN production in the Front Range. These species predominately come from oil and gas sources (*e.g.*, Gilman 2013, Abeleira, 2017); therefore we conclude that high ratios of PPN/PAN observed in the Front Range are driven by the oxidation of emissions from the oil and gas industry.

Chapter 4 presented the results of our second analysis, on a case study of the smoke-impacted periods to investigate the contribution of aged wildfire smoke on atmospheric composition and surface O_3 abundances at BAO. Clear anomalies in CO and $PM_{2.5}$ showed that aged wildfire smoke was present at ground level during two distinct periods (6 – 10 July and 16 – 30 August) during the nine week sampling campaign. The smoke, from wildfires in the Pacific Northwest and Canada, impacted a large area across much of the central and western U.S., and was several days old when it was sampled in Colorado. This wildfire smoke mixed with anthropogenic emissions in the Front Range, resulting in significant changes in the abundances of O_3 and many of its precursor species. Our measurements are unique because of 1) the length of time we sampled this smoke-impacted anthropogenic air mass, and 2) the detailed composition information that was collected.

During the smoke-impacted periods we observed significantly increased abundances of CO, CH_4 , and several VOCs with OH oxidation lifetimes longer than the transport time of the

smoke. We measured significant decreases in several of the most reactive alkene species, indicating possible enhanced oxidation processes occurring locally. Mixing ratios of acyl peroxy nitrates and some alkyl nitrates were enhanced and peak abundances were delayed by 3-4 hours, but there was no significant change in HNO₃ mixing ratios or its diurnal cycle. During the longer August smoke-impacted period we observed significant increases in NO₂ mixing ratios just after sunrise and sunset. We did not observe any consistent shifts in wind direction or changes in wind speed that can explain the observed changes in composition (e.g. Figure 12), and the changes in abundances that we observed for a given species were generally present across all directions and speeds. The smoke was ubiquitous across the Front Range as evidenced by enhanced PM_{2.5} at CAMP (Figure 2) and 9 other Front Range CDPHE monitoring sites.

We observed significantly enhanced O₃ abundances at BAO of about 10 ppbv for a given temperature during both smoke-impacted periods. The enhancements during the August smoke-period led to very high surface O₃ levels on several days; out of 9 high O₃ days at BAO during our study period, 2 were during the August smoke-impacted period. These enhancements were not due to higher temperatures, nor anomalous meteorological conditions. We found evidence of O₃ produced within the smoke plume during transit, and changes in the observed abundances of many O₃ precursors indicated that the smoke may have impacted local O₃ production as well.

It is important to note that the presence of smoke does not always result in very high O₃ abundances. Many other factors contribute to the overall level of surface O₃, and smoke can also be associated with relatively low O₃ at times, such as during the July smoke event described above. This case study describes two distinct smoke events where the presence of smoke likely increased O₃ abundances above those expected by coincident temperatures. However, we do not intend to claim that all high O₃ episodes in the Front Range are caused by smoke, nor that smoke

will always cause higher than expected O_3 . Each smoke event has unique characteristics and thus it is important to study and characterize more events such as these in the future.

Wildfire smoke during these time periods in 2015 most likely impacted atmospheric composition and photochemistry across much of the mountain west and great plains regions of the U.S. Given the BAO, Rocky Mountain and Walden research locations span an urban-rural gradient as well as a large altitudinal gradient, it is likely that both rural and urban locations impacted by this smoke could have experienced enhanced O_3 levels. Additionally, the Pacific Northwest wildfires that produced this smoke were among the most extreme in that region's history. We know that wildfires are increasing in both frequency and intensity throughout the western U.S. due to climate change, and thus wildfire smoke events such as this one will likely play an increasingly problematic role in U.S. air quality.

These analyses attempt to answer important questions at the intersection of air quality, human health, and climate. Future work is certainly needed to more fully understand and address these questions. In order to understand the response of air quality to both changing anthropogenic emission sources, and increasingly pervasive wildfire smoke events, it is clear that additional observations are needed in support of comprehensive modeling efforts. For example the mechanisms by which wildfire smoke produces O_3 , either en route to an urban area or when mixed with anthropogenic emissions, could be investigated through multi-scale modeling efforts. Additional intensive ground observation campaigns in other locations around the Front Range region may help better elucidate patterns in O_3 production and the mechanisms behind them. Combining as many different measurements at the same site as possible should be a priority. In addition to the measurements presented in this thesis, measurements of OH and HO_2 along with more oxygenated VOCs can be useful in probing VOC oxidation pathways, empirical jNO_2

values would help to estimate instantaneous O_3 production, O_3 LIDARs could allow an empirical estimate of residual O_3 , and aerosol mass, size distribution, and composition measurements give insights into heterogeneous chemistry which could be especially important for smoke chemistry. Last, but not least, on the wish list of measurements would be additional reactive nitrogen species, N_2O_5 , HONO, and NO_3 to be able to assess nighttime oxidation processes and other sources of the OH radical.

REFERENCES

- Abeleira, A., Pollack, I. B., Sive, B., Zhou, Y., Fischer, E. V., and Farmer, D. K.: Source Characterization of Volatile Organic Compounds in the Colorado Northern Front Range Metropolitan Area during Spring and Summer 2015, *Journal of Geophysical Research: Atmospheres*, 122, doi:10.1002/2016JD026227, 2017.
- Abeleira, A. J., and Farmer, D. K.: Summer ozone in the northern Front Range metropolitan area: weekend–weekday effects, temperature dependences, and the impact of drought, *Atmos. Chem. Phys.*, 17, 6517-6529, 10.5194/acp-17-6517-2017, 2017.
- Akagi, S. K., Yokelson, R. J., Wiedinmyer, C., Alvarado, M. J., Reid, J. S., Karl, T., Crounse, J. D., and Wennberg, P. O.: Emission factors for open and domestic biomass burning for use in atmospheric models, *Atmos. Chem. Phys.*, 11, 4039-4072, 10.5194/acp-11-4039-2011, 2011.
- Akagi, S. K., Craven, J. S., Taylor, J. W., McMeeking, G. R., Yokelson, R. J., Burling, I. R., Urbanski, S. P., Wold, C. E., Seinfeld, J. H., Coe, H., Alvarado, M. J., and Weise, D. R.: Evolution of trace gases and particles emitted by a chaparral fire in California, *Atmos. Chem. Phys.*, 12, 1397-1421, 10.5194/acp-12-1397-2012, 2012.
- Alvarado, M. J., Logan, J. A., Mao, J., Apel, E., Riemer, D., Blake, D., Cohen, R. C., Min, K. E., Perring, A. E., Browne, E. C., Wooldridge, P. J., Diskin, G. S., Sachse, G. W., Fuelberg, H., Sessions, W. R., Harrigan, D. L., Huey, G., Liao, J., Case-Hanks, A., Jimenez, J. L., Cubison, M. J., Vay, S. A., Weinheimer, A. J., Knapp, D. J., Montzka, D. D., Flocke, F. M., Pollack, I. B., Wennberg, P. O., Kurten, A., Crounse, J., Clair, J. M. S., Wisthaler, A., Mikoviny, T., Yantosca, R. M., Carouge, C. C., and Le Sager, P.: Nitrogen oxides and PAN in plumes from boreal fires during ARCTAS-B and their impact on ozone: an integrated analysis of aircraft and satellite observations, *Atmos. Chem. Phys.*, 10, 9739-9760, 10.5194/acp-10-9739-2010, 2010.
- Atkinson, R., and Arey, J.: Atmospheric Degradation of Volatile Organic Compounds, *Chemical Reviews*, 103, 4605-4638, 10.1021/cr0206420, 2003.
- Bates, D. V.: Ambient ozone and mortality, *Epidemiology*, 16, 427-429, 10.1097/01.ede.0000165793.71278.ec, 2005.
- Benedict, K. B., Carrico, C. M., Kreidenweis, S. M., Schichtel, B., Malm, W. C., and Collett, J. L.: A seasonal nitrogen deposition budget for Rocky Mountain National Park, *Ecological Applications*, 23, 1156-1169, 2013.
- Brey, S. J., and Fischer, E. V.: Smoke in the City: How Often and Where Does Smoke Impact Summertime Ozone in the United States?, *Environmental Science & Technology*, 50, 1288-1294, 10.1021/acs.est.5b05218, 2016.
- Brey, S. J., Ruminski, M., Atwood, S. A., and Fischer, E. V.: Connecting smoke plumes to sources using Hazard Mapping System (HMS) smoke and fire location data over North America, *Atmos. Chem. Phys. Discuss.*, 2017, 1-29, 10.5194/acp-2017-245, 2017.
- Brown, S. S., Thornton, J. A., Keene, W. C., Pszenny, A. A. P., Sive, B. C., Dubč, W. P., Wagner, N. L., Young, C. J., Riedel, T. P., Roberts, J. M., VandenBoer, T. C., Bahreini, R., ôztÅrk, F., Middlebrook, A. M., Kim, S., HÅbler, G., and Wolfe, D. E.: Nitrogen, Aerosol Composition, and Halogens on a Tall Tower (NACHTT): Overview of a

- wintertime air chemistry field study in the front range urban corridor of Colorado, *Journal of Geophysical Research: Atmospheres*, 118, 8067-8085, 10.1002/jgrd.50537, 2013.
- Calvert, J. D., RG; Orlando, JJ; Tyndall, GS; Wallington, TJ: *Mechanisms of Atmospheric Oxidation of the Alkanes*, Oxford University Press, New York, New York, 2008.
- Camalier, L., Cox, W., and Dolwick, P.: The effects of meteorology on ozone in urban areas and their use in assessing ozone trends, *Atmospheric Environment*, 41, 7127-7137, <http://dx.doi.org/10.1016/j.atmosenv.2007.04.061>, 2007.
- CDPHE: *For Recommended 8-Hour Ozone Designations*, Denver, CO, 2009.
- Cheadle LC, O. S., Petron G, Schnell RC, Mattson EJ, Herndon SC, Thompson AM, Blake DR, McClure-Begley A: Surface ozone in the Colorado northern Front Range and the influence of oil and gas development during FRAPPE/DISCOVER-AQ in summer 2014, *Elementa: Science of the Anthropocene*, 5, <http://doi.org/10.1525/elementa.254>, 2017.
- Cooper, O. R., Gao, R.-S., Tarasick, D., Leblanc, T., and Sweeney, C.: Long-term ozone trends at rural ozone monitoring sites across the United States, 1990–2010, *Journal of Geophysical Research: Atmospheres*, 117, n/a-n/a, 10.1029/2012JD018261, 2012.
- Creamean, J. M., Neiman, P. J., Coleman, T., Senff, C. J., Kirgis, G., Alvarez, R. J., and Yamamoto, A.: Colorado air quality impacted by long-range-transported aerosol: a set of case studies during the 2015 Pacific Northwest fires, *Atmos. Chem. Phys.*, 16, 12329-12345, 10.5194/acp-16-12329-2016, 2016.
- Crosson, E. R.: A cavity ring-down analyzer for measuring atmospheric levels of methane, carbon dioxide, and water vapor, *Applied Physics B*, 92, 403-408, 10.1007/s00340-008-3135-y, 2008.
- Ebben, C. J., Sparks, T. L., Wooldridge, P. J., Campos, T. L., Cantrell, C. A., Mauldin, R. L., Weinheimer, A. J., and Cohen, R. C.: Evolution of NO_x in the Denver Urban Plume during the Front Range Air Pollution and Photochemistry Experiment, *Atmos. Chem. Phys. Discuss.*, 2017, 1-13, 10.5194/acp-2017-671, 2017.
- Eilerman, S. J., Peischl, J., Neuman, J. A., Ryerson, T. B., Aikin, K. C., Holloway, M. W., Zondlo, M. A., Golston, L. M., Pan, D., Floerchinger, C., and Herndon, S.: Characterization of Ammonia, Methane, and Nitrous Oxide Emissions from Concentrated Animal Feeding Operations in Northeastern Colorado, *Environmental Science & Technology*, 50, 10885-10893, 10.1021/acs.est.6b02851, 2016.
- Elliott, C., Henderson, S., and Wan, V.: Time series analysis of fine particulate matter and asthma reliever dispensations in populations affected by forest fires, *Environmental Health*, 12, 11, 2013.
- Emmerson, K. M., and Evans, M. J.: Comparison of tropospheric gas-phase chemistry schemes for use within global models, *Atmos. Chem. Phys.*, 9, 1831-1845, 10.5194/acp-9-1831-2009, 2009.
- EPA: *Ground-level ozone—Regulatory actions*, 2015.
- Evans, J. M., and Helmig, D.: Investigation of the influence of transport from oil and natural gas regions on elevated ozone levels in the northern Colorado front range, *Journal of the Air & Waste Management Association*, 67, 196-211, 10.1080/10962247.2016.1226989, 2017.
- Farmer, D. K., Perring, A. E., Wooldridge, P. J., Blake, D. R., Baker, A., Meinardi, S., Huey, L. G., Tanner, D., Vargas, O., and Cohen, R. C.: Impact of organic nitrates on urban ozone production, *Atmos. Chem. Phys.*, 11, 4085-4094, 10.5194/acp-11-4085-2011, 2011.

- Fent, K. W., Eisenberg, J., Snawder, J., Sammons, D., Pleil, J. D., Stiegel, M. A., Mueller, C., Horn, G. P., and Dalton, J.: Systemic Exposure to PAHs and Benzene in Firefighters Suppressing Controlled Structure Fires, *Annals of Occupational Hygiene*, 10.1093/annhyg/meu036, 2014.
- Fischer, E. V., Jacob, D. J., Yantosca, R. M., Sulprizio, M. P., Millet, D. B., Mao, J., Paulot, F., Singh, H. B., Roiger, A., Ries, L., Talbot, R. W., Dzepina, K., and Pandey Deolal, S.: Atmospheric peroxyacetyl nitrate (PAN): a global budget and source attribution, *Atmos. Chem. Phys.*, 14, 2679-2698, 10.5194/acp-14-2679-2014, 2014.
- Flocke, F. M., Weinheimer, A. J., Swanson, A. L., Roberts, J. M., Schmitt, R., and Shertz, S.: On the Measurement of PANs by Gas Chromatography and Electron Capture Detection, *Journal of Atmospheric Chemistry*, 52, 19-43, 10.1007/s10874-005-6772-0, 2005.
- Fowler, D.: Effects of acidic pollutants on terrestrial ecosystems, *Atmospheric Acidity: Sources, Consequences and Abatement*, edited by: Radojevic M., H. R. M., Elsevier, Amsterdam, 341-361 pp., 1992.
- Giglio, L., Descloitres, J., Justice, C. O., and Kaufman, Y. J.: An Enhanced Contextual Fire Detection Algorithm for MODIS, *Remote Sensing of Environment*, 87, 273-282, [http://dx.doi.org/10.1016/S0034-4257\(03\)00184-6](http://dx.doi.org/10.1016/S0034-4257(03)00184-6), 2003.
- Giglio, L., Csiszar, I., and Justice, C. O.: Global distribution and seasonality of active fires as observed with the Terra and Aqua Moderate Resolution Imaging Spectroradiometer (MODIS) sensors, *Journal of Geophysical Research: Biogeosciences*, 111, n/a-n/a, 10.1029/2005JG000142, 2006.
- Gilman, J. B., Lerner, B. M., Kuster, W. C., and de Gouw, J. A.: Source signature of volatile organic compounds from oil and natural gas operations in northeastern Colorado, *Environ Sci Technol*, 47, 1297-1305, 10.1021/es304119a, 2013.
- Gilman, J. B., Lerner, B. M., Kuster, W. C., Goldan, P. D., Warneke, C., Veres, P. R., Roberts, J. M., de Gouw, J. A., Burling, I. R., and Yokelson, R. J.: Biomass burning emissions and potential air quality impacts of volatile organic compounds and other trace gases from fuels common in the US, *Atmos. Chem. Phys.*, 15, 13915-13938, 10.5194/acp-15-13915-2015, 2015.
- Giordano, M. R., Chong, J., Weise, D. R., and Asa-Awuku, A. A.: Does chronic nitrogen deposition during biomass growth affect atmospheric emissions from biomass burning?, *Environmental Research Letters*, 11, 034007, 2016.
- Goode, J. G., Yokelson, R. J., Ward, D. E., Susott, R. A., Babbitt, R. E., Davies, M. A., and Hao, W. M.: Measurements of excess O₃, CO₂, CO, CH₄, C₂H₄, C₂H₂, HCN, NO, NH₃, HCOOH, CH₃COOH, HCHO, and CH₃OH in 1997 Alaskan biomass burning plumes by airborne Fourier transform infrared spectroscopy (AFTIR), *Journal of Geophysical Research: Atmospheres*, 105, 22147-22166, 10.1029/2000JD900287, 2000.
- Guenther, A., Karl, T., Harley, P., Wiedinmyer, C., Palmer, P. I., and Geron, C.: Estimates of global terrestrial isoprene emissions using MEGAN (Model of Emissions of Gases and Aerosols from Nature), *Atmos. Chem. Phys.*, 6, 3181-3210, 10.5194/acp-6-3181-2006, 2006.
- Halliday, H. S., Thompson, A. M., Wisthaler, A., Blake, D. R., Hornbrook, R. S., Mikoviny, T., Müller, M., Eichler, P., Apel, E. C., and Hills, A. J.: Atmospheric benzene observations from oil and gas production in the Denver-Julesburg Basin in July and August 2014, *Journal of Geophysical Research: Atmospheres*, 121, 11,055-011,074, 10.1002/2016JD025327, 2016.

- Heilman, W. E., Liu, Y., Urbanski, S., Kovalev, V., and Mickler, R.: Wildland fire emissions, carbon, and climate: Plume rise, atmospheric transport, and chemistry processes, *Forest Ecology and Management*, 317, 70-79, <http://dx.doi.org/10.1016/j.foreco.2013.02.001>, 2014.
- Hobbs, P. V., Sinha, P., Yokelson, R. J., Christian, T. J., Blake, D. R., Gao, S., Kirchstetter, T. W., Novakov, T., and Pilewskie, P.: Evolution of gases and particles from a savanna fire in South Africa, *Journal of Geophysical Research: Atmospheres*, 108, n/a-n/a, 10.1029/2002JD002352, 2003.
- Ito, K., De Leon, S. F., and Lippmann, M.: Associations between ozone and daily mortality - Analysis and meta-analysis, *Epidemiology*, 16, 446-457, 10.1097/01.ede.0000165821.90114.7f, 2005.
- Jacob, D. J., Logan, J. A., Yevich, R. M., Gardner, G. M., Spivakovsky, C. M., Wofsy, S. C., Munger, J. W., Sillman, S., Prather, M. J., Rodgers, M. O., Westberg, H., and Zimmerman, P. R.: Simulation of summertime ozone over North America, *Journal of Geophysical Research: Atmospheres*, 98, 14797-14816, 10.1029/93JD01223, 1993.
- Jaegle, L., Steinberger, L., Martin, R. V., and Chance, K.: Global partitioning of NO_x sources using satellite observations: Relative roles of fossil fuel combustion, biomass burning and soil emissions, *Faraday Discussions*, 130, 407-423, 10.1039/B502128F, 2005.
- Jaffe, D. A., Chand, D., Hafner, W., Westerling, A., and Spracklen, D.: Influence of fires on O₃ concentrations in the western US, *Environmental Science & Technology*, 42, 5885-5891, 10.1021/es800084k, 2008.
- Jaffe, D. A., and Wigder, N. L.: Ozone production from wildfires: A critical review, *Atmospheric Environment*, 51, 1-10, <http://dx.doi.org/10.1016/j.atmosenv.2011.11.063>, 2012.
- Jenkin, M. E., Young, J. C., and Rickard, A. R.: The MCM v3.3.1 degradation scheme for isoprene, *Atmos. Chem. Phys.*, 15, 11433-11459, 10.5194/acp-15-11433-2015, 2015.
- Jin, L., Tonse, S., Cohan, D. S., Mao, X., Harley, R. A., and Brown, N. J.: Sensitivity Analysis of Ozone Formation and Transport for a Central California Air Pollution Episode, *Environmental Science & Technology*, 42, 3683-3689, 10.1021/es072069d, 2008.
- Kalnay, E., Kanamitsu, M., Kistler, R., Collins, W., Deaven, D., Gandin, L., Iredell, M., Saha, S., White, G., Woollen, J., Zhu, Y., Leetmaa, A., Reynolds, R., Chelliah, M., Ebisuzaki, W., Higgins, W., Janowiak, J., Mo, K. C., Ropelewski, C., Wang, J., Jenne, R., and Joseph, D.: The NCEP/NCAR 40-Year Reanalysis Project, *Bulletin of the American Meteorological Society*, 77, 437-471, 10.1175/1520-0477(1996)077<0437:TNYRP>2.0.CO;2, 1996.
- Kelly, T. J., Stedman, D. H., and Kok, G. L.: Measurements of H₂O₂ and HNO₃ in rural air, *Geophysical Research Letters*, 6, 375-378, 10.1029/GL006i005p00375, 1979.
- Kley, D., and McFarland, M.: Chemiluminescence detector for NO and NO₂, *Journal of Atmospheric Technology*, 12, 62-69, 1980.
- Knote, C., Tuccella, P., Curci, G., Emmons, L., Orlando, J. J., Madronich, S., Baró, R., Jiménez-Guerrero, P., Luecken, D., Hogrefe, C., Forkel, R., Werhahn, J., Hirtl, M., Pérez, J. L., San José, R., Giordano, L., Brunner, D., Yahya, K., and Zhang, Y.: Influence of the choice of gas-phase mechanism on predictions of key gaseous pollutants during the AQMEII phase-2 intercomparison, *Atmospheric Environment*, 115, 553-568, <https://doi.org/10.1016/j.atmosenv.2014.11.066>, 2015.

- Künzli, N., Avol, E., Wu, J., Gauderman, W. J., Rappaport, E., Millstein, J., Bennion, J., McConnell, R., Gilliland, F. D., Berhane, K., Lurmann, F., Winer, A., and Peters, J. M.: Health Effects of the 2003 Southern California Wildfires on Children, *American Journal of Respiratory and Critical Care Medicine*, 174, 1221-1228, 10.1164/rccm.200604-519OC, 2006.
- Lacaux, J. P., Delmas, R., Jambert, C., and Kuhlbusch, T. A. J.: NO_x emissions from African savanna fires, *Journal of Geophysical Research: Atmospheres*, 101, 23585-23595, 10.1029/96JD01624, 1996.
- Lindaas, J., Farmer, D. K., Pollack, I. B., Abeleira, A., Flocke, F., Roscioli, R., Herndon, S., and Fischer, E. V.: Changes in ozone and precursors during two aged wildfire smoke events in the Colorado Front Range in summer 2015, *Atmos. Chem. Phys.*, 17, 10691-10707, 10.5194/acp-17-10691-2017, 2017.
- Liu, X., Zhang, Y., Huey, L. G., Yokelson, R. J., Wang, Y., Jimenez, J. L., Campuzano-Jost, P., Beyersdorf, A. J., Blake, D. R., Choi, Y., St. Clair, J. M., Crouse, J. D., Day, D. A., Diskin, G. S., Fried, A., Hall, S. R., Hanisco, T. F., King, L. E., Meinardi, S., Mikoviny, T., Palm, B. B., Peischl, J., Perring, A. E., Pollack, I. B., Ryerson, T. B., Sachse, G., Schwarz, J. P., Simpson, I. J., Tanner, D. J., Thornhill, K. L., Ullmann, K., Weber, R. J., Wennberg, P. O., Wisthaler, A., Wolfe, G. M., and Ziemba, L. D.: Agricultural fires in the southeastern U.S. during SEAC4RS: Emissions of trace gases and particles and evolution of ozone, reactive nitrogen, and organic aerosol, *Journal of Geophysical Research: Atmospheres*, n/a-n/a, 10.1002/2016JD025040, 2016.
- Lu, X., Zhang, L., Yue, X., Zhang, J., Jaffe, D. A., Stohl, A., Zhao, Y., and Shao, J.: Wildfire influences on the variability and trend of summer surface ozone in the mountainous western United States, *Atmos. Chem. Phys.*, 16, 14687-14702, 10.5194/acp-16-14687-2016, 2016.
- Madronich, S.: Implications of recent total atmospheric ozone measurements for biologically active ultraviolet radiation reaching the Earth's surface, *Geophysical Research Letters*, 19, 37-40, 10.1029/91GL02954, 1992.
- Mason, S. A., Field, R. J., Yokelson, R. J., Kochivar, M. A., Tinsley, M. R., Ward, D. E., and Hao, W. M.: Complex effects arising in smoke plume simulations due to inclusion of direct emissions of oxygenated organic species from biomass combustion, *Journal of Geophysical Research: Atmospheres*, 106, 12527-12539, 10.1029/2001JD900003, 2001.
- McClure-Begley, A., Petropavlovskikh, I., and Oltmans, S.: NOAA Global Monitoring Surface Ozone Network. BAO, June 2015 - September 2015. National Oceanic and Atmospheric Administration, Earth Systems Research Laboratory Global Monitoring Division. Boulder, CO., doi: 10.7289/V5P8WBF, 2014.
- McDuffie, E. E., Edwards, P. M., Gilman, J. B., Lerner, B. M., Dubé, W. P., Trainer, M., Wolfe, D. E., Angevine, W. M., deGouw, J., Williams, E. J., Tevlin, A. G., Murphy, J. G., Fischer, E. V., McKeen, S., Ryerson, T. B., Peischl, J., Holloway, J. S., Aikin, K., Langford, A. O., Senff, C. J., Alvarez, R. J., Hall, S. R., Ullmann, K., Lantz, K. O., and Brown, S. S.: Influence of oil and gas emissions on summertime ozone in the Colorado Northern Front Range, *Journal of Geophysical Research: Atmospheres*, 121, 8712-8729, 10.1002/2016JD025265, 2016.

- McManus, J. B., Zahniser, M. S., and Nelson, D. D.: Dual quantum cascade laser trace gas instrument with astigmatic Herriott cell at high pass number, *Appl. Opt.*, 50, A74-A85, 10.1364/AO.50.000A74, 2011.
- McMeeking, G. R., Kreidenweis, S. M., Baker, S., Carrico, C. M., Chow, J. C., Collett, J. L., Hao, W. M., Holden, A. S., Kirchstetter, T. W., Malm, W. C., Moosmüller, H., Sullivan, A. P., and Wold, C. E.: Emissions of trace gases and aerosols during the open combustion of biomass in the laboratory, *Journal of Geophysical Research: Atmospheres*, 114, n/a-n/a, 10.1029/2009JD011836, 2009.
- Monks, P. S., Archibald, A. T., Colette, A., Cooper, O., Coyle, M., Derwent, R., Fowler, D., Granier, C., Law, K. S., Mills, G. E., Stevenson, D. S., Tarasova, O., Thouret, V., von Schneidemesser, E., Sommariva, R., Wild, O., and Williams, M. L.: Tropospheric ozone and its precursors from the urban to the global scale from air quality to short-lived climate forcer, *Atmos. Chem. Phys.*, 15, 8889-8973, 10.5194/acp-15-8889-2015, 2015.
- Moody, J. L., Munger, J. W., Goldstein, A. H., Jacob, D. J., and Wofsy, S. C.: Harvard Forest regional-scale air mass composition by Patterns in Atmospheric Transport History (PATH), *Journal of Geophysical Research: Atmospheres*, 103, 13181-13194, 10.1029/98JD00526, 1998.
- Morris, G. A., Hersey, S., Thompson, A. M., Pawson, S., Nielsen, J. E., Colarco, P. R., McMillan, W. W., Stohl, A., Turquety, S., Warner, J., Johnson, B. J., Kucsera, T. L., Larko, D. E., Oltmans, S. J., and Witte, J. C.: Alaskan and Canadian forest fires exacerbate ozone pollution over Houston, Texas, on 19 and 20 July 2004, *Journal of Geophysical Research: Atmospheres*, 111, n/a-n/a, 10.1029/2006JD007090, 2006.
- Pétron, G., Frost, G., Miller, B. R., Hirsch, A. I., Montzka, S. A., Karion, A., Trainer, M., Sweeney, C., Andrews, A. E., Miller, L., Kofler, J., Bar-Ilan, A., Dlugokencky, E. J., Patrick, L., Moore, C. T., Ryerson, T. B., Siso, C., Kolodzey, W., Lang, P. M., Conway, T., Novelli, P., Masarie, K., Hall, B., Guenther, D., Kitzis, D., Miller, J., Welsh, D., Wolfe, D., Neff, W., and Tans, P.: Hydrocarbon emissions characterization in the Colorado Front Range: A pilot study, *Journal of Geophysical Research: Atmospheres*, 117, n/a-n/a, 10.1029/2011JD016360, 2012.
- Pétron, G., Karion, A., Sweeney, C., Miller, B. R., Montzka, S. A., Frost, G. J., Trainer, M., Tans, P., Andrews, A., Kofler, J., Helmig, D., Guenther, D., Dlugokencky, E., Lang, P., Newberger, T., Wolter, S., Hall, B., Novelli, P., Brewer, A., Conley, S., Hardesty, M., Banta, R., White, A., Noone, D., Wolfe, D., and Schnell, R.: A new look at methane and nonmethane hydrocarbon emissions from oil and natural gas operations in the Colorado Denver-Julesburg Basin, *Journal of Geophysical Research: Atmospheres*, 119, 6836-6852, 10.1002/2013JD021272, 2014.
- Pfister, G., Flocke, F., Hornbrook, R. S., Orlando, J. J., Lee, S., and Schroeder, J. R.: Process-Based and Regional Source Impact Analysis for FRAPPÉ and DISCOVER-AQ 2014, National Center for Atmospheric Research, Boulder, CO, 48, 2017a.
- Pfister, G. G., Wiedinmyer, C., and Emmons, L. K.: Impacts of the fall 2007 California wildfires on surface ozone: Integrating local observations with global model simulations, *Geophysical Research Letters*, 35, n/a-n/a, 10.1029/2008GL034747, 2008.
- Pfister, G. G., Reddy, P. J., Barth, M. C., Flocke, F. F., Fried, A., Herndon, S. C., Sive, B. C., Sullivan, J. T., Thompson, A. M., Yacovitch, T. I., Weinheimer, A. J., and Wisthaler, A.: Using Observations and Source-Specific Model Tracers to Characterize Pollutant

- Transport During FRAPPÉ and DISCOVER-AQ, *Journal of Geophysical Research: Atmospheres*, 122, 10,510-510,538, 10.1002/2017JD027257, 2017b.
- Pinder, R. W., Gilliland, A. B., and Dennis, R. L.: Environmental impact of atmospheric NH₃ emissions under present and future conditions in the eastern United States, *Geophysical Research Letters*, 35, n/a-n/a, 10.1029/2008GL033732, 2008.
- Rappold, A. G., Stone, S. L., Cascio, W. E., Neas, L. M., Kilaru, V. J., Carraway, M. S., Szykman, J. J., Ising, A., Cleve, W. E., Meredith, J. T., Vaughan-Batten, H., Deyneka, L., and Devlin, R. B.: Peat Bog Wildfire Smoke Exposure in Rural North Carolina Is Associated with Cardiopulmonary Emergency Department Visits Assessed through Syndromic Surveillance, *Environmental Health Perspectives*, 119, 1415-1420, 10.1289/ehp.1003206, 2011.
- Reddy, P. J., and Pfister, G. G.: Meteorological factors contributing to the interannual variability of midsummer surface ozone in Colorado, Utah, and other western U.S. states, *Journal of Geophysical Research: Atmospheres*, 121, 2434-2456, 10.1002/2015JD023840, 2016.
- Rhew, R. C., Deventer, M. J., Turnipseed, A. A., Warneke, C., Ortega, J., Shen, S., Martinez, L., Koss, A., Lerner, B. M., Gilman, J. B., Smith, J. N., Guenther, A. B., and de Gouw, J. A.: Ethene, propene, butene and isoprene emissions from a ponderosa pine forest measured by relaxed eddy accumulation, *Atmos. Chem. Phys.*, 17, 13417-13438, 10.5194/acp-17-13417-2017, 2017a.
- Rhew, R. C., Deventer, M. J., Turnipseed, A. A., Warneke, C., Ortega, J., Shen, S., Martinez, L., Koss, A., Lerner, B. M., Gilman, J. B., Smith, J. N., Guenther, A. B., and de Gouw, J. A.: Ethene, propene, butene and isoprene emissions from a ponderosa pine forest measured by Relaxed Eddy Accumulation, *Atmos. Chem. Phys. Discuss.*, 2017, 1-35, 10.5194/acp-2017-363, 2017b.
- Roberts, J. M., Williams, J., Baumann, K., Buhr, M. P., Goldan, P. D., Holloway, J., Hübler, G., Kuster, W. C., McKeen, S. A., Ryerson, T. B., Trainer, M., Williams, E. J., Fehsenfeld, F. C., Bertman, S. B., Nouaime, G., Seaver, C., Grodzinsky, G., Rodgers, M., and Young, V. L.: Measurements of PAN, PPN, and MPAN made during the 1994 and 1995 Nashville Intensives of the Southern Oxidant Study: Implications for regional ozone production from biogenic hydrocarbons, *Journal of Geophysical Research: Atmospheres*, 103, 22473-22490, 10.1029/98JD01637, 1998.
- Roberts, J. M., Stroud, C. A., Jobson, B. T., Trainer, M., Hereid, D., Williams, E., Fehsenfeld, F., Brune, W., Martinez, M., and Harder, H.: Application of a sequential reaction model to PANs and aldehyde measurements in two urban areas, *Geophysical Research Letters*, 28, 4583-4586, 10.1029/2001GL013507, 2001.
- Roberts, J. M., Jobson, B. T., Kuster, W., Goldan, P., Murphy, P., Williams, E., Frost, G., Riemer, D., Apel, E., Stroud, C., Wiedinmyer, C., and Fehsenfeld, F.: An examination of the chemistry of peroxy-carboxylic nitric anhydrides and related volatile organic compounds during Texas Air Quality Study 2000 using ground-based measurements, *Journal of Geophysical Research: Atmospheres*, 108, 10.1029/2003JD003383, 2003.
- Roberts, J. M., Marchewka, M., Bertman, S. B., Sommariva, R., Warneke, C., de Gouw, J., Kuster, W., Goldan, P., Williams, E., Lerner, B. M., Murphy, P., and Fehsenfeld, F. C.: Measurements of PANs during the New England Air Quality Study 2002, *Journal of Geophysical Research: Atmospheres*, 112, 10.1029/2007JD008667, 2007.
- Roberts, J. M.: PAN and Related Compounds, in: *Volatile Organic Compounds in the Atmosphere*, edited by: Koppmann, R., Wiley-Blackwell, 221-268, 2008.

- Rolph, G. D., Draxler, R. R., Stein, A. F., Taylor, A., Ruminski, M. G., Kondragunta, S., Zeng, J., Huang, H.-C., Manikin, G., McQueen, J. T., and Davidson, P. M.: Description and Verification of the NOAA Smoke Forecasting System: The 2007 Fire Season, *Weather and Forecasting*, 24, 361-378, 10.1175/2008WAF2222165.1, 2009.
- Roscioli, J. R., Zahniser, M. S., Nelson, D. D., Herndon, S. C., and Kolb, C. E.: New Approaches to Measuring Sticky Molecules: Improvement of Instrumental Response Times Using Active Passivation, *The Journal of Physical Chemistry A*, 120, 1347-1357, 10.1021/acs.jpca.5b04395, 2016.
- Rudolph, J., and Ehhalt, D. H.: Measurements of C2–C5 hydrocarbons over the North Atlantic, *Journal of Geophysical Research: Oceans*, 86, 11959-11964, 10.1029/JC086iC12p11959, 1981.
- Sandu, A., Daescu, D. N., and Carmichael, G. R.: Direct and adjoint sensitivity analysis of chemical kinetic systems with KPP: Part I—theory and software tools, *Atmospheric Environment*, 37, 5083-5096, <https://doi.org/10.1016/j.atmosenv.2003.08.019>, 2003.
- Schreier, S. F., Richter, A., Schepaschenko, D., Shvidenko, A., Hilboll, A., and Burrows, J. P.: Differences in satellite-derived NO_x emission factors between Eurasian and North American boreal forest fires, *Atmospheric Environment*, 121, 55-65, <http://dx.doi.org/10.1016/j.atmosenv.2014.08.071>, 2015.
- Sillman, S., Al-Wali, K. I., Marsik, F. J., Nowacki, P., Samson, P. J., Rodgers, M. O., Garland, L. J., Martinez, J. E., Stoneking, C., Imhoff, R., Lee, J. H., Newman, L., Weinstein-Lloyd, J., and Aneja, V. P.: Photochemistry of ozone formation in Atlanta, GA—Models and measurements, *Atmospheric Environment*, 29, 3055-3066, [https://doi.org/10.1016/1352-2310\(95\)00217-M](https://doi.org/10.1016/1352-2310(95)00217-M), 1995.
- Sillman, S., and Samson, P. J.: Impact of temperature on oxidant photochemistry in urban, polluted rural and remote environments, *Journal of Geophysical Research: Atmospheres*, 100, 11497-11508, 10.1029/94JD02146, 1995.
- Sillman, S.: The relation between ozone, NO_x, and hydrocarbons in urban and polluted rural environments, *Atmospheric Environment*, 33, 1821-1845, 1999.
- Singh, H. B., and Hanst, P. L.: Peroxyacetyl nitrate (PAN) in the unpolluted atmosphere: An important reservoir for nitrogen oxides, *Geophysical Research Letters*, 8, 941-944, 10.1029/GL008i008p00941, 1981.
- Singh, H. B., Cai, C., Kaduwela, A., Weinheimer, A., and Wisthaler, A.: Interactions of fire emissions and urban pollution over California: Ozone formation and air quality simulations, *Atmospheric Environment*, 56, 45-51, 10.1016/j.atmosenv.2012.03.046, 2012.
- Sive, B. C., Zhou, Y., Troop, D., Wang, Y., Little, W. C., Wingenter, O. W., Russo, R. S., Varner, R. K., and Talbot, R.: Development of a Cryogen-Free Concentration System for Measurements of Volatile Organic Compounds, *Analytical Chemistry*, 77, 6989-6998, 10.1021/ac0506231, 2005.
- Sommariva, R., de Gouw, J. A., Trainer, M., Atlas, E., Goldan, P. D., Kuster, W. C., Warneke, C., and Fehsenfeld, F. C.: Emissions and photochemistry of oxygenated VOCs in urban plumes in the Northeastern United States, *Atmos. Chem. Phys.*, 11, 7081-7096, 10.5194/acp-11-7081-2011, 2011.
- Stein, A. F., Draxler, R. R., Rolph, G. D., Stunder, B. J. B., Cohen, M. D., and Ngan, F.: NOAA's HYSPLIT Atmospheric Transport and Dispersion Modeling System, *Bulletin of*

- the American Meteorological Society, 96, 2059-2077, 10.1175/BAMS-D-14-00110.1, 2015.
- Stockwell, C. E., Veres, P. R., Williams, J., and Yokelson, R. J.: Characterization of biomass burning emissions from cooking fires, peat, crop residue, and other fuels with high-resolution proton-transfer-reaction time-of-flight mass spectrometry, *Atmos. Chem. Phys.*, 15, 845-865, 10.5194/acp-15-845-2015, 2015.
- Sullivan, J. T., McGee, T. J., Langford, A. O., Alvarez, R. J., Senff, C. J., Reddy, P. J., Thompson, A. M., Twigg, L. W., Sumnicht, G. K., Lee, P., Weinheimer, A., Knute, C., Long, R. W., and Hoff, R. M.: Quantifying the contribution of thermally driven recirculation to a high-ozone event along the Colorado Front Range using lidar, *Journal of Geophysical Research: Atmospheres*, 121, 3377-3390, 10.1002/2016JD025229, 2016.
- Swarthout, R. F., Russo, R. S., Zhou, Y., Hart, A. H., and Sive, B. C.: Volatile organic compound distributions during the NACHTT campaign at the Boulder Atmospheric Observatory: Influence of urban and natural gas sources, *Journal of Geophysical Research: Atmospheres*, 118, 614-637, 10.1002/jgrd.50722, 2013.
- Tabazadeh, A., Jacobson, M. Z., Singh, H. B., Toon, O. B., Lin, J. S., Chatfield, R. B., Thakur, A. N., Talbot, R. W., and Dibb, J. E.: Nitric acid scavenging by mineral and biomass burning aerosols, *Geophysical Research Letters*, 25, 4185-4188, 10.1029/1998GL900062, 1998.
- Tevlin, A. G., Li, Y., Collett, J. L., McDuffie, E. E., Fischer, E. V., and Murphy, J. G.: Tall Tower Vertical Profiles and Diurnal Trends of Ammonia in the Colorado Front Range, *Journal of Geophysical Research: Atmospheres*, 122, 10.1002/2017JD026534, 2017.
- Thompson, C. R., Hueber, J., and Helmig, D.: Influence of oil and gas emissions on ambient atmospheric non-methane hydrocarbons in residential areas of Northeastern Colorado, *Elementa: Science of the Anthropocene*, 2, 000035, 10.12952/journal.elementa.000035, 2014.
- Thornton, J. A., Wooldridge, P. J., Cohen, R. C., Martinez, M., Harder, H., Brune, W. H., Williams, E. J., Roberts, J. M., Fehsenfeld, F. C., Hall, S. R., Shetter, R. E., Wert, B. P., and Fried, A.: Ozone production rates as a function of NO_x abundances and HO_x production rates in the Nashville urban plume, *Journal of Geophysical Research: Atmospheres*, 107, ACH 7-1-ACH 7-17, 10.1029/2001JD000932, 2002.
- Townsend-Small, A., Botner, E. C., Jimenez, K. L., Schroeder, J. R., Blake, N. J., Meinardi, S., Blake, D. R., Sive, B. C., Bon, D., Crawford, J. H., Pfister, G., and Flocke, F. M.: Using stable isotopes of hydrogen to quantify biogenic and thermogenic atmospheric methane sources: A case study from the Colorado Front Range, *Geophysical Research Letters*, 43, 411,462-411,471, 10.1002/2016GL071438, 2016.
- Trainer, M., Parrish, D. D., Buhr, M. P., Norton, R. B., Fehsenfeld, F. C., Anlauf, K. G., Bottenheim, J. W., Tang, Y. Z., Wiebe, H. A., Roberts, J. M., Tanner, R. L., Newman, L., Bowersox, V. C., Meagher, J. F., Olszyna, K. J., Rodgers, M. O., Wang, T., Berresheim, H., Demerjian, K. L., and Roychowdhury, U. K.: Correlation of ozone with NO_y in photochemically aged air, *Journal of Geophysical Research: Atmospheres*, 98, 2917-2925, 10.1029/92JD01910, 1993.
- Trentmann, J., Yokelson, R. J., Hobbs, P. V., Winterrath, T., Christian, T. J., Andreae, M. O., and Mason, S. A.: An analysis of the chemical processes in the smoke plume from a

- savanna fire, *Journal of Geophysical Research: Atmospheres*, 110, n/a-n/a, 10.1029/2004JD005628, 2005.
- Val Martin, M., Heald, C. L., Lamarque, J. F., Tilmes, S., Emmons, L. K., and Schichtel, B. A.: How emissions, climate, and land use change will impact mid-century air quality over the United States: a focus on effects at national parks, *Atmos. Chem. Phys.*, 15, 2805-2823, 10.5194/acp-15-2805-2015, 2015.
- Vu, K. T., Dingle, J. H., Bahreini, R., Reddy, P. J., Apel, E. C., Campos, T. L., DiGangi, J. P., Diskin, G. S., Fried, A., Herndon, S. C., Hills, A. J., Hornbrook, R. S., Huey, G., Kaser, L., Montzka, D. D., Nowak, J. B., Pusede, S. E., Richter, D., Roscioli, J. R., Sachse, G. W., Shertz, S., Stell, M., Tanner, D., Tyndall, G. S., Walega, J., Weibring, P., Weinheimer, A. J., Pfister, G., and Flocke, F.: Impacts of the Denver Cyclone on regional air quality and aerosol formation in the Colorado Front Range during FRAPPÉ 2014, *Atmos. Chem. Phys.*, 16, 12039-12058, 10.5194/acp-16-12039-2016, 2016.
- Wang, L., Newchurch, M. J., Alvarez Ii, R. J., Berkoff, T. A., Brown, S. S., Carrion, W., De Young, R. J., Johnson, B. J., Gano, R., Gronoff, G., Kirgis, G., Kuang, S., Langford, A. O., Leblanc, T., McDuffie, E. E., McGee, T. J., Pliutau, D., Senff, C. J., Sullivan, J. T., Sunnicht, G., Twigg, L. W., and Weinheimer, A. J.: Quantifying TOLNet ozone lidar accuracy during the 2014 DISCOVER-AQ and FRAPPÉ campaigns, *Atmos. Meas. Tech.*, 10, 3865-3876, 10.5194/amt-10-3865-2017, 2017.
- Westerling, A. L.: Increasing western US forest wildfire activity: sensitivity to changes in the timing of spring, *Philosophical Transactions of the Royal Society B: Biological Sciences*, 371, 2016.
- Wild, R. J., Dubé, W. P., Aikin, K. C., Eilerman, S. J., Neuman, J. A., Peischl, J., Ryerson, T. B., and Brown, S. S.: On-road measurements of vehicle NO₂/NO_x emission ratios in Denver, Colorado, USA, *Atmospheric Environment*, 148, 182-189, <https://doi.org/10.1016/j.atmosenv.2016.10.039>, 2017.
- Williams, J., Roberts, J. M., Fehsenfeld, F. C., Bertman, S. B., Buhr, M. P., Goldan, P. D., Hübler, G., Kuster, W. C., Ryerson, T. B., Trainer, M., and Young, V.: Regional ozone from biogenic hydrocarbons deduced from airborne measurements of PAN, PPN, and MPAN, *Geophysical Research Letters*, 24, 1099-1102, 10.1029/97GL00548, 1997.
- Yates, E. L., Iraci, L. T., Singh, H. B., Tanaka, T., Roby, M. C., Hamill, P., Clements, C. B., Lareau, N., Contezac, J., Blake, D. R., Simpson, I. J., Wisthaler, A., Mikoviny, T., Diskin, G. S., Beyersdorf, A. J., Choi, Y., Ryerson, T. B., Jimenez, J. L., Campuzano-Jost, P., Loewenstein, M., and Gore, W.: Airborne measurements and emission estimates of greenhouse gases and other trace constituents from the 2013 California Yosemite Rim wildfire, *Atmospheric Environment*, 127, 293-302, <http://dx.doi.org/10.1016/j.atmosenv.2015.12.038>, 2016.
- Yokelson, R. J., Crouse, J. D., DeCarlo, P. F., Karl, T., Urbanski, S., Atlas, E., Campos, T., Shinozuka, Y., Kapustin, V., Clarke, A. D., Weinheimer, A., Knapp, D. J., Montzka, D. D., Holloway, J., Weibring, P., Flocke, F., Zheng, W., Toohey, D., Wennberg, P. O., Wiedinmyer, C., Mauldin, L., Fried, A., Richter, D., Walega, J., Jimenez, J. L., Adachi, K., Buseck, P. R., Hall, S. R., and Shetter, R.: Emissions from biomass burning in the Yucatan, *Atmos. Chem. Phys.*, 9, 5785-5812, 10.5194/acp-9-5785-2009, 2009.
- Zaragoza, J.: Observations of acyl peroxy nitrates during the Front Range Air Pollution And Photochemistry Experiment (FRAPPÉ), Master of Science (M.S.), Atmospheric Science, Colorado State University, 78 pp., 2016.

Zaragoza, J., Callahan, S., McDuffie, E. E., Kirkland, J., Brophy, P., Durrett, L., Farmer, D. K., Zhou, Y., Sive, B., Flocke, F., Pfister, G., Knote, C., Tevlin, A., Murphy, J., and Fischer, E. V.: Observations of Acyl Peroxy Nitrates During the Front Range Air Pollution and Photochemistry Experiment (FRAPPÉ), *Journal of Geophysical Research: Atmospheres*, 122, 10.1002/2017JD027337, 2017.

APPENDIX A: SUPPLEMENTARY INFORMATION TO CHAPTER 3

Table 3. Input parameters to the NCAR Tropospheric Ultraviolet and Visible radiation model.

Latitude	Longitude	Solar zenith angle	Assumed Cloud optical depth	Assumed Aerosol optical depth	Assumed Overhead O ₃ column	Assumed surface albedo	Ground elevation (masl)	Assumed Box elevation
40° N	105° W	25.23	0	0	290	0.1	1700 m	0 m

Sensitivity of PPN mixing ratio to 10% perturbations in PPN precursor species

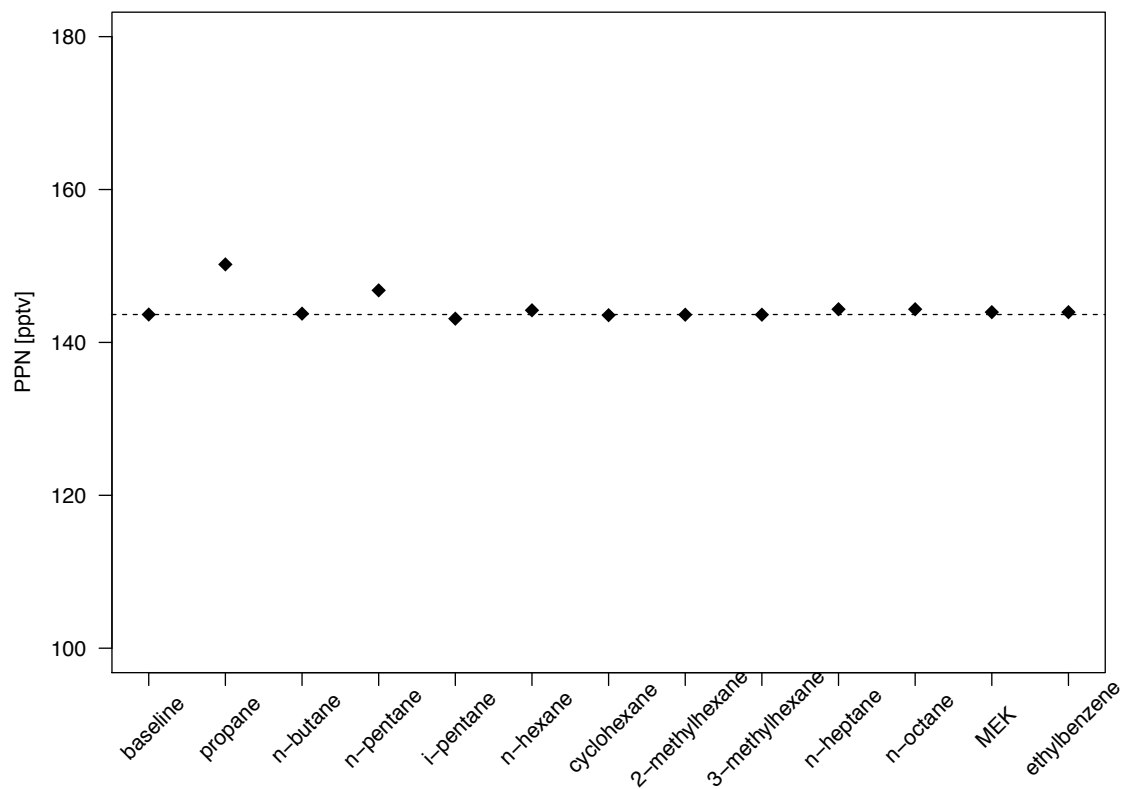


Figure 17. Sensitivity of the final PPN mixing ratio in BOXMOX simulations to a 10% increase in the initial mixing ratio of all PPN precursor species measured at BAO in summer 2015. Propane and n-pentane show the largest increase in PPN, indicating that they are the dominant PPN precursors among the species measured.

Sensitivity of PAN mixing ratio to 10% perturbations in PPN precursor species

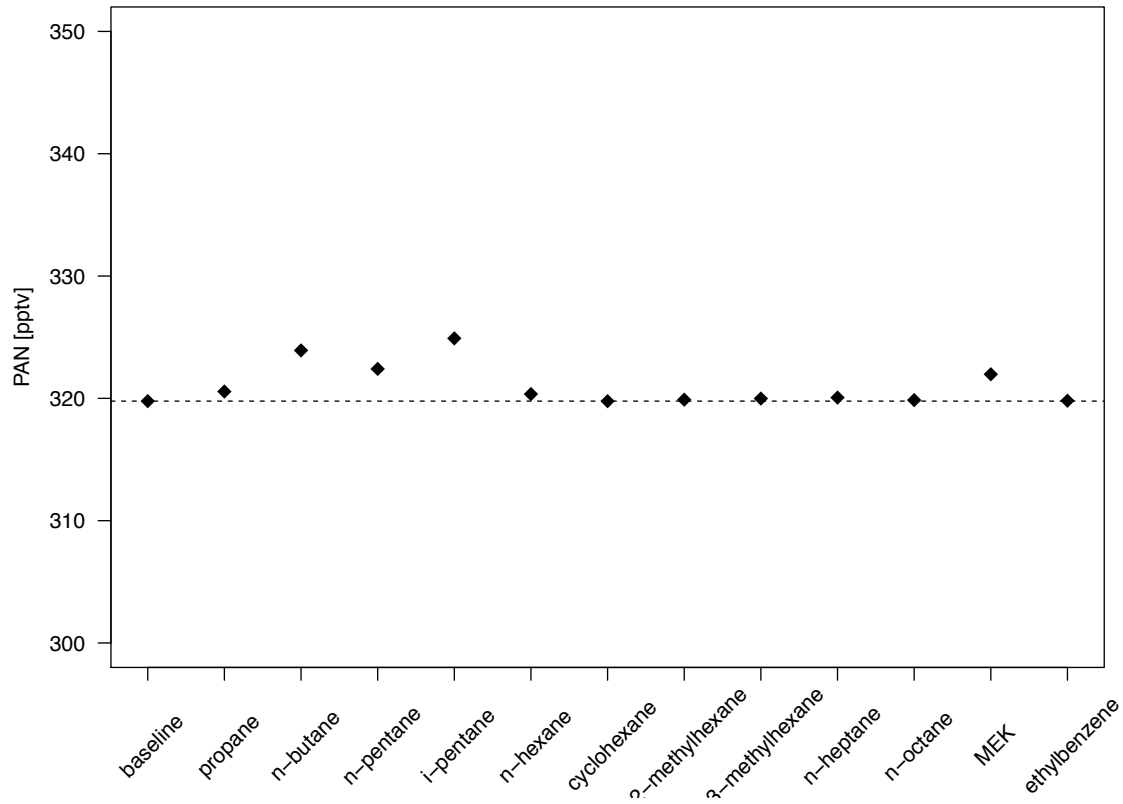


Figure 18. Sensitivity of the final PAN mixing ratio in BOXMOX simulations to a 10% increase in the initial mixing ratio of all PPN precursor species measured at BAO in summer 2015.

APPENDIX B: SUPPLEMENTARY INFORMATION TO CHAPTER 4

Table 4. Summary of Statistics for GC measurements at the Boulder Atmospheric Observatory in summer 2015.

^a Standard deviation in parentheses

* Indicates statistically significant change in mean during August smoke-impacted period as compared to the smoke-free period

Compound	Smoke-free period				August smoke-impacted period			
	min	median	mean ^a	max	min	median	mean ^a	max
ethane	0.341	12.4	23 (32.3)	338	0.981	11.5	20.5 (33.7)	362
propane	0.04	4.37	8.09 (11.2)	149	0.218	5.02	8.88 (12.9)	135
i-butane	0.002	0.841	1.52 (1.89)	14	0.028	0.952	1.75 (2.98)	36.3
n-butane	0.023	1.92	3.8 (5.67)	78.2	0.072	2.17	4.16 (7.01)	82.5
i-pentane	0.001	1.63	2.93 (4.94)	82.2	0.048	1.65	2.74 (4.39)	54.6
n-pentane	0.029	1.45	2.84 (5.03)	81.6	0.053	1.42	2.8 (6.6)	91.6
cyclopentane	0.001	0.115	0.679 (0.977)	3.74	0.001	0.104	0.43 (0.665)	3.33
n-hexane	0.001	0.208	0.365 (0.511)	6.82	0.01	0.222	0.387 (0.634)	7.83
cyclohexane	0.005	0.108	0.178 (0.208)	2.15	0.007	0.123	0.194 (0.26)	2.64
2,3-dimethylpentane	0.002	0.057	0.0865 (0.0928)	0.758	0.006	0.073	0.111 (0.144)	1.42
2-methylhexane	0.002	0.055	0.085 (0.092)	0.72	0	0.031	0.046 (0.053)	0.46
3-methylhexane	0.001	0.046	0.0847 (0.121)	1.26	0.007	0.093	0.148 (0.191)	1.86
n-heptane	0.001	0.082	0.129 (0.149)	1.52	0.004	0.085	0.136 (0.188)	1.98
methylcyclohexane	0.005	0.104	0.186 (0.235)	2.33	0.004	0.113	0.2 (0.3)	3.17
2,2,4-trimethylpentane	0.001	0.048	0.061 (0.063)	0.66	0.004	0.048	0.056 (0.055)	0.5
2,2,3-trimethylpentane	0.002	0.017	0.028 (0.044)	0.55	0.002	0.006	0.023 (0.029)	0.24
2-methylheptane	0	0.033	0.044 (0.052)	0.54	0.003	0.027	0.04 (0.054)	0.47
3-methylheptane	0.003	0.045	0.063 (0.067)	0.56	0.005	0.051	0.074 (0.091)	0.77
n-octane	0.005	0.038	0.059 (0.065)	0.54	0.004	0.036	0.057 (0.078)	0.6
ethene*	0.001	0.2	0.253 (0.212)	1.94	0.001	0.001	0.0464 (0.128)	0.918
propene*	0.002	0.041	0.051 (0.04)	0.41	0.002	0.008	0.011 (0.012)	0.086
cis-2-butene	0.001	0.018	0.0236 (0.0292)	0.345	0.001	0.014	0.023 (0.07)	1.08

isoprene*	0.003	0.141	0.223 (0.268)	2.02	0.001	0.048	0.0804 (0.114)	1.16
benzene*	0.009	0.143	0.175 (0.131)	1.12	0.042	0.241	0.292 (0.189)	1.48
toluene	0.008	0.252	0.297 (0.215)	1.5	0.008	0.237	0.298 (0.26)	1.68
ethylbenzene	0	0.026	0.035 (0.053)	0.95	0.002	0.017	0.028 (0.037)	0.35
ortho-xylene	0.003	0.037	0.045 (0.046)	0.46	0.003	0.022	0.035 (0.041)	0.22
ethyne*	0.002	0.203	0.242 (0.168)	2.09	0.092	0.357	0.405 (0.255)	2.43
acetaldehyde	0.202	1.82	1.86 (0.614)	5.7	0.463	1.79	1.78 (0.509)	3.88
acetone	0.297	3.39	3.46 (1.05)	7.68	0.061	3.56	3.62 (1.21)	7.2
methyl ethyl ketone	0.021	0.353	0.407 (0.25)	2.47	0.021	0.399	0.45 (0.256)	1.6
CFCl ₃ (CFC-11)	0.11	0.19	0.2 (0.022)	0.36	0.15	0.19	0.19 (0.024)	0.35
CCl ₂ FCClF ₂ (CFC- 113)	0.002	0.061	0.061 (0.007)	0.11	0.047	0.064	0.063 (0.006)	0.08 7
CH ₂ Cl ₂	0.002	0.025	0.029 (0.019)	0.2	0.002	0.022	0.025 (0.013)	0.08 6
MeCCl ₃	0	0.014	0.013 (0.0015)	0.022	0.01	0.014	0.014 (0.0014)	0.01 8
CHCl ₃	0	0.008	0.0087 (0.0031)	0.022	0.001	0.008	0.0087 (0.0026)	0.01 8
C ₂ Cl ₄	0	0.005	0.0057 (0.0036)	0.025	0.001	0.004	0.006 (0.0049)	0.03 6
CH ₂ Br ₂	0	0.001	0.0011 (4e- 04)	0.003	0	0.001	0.0011 (5e-04)	0.00 4
CHBrCl ₂	0	0.001	0.00074 (9e-04)	0.006	0	0.001	0.00066 (8e- 04)	0.00 4
methylnitrate*	0.001	0.003	0.003 (0.0017)	0.021	0	0.004	0.0042 (0.002)	0.01 6
ethylnitrate*	0	0.002	0.0024 (0.0018)	0.023	0.001	0.003	0.0032 (0.0013)	0.00 8
2-propylnitrate	0.001	0.009	0.011 (0.0062)	0.045	0.004	0.011	0.012 (0.0061)	0.03 5
2-butylnitrate	0.001	0.014	0.018 (0.016)	0.12	0.002	0.015	0.021 (0.015)	0.07 8
3-pentylnitrate	0	0.003	0.0048 (0.0047)	0.035	0	0.004	0.006 (0.0049)	0.02 5
2-pentylnitrate	0	0.005	0.0072 (0.0072)	0.055	0	0.007	0.009 (0.0075)	0.03 9

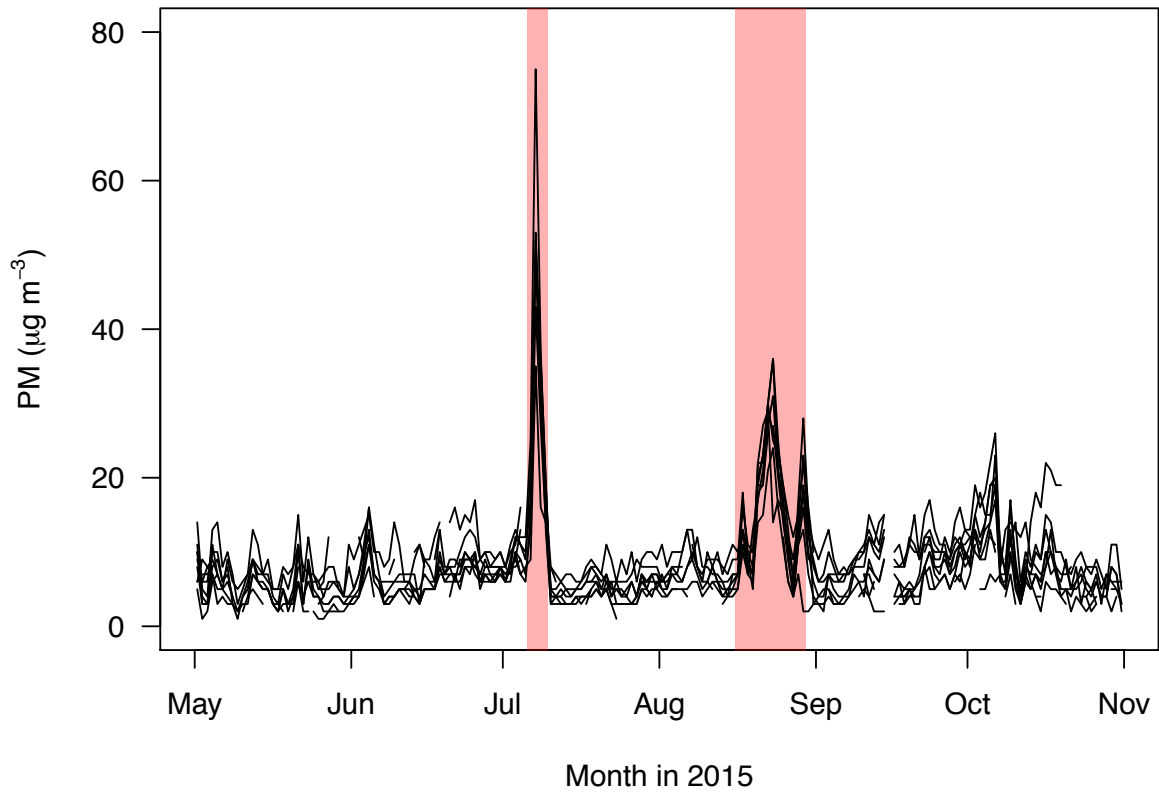


Figure 19. Timeseries of daily average PM measurements for May – November 2015 from 10 PM monitors in the Front Range: CAMP, BOU, CASA, CHAT, COMM, FTCF, GREH, I25, LNGM, NJH. All monitors show similar and consistent excursions during the same smoke-impacted time periods defined at BAO (shown in red shading).

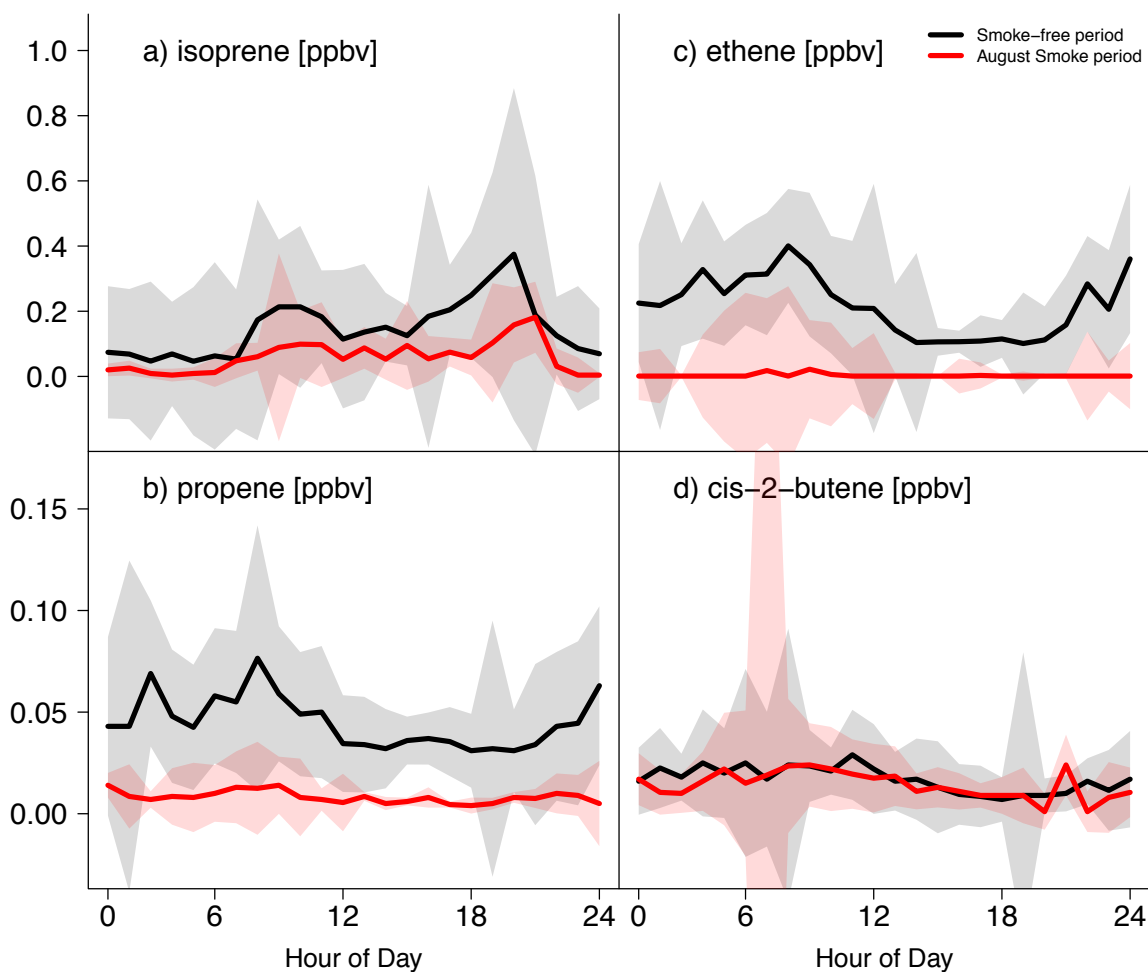


Figure 20. Diurnal cycles of a) isoprene, b) propene, c) ethene, and d) cis-2-butene, during the smoke-free period (black lines and shading) and the August smoke-impacted period (red lines and shading) at the Boulder Atmospheric Observatory in summer 2015. Lines show median values for 2 hour bins, and shading represents \pm one standard deviation.

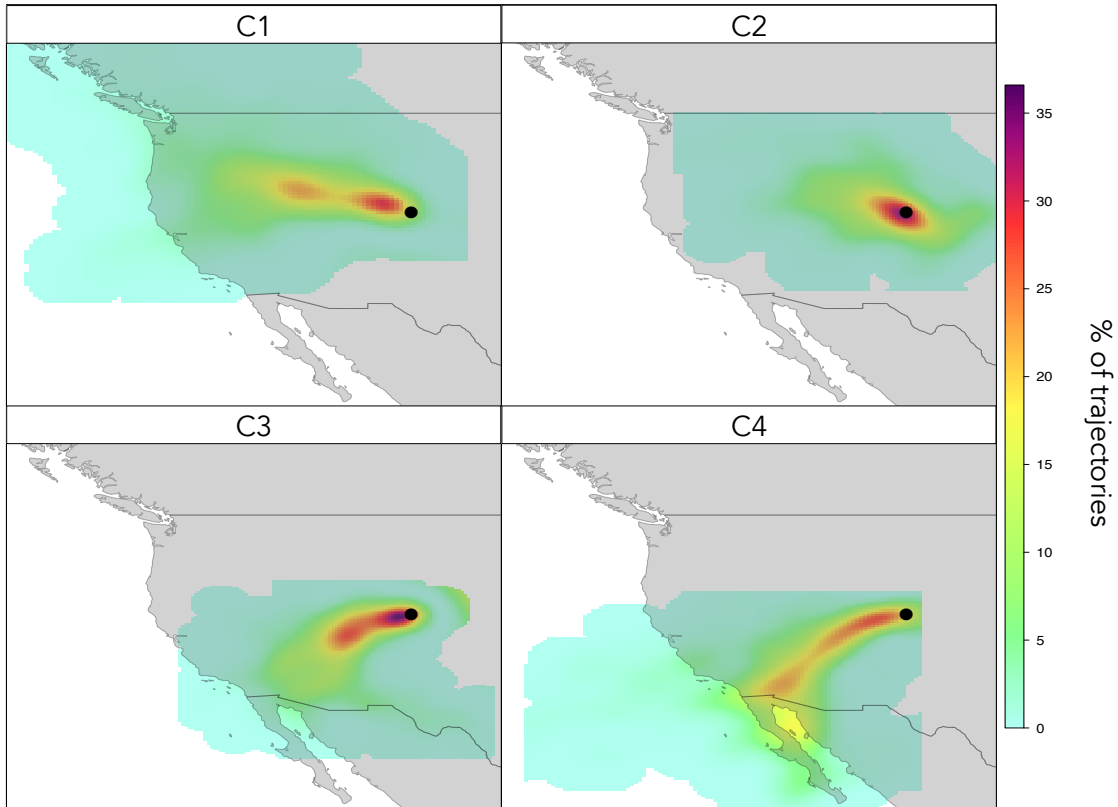


Figure 21. Trajectory clusters calculated for hourly HYSPLIT back trajectories initiated from BAO. Clusters are calculated using k-means cluster analysis. 66% of all hours during the campaign were able to be clustered. C1 shows northwesterly flow, and contains the majority of the smoke-impacted hours. C2 shows stagnant or uncertain flow. C3 shows weak southwesterly flow, and C4 shows strong westerly/southwesterly flow.

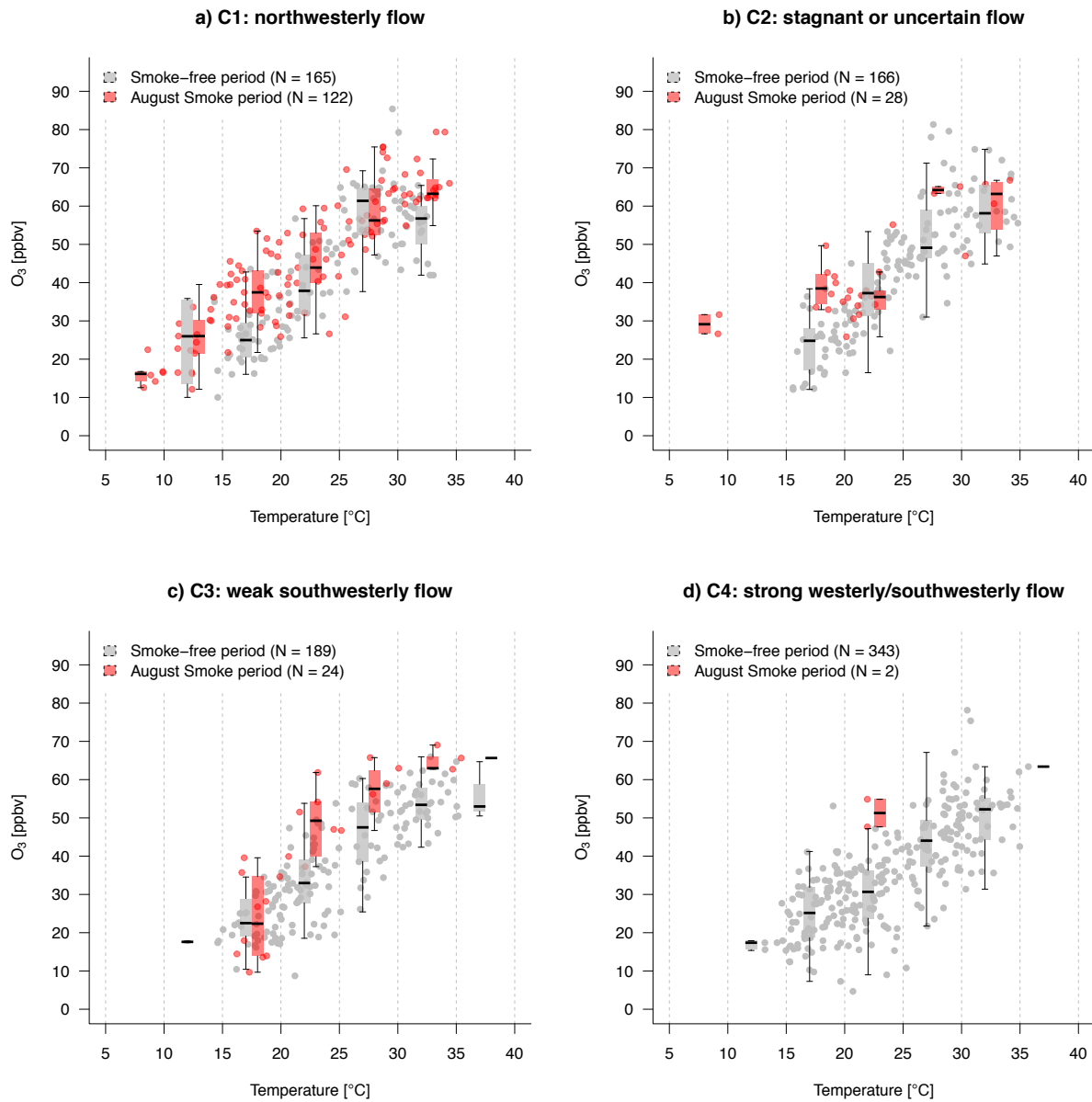


Figure 22. Hourly O_3 versus temperature for the four k-means trajectory clusters: a) C1: northwesterly flow, b) C2: stagnant or uncertain flow, c) C3: weak southwesterly flow, and d) C4: strong westerly/southwesterly flow. Plotted here are hourly data, with boxplots showing standard percentiles of 5 $^{\circ}C$ binned O_3 data. Smoke-free days are shown in black and August smoke-impacted days are shown in red as in Figure 14 and Figure 16.

a) Unclustered

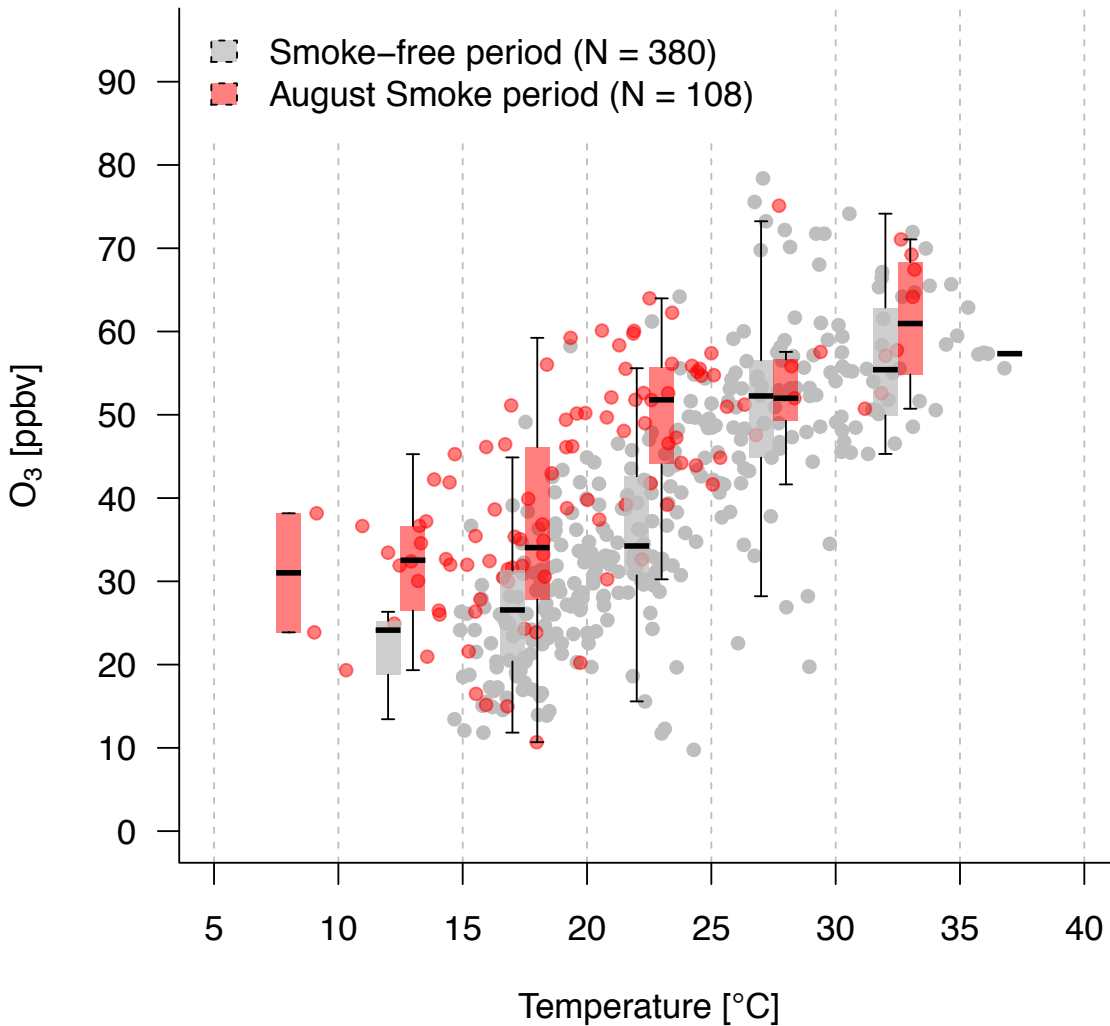


Figure 23. Hourly O₃ versus temperature for the unclustered HYSPLIT trajectory hours. Plotted here are hourly data, with boxplots showing standard percentiles of 5 °C binned O₃ data the same as is shown in Figure 14 and Figure 16.